Order Number 9100490

Modeling and control of a two-arm elastic robot in gravity

Oh, Chaeyoun, Ph.D.

Iowa State University, 1990

U·M·I
300 N. Zeeb Rd.
Ann Arbor, MI 48106

Modeling and control of a two-arm elastic robot in gravity

by

Chaeyoun Oh

A Dissertation Submitted to the
Graduate Faculty in Partial Fulfillment of the
Requirements for the Degree of
DOCTOR OF PHILOSOPHY

Major: Mechanical Engineering

Approved:

Signature was redacted for privacy.

In Charge of Major Work

Signature was redacted for privacy.

For the Major Department

Signature was redacted for privacy.

For the Graduate College

Iowa State University
Ames, Iowa
1990

TABLE OF CONTENTS

LIST OF TABLES

LIST OF FIGURES

ACKNOWLEDGEMENTS

I would like to express sincere gratitude to my advisor and good friend, Martin Vanderploeg, for his valuable guidance and encouragement throughout my graduate program. I would also like to thank Professors Bernard, Pierson, Huston and Flugrad for their input while serving on my doctoral committee.

In addition, I would like to thank my colleagues in 0095E, Jeff Trom, Jay Shannan and Jim Lynch, for their encouragement during my dissertation work.

Finally, I would like to thank my family for their love and support.

DESCRIPTION OF NOMENCLATURE

This section presents the mathematical symbols used in this thesis. The subscripts 1 and 2 (e.g., ρ_1, ρ_2) are usually reserved for the indication of the location of variables. The subscript 1 is for the upper arm and the subscript 2 is for the lower arm. A variable of bold-faced lower case (e.g., $\mathbf{q}$) or with a arrow on the top of it is a vector. A variable of bold-faced upper case (e.g., $\mathbf{S}$) or with double subscripts (e.g., S_{ij}) is a matrix. The superscript T (e.g., $\mathbf{q}^{\mathbf{T}}$) means a transpose of a vector or a matrix. A dot or dots on a variable (e.g., $\dot{\mathbf{q}}$, $\ddot{\mathbf{q}}$) means that the variable is differentiated with respect to time. Prime or primes on a variable(e.g., w_1', w_2'') means that the variable is differentiated with respect to spatial variable r_1 or r_2.

LIST OF NOMENCLATURE

A_1, A_2	cross sectional area of the upper and lower arms
a	generalized coordinate vector for elastic deformation of the upper arm
a_i	i^{th} element of a
b_i	coefficients of mode shape for the upper arm
c	generalized coordinate vector for elastic deformation of the lower arm
c_i	i^{th} element of c
d_i	coefficients of mode shape for the lower arm
E_1, E_2	modulus of elasticity of the upper and lower arm
g	gravitational acceleration
I_1, I_2	area moment of inertia of the upper and lower arm
$\hat{I}$, $\hat{J}$	global coordinates
$\hat{i}_1$, $\hat{j}_1$	local coordinate system fixed to the upper arm
$\hat{i}_2$, $\hat{j}_2$	local coordinate system fixed to the lower arm
J_1	mass moment of inertia of the actuator at the upper joint
J_2	mass moment of inertia of the actuator at the lower joint $(= J_a + J_b)$

J_a	portion of the mass moment of inertia of the actuator fixed to the lower end of the upper arm
J_b	portion of the mass moment of inertia of the actuator fixed to the top of the lower arm
J_p	mass moment of inertia of the end effector and payload
K_{t_1}	torsional spring constant at the upper joint
K_{t_2}	torsional spring constant at the lower joint
L	Lagrangian ($= T + \Pi$)
ℓ_1, ℓ_2	length of the upper and lower arms
m_2	mass of the actuator at the lower joint ($= m_a + m_b$)
m_a	portion of the mass of the actuator fixed to the lower end of the upper arm
m_b	portion of the mass of the actuator fixed to the top of the lower arm
m_p	mass of the end effector and payload
$\vec{p}_1, \vec{p}_2$	location of a point on the upper and lower arms
$(Qnc)_i$	generalized forces
$\mathbf{q}(t)$	generalized coordinates
r_1, r_2	distance along the $\hat{j}_1$ and $\hat{j}_2$ axes of the upper and lower arms
T	Kinetic energy
t	time
u_1, u_2	upper and lower joint torques
$\mathbf{u}(t)$	control vector
$\mathbf{u}(t)^\diamond$	shifted control vector

$\hat{\mathbf{u}}(t)$	modified control vector for a prescribed degree of stability
$\mathbf{u}(t)^*$	optimal control vector
$\vec{V}_{p_1}$	linear velocity at a point on the upper arm
$\vec{V}_{\ell_1}$	linear velocity at the lower joint
$\vec{V}_{p_2}$	linear velocity at a point on the lower arm
$\vec{V}_{\ell_2}$	linear velocity at the end of the lower arm
W_{nc}	nonconservative work
$w_1(r_1,t)$, $w_2(r_2,t)$	elastic deformation of the upper and lower arms
$\mathbf{x}(t)$	state vector
$\mathbf{x}(t)^\diamond$	shifted state vector
$\hat{\mathbf{x}}(t)$	modified state vector for a prescribed degree of stability
$\mathbf{x}(t)^*$	optimal state vector
$\mathbf{y}(t)$	output vector
$\mathbf{y}(t)^\diamond$	shifted output vector
$\hat{\mathbf{y}}(t)$	modified output vector for a prescribed degree of stability
α_i	frequency parameter in boundary value problem for the upper arm
α	prescribed degree of stability
β_i	frequency parameter in boundary value problem for the lower arm
δ	variational operator
θ_1, θ_2	rigid motion of the upper and lower arms
Π	potential energy
ρ_1, ρ_2	mass density of the upper and lower arms

ϕ	assumed mode shapes for the upper arm
ψ	assumed mode shapes for the lower arm
ω	circular natural frequency
ω_{m_1}	angular velocity of the hub
ω_1	angular velocity of a local coordinate attached on the upper arm
ω_{m_a}	angular velocity at the end of upper arm
ω_{m_b}	angular velocity at the top of lower arm
ω_2	angular velocity of a local coordinate attached on the lower arm
ω_{m_p}	angular velocity at the end of the lower arm

1. INTRODUCTION

Over past fifty years, many researchers have investigated the dynamics of large motion systems which have elastic bodies. Recently, these studies have looked at elastic robot arms. This is the result of a desire to have robots operate at higher speeds and precision, and at the same time reduce power demands. An obvious way to increase operating speed with less power demand is to reduce the weight of robot arms. As speed increases and weight decreases, the structural flexibility of the robot becomes significant. This flexibility then affects accuracy and response time of the robot system. Therefore, development of good models of elastic manipulators is necessary to better understanding the dynamic behavior of flexible robot systems and to develop the necessary control techniques.

The assumed modes method and the finite element method are the most commonly used modeling methods. Both convert a continuous dynamic system to a finite dimensional one. The assumed modes method is widely used because it transforms a continuous system with flexible links to finite dimensional one with a relatively small number of generalized coordinates. The finite element method can easily model complex elastic systems, but the number of degrees of freedom increases rapidly as the number of elements increases.

Since a flexible manipulator has more degrees of freedom than control inputs,

the conventional control schemes developed for the rigid manipulator are not appropriate for flexible manipulator control. Thus, a flexible manipulator requires more sophisticated control algorithms as well as more accurate dynamic models to obtain satisfactory stability and performance.

This thesis develops an analytical model for a two elastic arm robot system in a gravitational field. The model includes the shortening effect due to the elastic deflection of the arms. The equations of motion are derived using two methods; the extended Hamilton's principle and the assumed modes method. Assumed mode shapes are developed for the assumed modes method. The accuracy of the assumed mode shapes is shown by comparing the eigenvalues from the assumed modes solution to eigenvalues computed from an exact solution derived in this thesis. The analytical models are experimentally validated by comparing the eigenvalues to those obtained from experimental measurements.

A control algorithm is developed to control the movement of the end point of the two arm elastic robot. A linear quadratic optimal control technique on an infinite time interval with the prescribed degree of stability method results in good end point control.

2. LITERATURE REVIEW

The dynamics of multibody systems with elastic components has received considerable attention over past fifty years. However, the study of elastic robot arms has been a more recent development. As robots have been required to work at higher speeds with less power, this has naturally lead to the desire to reduce the weight. As weight reduces, and speed increases, flexibility in the system can degrade accuracy and response time. This chapter reviews literature related to modeling and control of elastic robot arms. This chapter is divided into two parts. The first surveys modeling techniques, and the second reviews control schemes applied to elastic robot arms.

2.1 Modeling Techniques

Development of a good model is essential for understanding the dynamic behavior of the flexible arm robot and for developing control techniques. The assumed modes method and the finite element method are the most commonly used modeling methods. As computing power has increased, symbolic modeling has been used to derive analytical models using programs such as MACSYMA, MAPLE and REDUCE. This section will review the literature relating to these three modeling techniques.

2.1.1 Assumed Modes Method

The assumed modes method [1] is widely used because it approximates a continuous system with elastic arms to a finite dimensional system with a relatively small number of generalized coordinates. The method assumes that the elastic deformation of a flexible link consists of a linear combination of basis functions which are functions of the spatial coordinates and time-dependent generalized coordinates.

$$w(r,t) = \sum_{i=1}^{n} \phi_i(r) q_i(t) \tag{2.1}$$

The assumed mode shapes are required to satisfy the essential boundary conditions of the system as a minimum, but the proper choice of assumed modes is not clearly defined in many cases. The accuracy of this approximation depends on the number of functions and the specific basis functions used for the model.

Book, Maizza-Neto and Whitney [2] developed a frequency domain model and a time domain model of a two elastic arm and two joint system. The time domain model used the assumed modes method. Admissible functions satisfying the geometric boundary conditions was used as the assumed modes. The time domain model included the first two assumed modes because the contribution of the higher frequency modes to the deflection was small compared with the first two modes. The equations of motion were derived using Lagrange's equations. The developed model was used to compare three linear feedback control schemes.

Cannon and Schmitz [3] performed an experiment to demonstrate control strategies for a single flexible manipulator moving in a horizontal plane. The flexible manipulator was modeled as a pinned-free beam. Hamilton's principle was used to obtain the partial differential equations of motion and boundary conditions. The

general form of the ordinary differential equations of motion was derived using Lagrange's equations and the assumed modes method in which eigenfunctions of a pinned-free beam without end mass were used as assumed modes. The coefficients in the equations of motion were found by an experimental identification procedure. The developed dynamic model was used to design a controller. The paper showed that satisfactory stability of end point control of a flexible arm requires a good model.

Krishnan and Vidyasagar [4] developed a dynamic model for a single link flexible arm using the assumed modes method. The model included one rigid mode and the first five flexible modes. Normal mode eigenfunctions obtained by solving the equations of motion of a pinned beam were used as assumed mode shapes. The Hankel norm minimization was used to reduce the order of the model for controller design.

Tsujisawa and Book [5] used the first five flexible modes of an analytical model of two flexible robotic arms and an actuator link which was parallel to the lower arm. A reduced order model which used the first two modes was obtained by the modal cost analysis approach. The governing equations of motion of the flexible system were derived by using Lagrange's equations and the assumed modes method. Admissible functions were used for the assumed modes. By comparing natural frequencies of two different sets of boundary conditions, paper showed that the selection of mode shapes may lead to a different analysis result.

Oakley and Cannon [6] presented a modeling technique for a two-link manipulator having a rigid upper arm and a flexible forearm, and moving in a horizontal plane. The model included the foreshortening effects due to the deflection of forearm. The transverse deflection was expressed by the assumed modes method. By

an experimental procedure, the paper showed the importance of the selection of assumed mode shapes by comparing the natural frequencies between a model with the cantilever mode shapes and a model with the cantilever mode shapes with a payload.

Johanni [7] presented a modeling method for deriving the governing equations of motion of a robot with elastic arms. D'Alembert's principle was used to derive the equations of motion. An elastic arm was modeled as an Euler-Bernoulli beam, and axial deformation was neglected. The elastic deformations were approximated by assumed mode shapes. It was pointed out that incorrect results can be induced if the second order terms of the deformation geometry are neglected in the linearized equations of motion in presence of significant centrifugal and gravity forces.

Schmitz [8] presented a nonlinear dynamic model for a planar two-link manipulator having a rigid inner link and an elastic forearm. The elastic link was assumed inextensible along the elastic axis and was modeled as Euler-Bernoulli beam. The foreshortening effect due to deflection of the elastic link was included in the model through a nonlinear strain-displacement relationship. Kane's method was utilized to obtain the governing equations of motion. The deflection was expressed by a finite series of assumed modes. Mode shapes for a cantilever beam with orthogonality properties were chosen for the assumed modes.

Yigit, Scott and Ulsoy [9] studied the flexible behavior of a radially rotating beam attached to a rigid body. The extended Hamilton's principle was applied to derive a coupled nonlinear partial differential equation of motion and the associated boundary conditions. The extended Galerkin method was used to obtain ordinary differential equations of motion. The model assumed that the arm was inextensible along longitudinal axis, and included foreshortening effects due to deflection. Admis-

sible functions were used as assumed modes, and the first three modes were included in the model. The study showed that the frequencies were increased due to coupling, and the effect of elastic behavior on the rigid motion became more important as the ratio of mass moment of inertia of the rigid shaft and that of the flexible beam decreased. It also showed that the uncoupled equations can result in incorrect frequencies.

Biswas and Klafter [10] presented a modeling method for a flexible manipulator rotating in a horizontal plane. It was assumed that the arm was not deformed along the elastic axis. The equation of motion and the associated boundary conditions were derived using Hamilton's principle. A finite dimensional system was obtained using the assumed modes method. The eigenfunctions were used as the assumed mode shapes for approximating the deflection of the elastic link. The dynamic model was used to control angular rotation of a flexible arm.

Nathan and Singh [11] developed a set of equations of motion for a robot arm with two elastic links moving in a horizontal plane. Lagrange's equations were used for deriving the equation of motion. Elastic deflections were expressed in the modal expansion. Eigenfunctions of a clamped-free beam were used for the assumed mode shapes.

Schmitz [12] developed a linearized model of a planar arm with two elastic links moving in a horizontal plane. In the model, axial elastic deformations were not considered, but energy dissipation effects were included. The assumed mode method was used to express the elastic deformation under the assumption that the deflection was small. The mode shapes for a cantilever beam were chosen as the assumed mode shapes for both links. The convergence of the system mode shapes as a function of

the number of assumed modes used in the model as well as the natural frequencies was shown. The linearized dynamic model was used for control design.

Chassiakos and Bekey [13] modeled a single link flexible manipulator moving in a horizontal plane for pointwise control. The model included the effects of the pointwise actuators, an end mass, and damping effects. A partial differential equation of motion and four boundary conditions were derived using Hamilton's principle. The elastic deflections were approximated by assumed mode shapes. The assumed mode shapes were determined by solving the partial differential equation of motion with boundary conditions, and to satisfy certain orthogonality relations.

Yang and Donath [14] developed two dynamic models including both link and joint flexibility for a single link robot arm. One model was simplified based on the assumed modes method and the orthogonality relationships. The other model was more detailed, incorporating cross coupling terms in the final equations of motion. Hamilton's principle was used to derive a partial differential equation of motion and the associated boundary conditions. The discretized equations of motion were obtained by Lagrange's equations and the assumed modes method. Admissible functions were utilized as assumed modes. A numerical simulation showed that a simplified model was enough to study the dynamic behavior of the elastic link when both joint and link flexibility were considered, and the contribution of higher frequency modes to the deflection was very small compared to the first two modes. It also showed that the joint flexibility reduced the total deflections but increased the oscillatory motion of the elastic link.

Book [15] described a modeling methodology for flexible manipulator arms connected by rotary joints. The method utilized 4×4 transformation matrices for both

the joint and deflection motion. Lagrange's equations were used for deriving the equations of motion, and some recursion relations were used to reduce the number of computations. The modal expansion method was used to express the deflections of links. A calculation count was used to compare the computational speed of this modeling method to rigid link results. The paper did not comment on the accuracy of the method.

Djerassi and Kane [16] presented a modeling method for deriving the equations of motion for a flexible linkage using Kane's equations. The model can handle closed loops and any number of links. Assumed mode shapes were used to approximate the deflection of links. The assumed mode shapes were obtained by solving the partial differential equation for cantilever beam motion. As a demonstration of the method, two simulation results of a ten link system were given.

Kane, Ryan and Banerjee [17] developed an analytical model for the study of dynamic behavior of a beam built into a base which underwent a prescribed motion of rotation or translation. The equations of motion were derived by using Kane's method. The model included the deformation along the elastic axis, transverse deflections, and torsional deflections which were expressed by the assumed modes method. Eigenfunctions of a cantilever beam were used as the assumed modes. The paper showed that, in a numerical simulation with a flexible beam attached to a rigid base, the results from the presented model differed from the results of some multibody dynamic programs.

2.1.2 Finite Element Method

The finite element method discretizes each flexible link into a set of elements connected at nodal points. The finite element method can easily model complex shapes, but the number of degrees of freedom increases rapidly as the number of elements is increased. The elastic deformation of each element is approximated by a linear combination of shape functions which satisfy boundary conditions and nodal deflections such as displacements and rotations.

Usoro, Nadira and Mahil [18] derived an analytical model for a two-link flexible manipulator moving in a vertical plane with a payload. The governing equations of motion were derived by Lagrange's equations. Shape functions were used to express the deflections. Hermitian polynomials were adapted for shape functions. The final model was verified by the response of the system in free vibration.

Sunada and Dubowsky [19] developed a method to model for dynamic analysis of robotic manipulators with elastic links. The dynamic model incorporated the control system by changing transfer functions into second order forms in terms of a Laplace variable. The dynamic motion of flexible links was described by a Hartenberg-Denavit 4×4 transformation matrix. A finite element analysis program, NASTRAN was used to develop the finite element model. Lagrange's equations were applied to derive the equations of motion. A component mode synthesis procedure was applied to reduce the number of degrees of freedom. A model for an industrial robot was developed using the method. The model was verified by comparing analytical results and experimental data. The study showed that system stability and performance were affected by flexibility of links.

Levinson and Kane [20] suggested a modeling method for numerical simulations

of large motions of a nonuniform cantilever beam in orbit. The procedure was based on Kane's method to generate the equations of motion and the finite element method to set shape functions for the deformation. Cubic polynomials were used for the shape functions. The model was tested with a uniform beam. The comparison between the exact solution and the model showed that the model yielded good results for a beam discretized with 10 elements. Furthermore, numerical simulation showed that a colocated control system led to stable results, but a noncolocated control system led to instability results.

Chedmail and Bardiaux [21] developed an analytical model for n elastic links connected with rotational joints. The analytical model was derived based on virtual work and the finite element method was used to discretize the flexible links. Hermite's interpolation functions were used for the shape functions to represent the elastic displacement. The model was verified experimentally with a two elastic link manipulator in a horizontal plane. The paper showed that, in dynamic response of two links and two rotational joints excited with sinusoidal torques, the simulation results with the model using one element on each link agreed with experimental results within 10%.

Van Den Bossche, Dugard and Landau [22] developed a model for a flexible arm moving in the horizontal plane. The elastic arm was discretized by the finite element method. Cubic polynomials were used as shape functions to approximate the transverse deflections. The equations of motion were derived using Lagrange's equations. Numerical results with the model for a flexible arm were verified by two experimental identification methods. One identification method used a spectral analyzer which analyzed the signal from the tip of the arm. The other method used

an identification software package and recursively performed on and off line according to the sampling time.

Menq and Chen [23] used the finite element method to model a flexible one link pinned-free arm moving in a horizontal plane. The model ignored longitudinal deformation and torsional deformation. Transverse deflection was approximated by using cubic shape functions. Lagrange's equations were used for deriving the equations of motion.

Bayo and Moulin [24] proposed a time domain algorithm for the solution of an inverse dynamic problem for the control of the end point of a one link flexible arm moving in a horizontal plane. The dynamic model included internal viscous damping but did not include Coriolis and centrifugal forces. The finite element method was used to discretize the elastic links. The paper showed that simulation results with the time domain method for a flexible arm using 5 elements were identical to the results with the frequency domain method.

Bayo [25] presented a frequency domain method for the solution of the inverse dynamics of flexible robots. The analytical model for the study included nonlinear Coriolis and centrifugal effects. An elastic link was modeled as Timoshenko beam which considered the shear deformation and rotary inertia. The equations of motion were derived using the principle of virtual displacement and the finite element method. The input torque history for a specified tip trajectory was found in the frequency domain. The method was applied to a two elastic link robot using 5 elements on each link. A Gaussian tip trajectory for the calculation of input joint torques was used to avoid the high frequency of the torque profile and to provide a smooth behavior of the tip trajectory.

Naganathan and Soni [26] developed a nonlinear model based on the finite element method for flexible manipulators. The nonlinear model considered rotary inertia, shear deformation, and the gross nonlinear motion effects of each link. The elastic links were modeled as a Timoshenko beam. The partial differential equations of motion were derived by the Newton-Euler formalism and transformed into integral form using Galerkin's method for the finite element method. The displacements and rotations for elastic elements were approximated using shape functions. A simulation with a three elastic link manipulator showed that linear and nonlinear coupled equations of motion yielded different deformation time histories.

Christensen and Lee [27] developed an analytical model based on the finite element method to determine the time response of unrestrained flexible structures undergoing rigid body translational and rotational motions. In the model, transverse shear was considered but warping of the cross section was neglected. The equations of motion were derived by momentum conservation principles and virtual work. In a numerical simulation with a beam rotating with respect to a fixed axis, it was shown that equations of motion using linear beam theory and using nonlinear beam theory can predict different natural frequencies as well as a different tip displacement history.

2.1.3 Symbolic Modeling

Deriving an accurate analytical model for flexible links is algebraically complex and a time-consuming. Therefore, when the model is derived manually, there is a tendency to make mistakes [28]. Symbolic languages such as MACSYMA, REDUCE and MAPLE have been used to meet this challenge. However, these programs require

large memory because the final equations of motion are very complex. Among the symbolic algebraic languages, MACSYMA is most widely used. One advantage is that it can produce FORTRAN code from its internal LISP code and has simplification code for trigonometric function reductions.

Cetinkunt and Book [28] presented a symbolic modeling method based on Lagrange's equations and the assumed modes method to derive the equations of motion of a multi-link flexible manipulator. The modeling method used a recursive method to relieve memory problems as the system dimension gets large. Assumed modes were supplied as an input. The method may show explicitly the effect of the selection of mode shapes and system parameters on the model. The model was verified by comparing the responses of two-link planar flexible arm with payload to those of a rigid arm.

Lucibello, Nicolò and Pimpinelli [29] used a method for symbolic modeling of a robot with up to four links and rotational joints in which only one link was elastic. The model included gravitational effects. Lagrange's equations were used to derive the equations of motion, and a few approximations were suggested to avoid the complexity of the final model.

Nicosia, Tomei and Tornambe [30] developed a symbolic model for one or two flexible arms. The model assumed a small deflection and included the gravitational effects. The finite dimensional model was obtained by using Ritz-Kantorovitch method. A set of functions was used as the assumed modes to approximate the deflection. Lagrange's equations were applied to derived the equations of motion.

Tzes, Yurkovich and Langer [31] utilized a symbolic algebraic language to model flexible manipulators. Kinematic relationships were given by a Denavit-Hartenberg

transformation matrix. Lagrange equations were applied to obtain coupled differential equations of motion. The model reduced the required memory space and execution time by using symmetric and anti-symmetric properties of the dynamic matrices.

De Luca, Lucibello and Nicolò [32] presented a symbolic modeling method for a robot with flexible links. The model included gravitational effects and damping effects but did not include torsional deformation. The model can handle up to six flexible links with rotational or prismatic joints if computer memory is sufficient. Lagrange's method was used to derive the equations of motion.

2.2 Control Techniques

A rigid manipulator has the same number of generalized coordinates as control inputs, however flexibility adds additional degrees of freedom. Thus, conventional control schemes developed for the rigid manipulator control may not be appropriate for flexible manipulator control. A flexible manipulator requires more sophisticated control algorithms as well as more accurate dynamic models to obtain satisfactory stability and performance.

Recently, there have been a number of control techniques proposed for flexible manipulators. Some of them are summarized below.

Book, Maizza-Neto and Whitney [2] compared the relative characteristics of three linear feedback control schemes for two flexible beams with two joints; independent joint control, general rigid control and flexible feedback control. Independent joint control and general rigid control based on a rigid arms model utilized joint angle and angular velocity measurements. Independent joint control did not include

interjoint feedback, but general rigid control included interjoint feedback. Flexible feedback control based on the linearized flexible arms model used a pole placement method to obtain the gain matrix. The simulation results showed that independent joint control was limited in bandwidth, general rigid control improved bandwidth and flexible feedback control had high sensitivities to parameter variations.

Oakley and Cannon [6] developed a noncolocated controller in which the actuator was not colocated with a sensor (e.g., end point sensor with joint controller). The controller was applied to end point control of a two-link manipulator whose upper arm was rigid and forearm was flexible. The controller was composed of linear quadratic regulator and a nonlinear estimator. A colocated proportional-derivative controller was also designed and implemented to experimentally compare with the above noncolocated controller. The experimental results showed that the noncolocated end point controller had better performance in the settling time, overshoot amplitude and commanded input tracking than the colocated proportional-derivative controller.

Cannon and Schmitz [3] developed a noncolocated controller for the end point control of a flexible one-link manipulator moving in a horizontal plane. The controller was implemented in an experimental test bed. The controller was designed using linear quadratic Gaussian regulator and a discrete estimator using measurements of the end point sensor and a colocated sensor. The end point position was measured using an optical sensor. Experiments showed that the noncolocated controller resulted in stable and precise end point control of the flexible arm.

Biswas and Klafter [10] designed an optimal controller for the control of a flexible robot arm moving in a horizontal plane. The control gain was calculated by

solving an optimal regulator problem with the prescribed terminal time, a quadratic performance index and nonlinear state and costate equations. Numerical simulations showed that structural vibrations were suppressed during angular rotation.

Nathan and Singh [11] presented a control scheme for the joint angle control of a flexible two-link arm. The control scheme was composed of two stages. The first stage was to move the joint angles to a specified neighborhood of terminal states with a discontinuous control law based on the theory of variable structure system. In the second stage, a stabilizer based on pole placement was incorporated into the discontinuous control law to suppress the elastic oscillations.

Schmitz [12] used a colocated control scheme with joint angle and joint angle rate sensors (colocated sensors) for a linear control simulation of an elastic two-link manipulator. The control scheme was based on a proportional-derivative compensator and the root locus technique which was used to obtain the gain matrix. The paper suggested that this compensator can be used for the comparison of performance of other controllers.

Schmitz [8] compared an independent joint proportional-derivative control law with a linear quadratic control law for the straight line commanded tip position control of an elastic two-link arm. The gain matrix was found using the method of successive loop closure. Using computer simulation, the paper showed that the linear quadratic controller had a better performance in damping of the elastic modes and the residual elastic vibrations control at the end of the trajectory.

Sakawa, Matsuno and Fukushima [33] developed a compensator to control a flexible arm moving in a horizontal plane. The optimal regulator gain matrix was obtained by solving an optimal linear quadratic regulator problem with the prescribed

degrees of stability and the observer gain matrix was obtained by pole assignment. The compensator was implemented in an experimental test-bed. Experimental results showed that the compensator stabilized the elastic oscillation. The deflection of the arm was measured by strain gages.

Chassiakos and Bekey [13] presented the theory of a pointwise control scheme to avoid the problem that was induced by the difference of the number of generalized coordinates and the number of control inputs for a flexible one-link manipulator moving in a horizontal plane with a payload. The control method used pointwise actuators along the link to apply force pulses in addition to input torque actuator. The optimal gain matrix was obtained by solving an optimal linear quadratic regulator problem. In the study, the optimal locations of the pointwise controllers were suggested.

Alberts, Dickerson and Book [34] suggested a combined active and passive control of a flexible link moving in a horizontal plane. The active control of the lower frequency modes was designed by solving the linear quadratic regulator problem with prescribed degrees of stability. The controller was implemented in numerical simulation. The passive control which was achieved by attaching a viscoelastic layer on the elastic beam was suggested to avoid the spillover problem due to the neglecting of higher frequency modes, and to permit the use a low order controller.

Carusone, Buchan and D'Eleuterio [35] derived a control law for the control of flexible manipulators. The control law was derived by using the optimal linear quadratic regulator problem whose performance index incorporated the first and second time derivatives of the control inputs to produce smooth control inputs. In an example using a flexible two-link manipulator in a horizontal plane, computer simulation showed that the control scheme had a good tracking performance.

Menq and Chen [23] developed an adaptive control scheme for a flexible manipulator carrying varying payloads. The control scheme was based on a compensator including regulator and estimator designed using linear quadratic Gaussian problem. The control scheme included an interpolation process to modify regulator and estimator gain matrices with changing payload. The interpolation was a least squares fit based on a look-up table of regulator and estimator gain matrices prepared off-line with a set of different payloads. The control scheme used a modified gradient method for payload identification. Simulation results with an abrupt change of payload showed that the adaptive control scheme had a good payload tracking.

Feliu, Ratten and Brown [36] proposed an adaptive control scheme for a single-link flexible manipulator moving in a horizontal plane with varying payload. The control scheme entails of four loops. An inner loop was to compensate for friction and make the motor response faster than the tip position response. A middle loop was to simplify the dynamics of the system by implementing a simple decoupling loop. An outer loop used a proportional-derivative controller and a feedforward acceleration term for fast and accurate tip position control. An adaptation loop used an adaptive controller to account for changes in the payload. The effectiveness of the adaptive control scheme was shown experimentally.

Rovner and Cannon [37] developed and implemented an adaptive control scheme for a flexible one-link manipulator moving in a horizontal plane with varying payload. The adaptive control scheme was composed of on-line identification process using a filtered version of the recursive least squares algorithm to identify the system model and a controller design process using a linear quadratic regulator and Kalman filter estimator using the results of the identification process. The tip position was mea-

sured by using a silicon lateral effect photodiode detector which sensed an infrared light from the tip of the manipulator. On-line identification process and controller design process were experimentally verified. The paper showed that the control scheme had better performance than a robust fixed gain controller in the response with a payload.

Book and Lee [38] applied two time scale control schemes for the vibration control of a large flexible manipulator using a small robotic arm. The slow motion due to the rigid motion of the manipulator was controlled using nonlinear feedback. The fast motion due to flexible behavior was controlled by pole assignment. A composite control law was then used to include the effect of the slow and fast motion.

Siciliano and Book [39] applied a singular perturbation method for order reduction of a dynamic model for a flexible manipulator. The reduced order models were a slow submodel which was the rigid model of the arm and a fast submodel which included the effects of the slow submodel. The slow submodel was controlled by a control scheme used for rigid manipulators. The fast submodel was controlled using a linear-state feedback control including the slow state variables.

Singer and Seering [40] developed a command shaping technique in the time domain which yielded an output trajectory with little or no residual vibration. Time domain shaping was compared with frequency domain filters with a step input. The comparisons showed the effectiveness of the method.

3. ANALYTICAL MODEL

3.1 Introduction

This chapter derives the equations of motion for a robot system which has two elastic arms in a gravitational field. Figure 3.1 presents a schematic diagram of the elastic robot system. The system has an end effector at the end of the second arm. The two elastic arms are connected by rotational joints which allow rotational movements only, and the flexible motion is assumed to be in the same plane of motion as the rotational joints. Therefore the robot system moves in a vertical plane.

Actuators are modeled at each joint and are assumed to apply moments at the two joints. The mass and inertia for the actuators is denoted as m_1 and J_1 at joint 1, and m_2 and J_2 at joint 2. The mass m_2 and mass moment of inertia J_2 are decomposed into two masses m_a and m_b which have mass moments of inertia J_a and J_b respectively. m_a and J_a are the portion of the actuator fixed to the lower end of the upper arm and m_b and J_b are the portion of the actuator fixed to the upper end of the lower arm. The mass and inertia of the end effector and payload are denoted as m_p and J_p. Torsional springs at each of the rotational joints with torsional spring constants K_{t_1} and K_{t_2} are also included in the model.

The elastic arms are assumed to have small cross sectional dimensions compared with the length of arms and therefore the shear deformation and rotary inertia effects

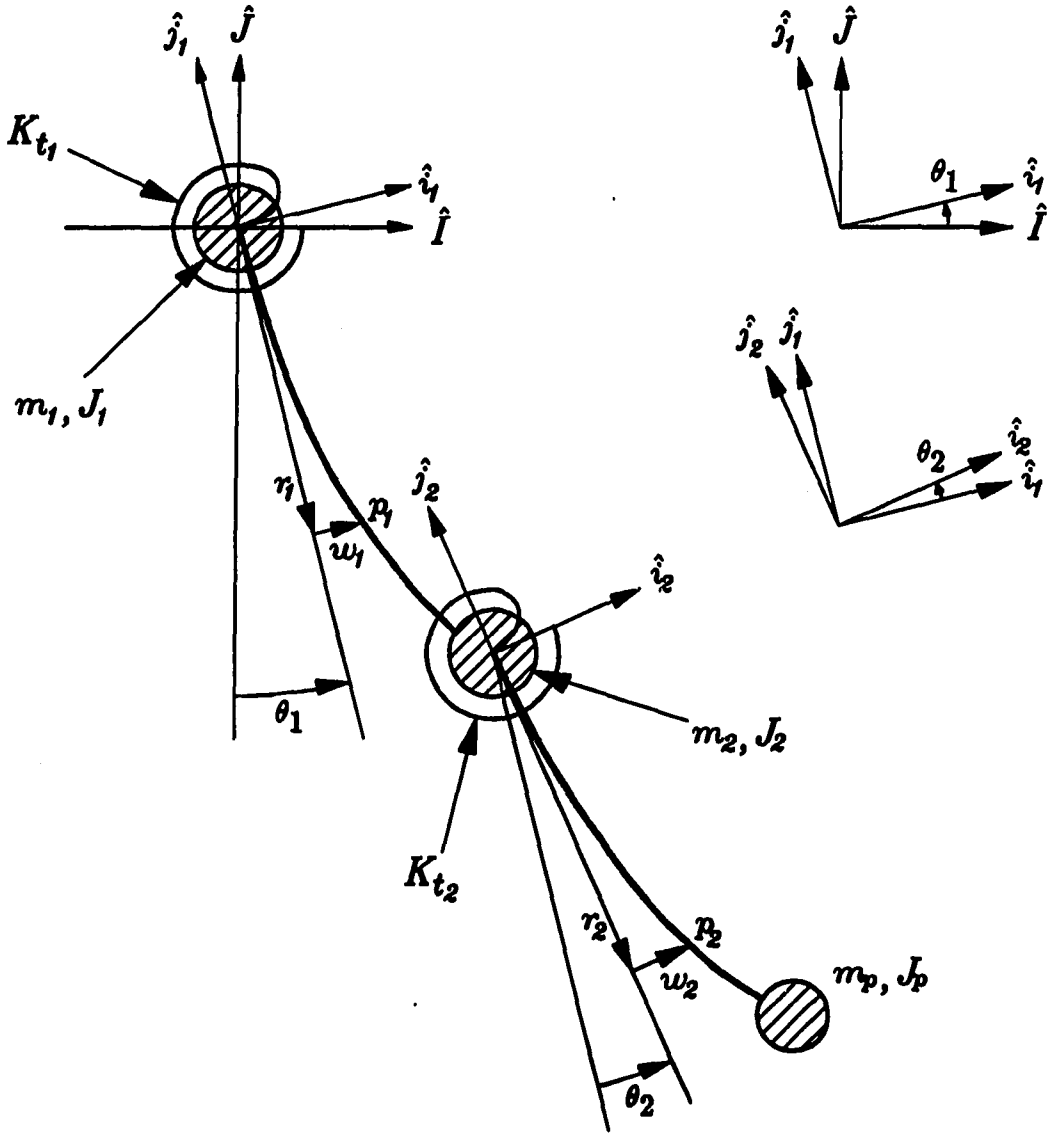

Figure 3.1: A schematic diagram of the elastic robot system

are neglected. Therefore, the elastic arms are modeled as Euler-Bernoulli beams. It is assumed that there is no twist in each arm. The elastic arms are assumed to have homogeneous material properties and constant cross sectional areas with densities ρ_1 and ρ_2, flexural rigidities or bending moduli $(EI)_1$ and $(EI)_2$, and cross sectional areas A_1 and A_2. Friction at the joints is not included in the model. Structural damping of elastic arms is neglected.

One global $(\hat{I}\hat{J}\hat{k})$ and two local coordinate systems are defined. One local coordinate system $(\hat{\imath}_1\hat{\jmath}_1\hat{k})$ is fixed to the upper arm at the first rotational joint and rotates with respect to the global coordinate system. The second local coordinate system $(\hat{\imath}_2\hat{\jmath}_2\hat{k})$ is attached to the lower arm at the second rotational joint and rotates with respect to the upper arm. The angle θ_2 represents the rigid motion of the lower arm with respect to the upper local coordinate system $(\hat{\imath}_1\hat{\jmath}_1\hat{k})$. The transformation matrix from the first local coordinate system $(\hat{\imath}_1\hat{\jmath}_1\hat{k})$ to the second local coordinate system $(\hat{\imath}_2\hat{\jmath}_2\hat{k})$ is defined in Equation 3.1 as

$$\begin{Bmatrix} \hat{\imath}_2 \\ \hat{\jmath}_2 \end{Bmatrix} = \begin{bmatrix} cos\theta_2 & sin\theta_2 \\ -sin\theta_2 & cos\theta_2 \end{bmatrix} \begin{Bmatrix} \hat{\imath}_1 \\ \hat{\jmath}_1 \end{Bmatrix} \tag{3.1}$$

The angle θ_1 represents the rigid motion of the upper arm with respect to the global coordinate system. The transformation matrix from the global coordinate system $(\hat{I}\hat{J}\hat{k})$ to the first local coordinate system $(\hat{\imath}_1\hat{\jmath}_1\hat{k})$ is similarly defined in Equation 3.2.

$$\begin{Bmatrix} \hat{\imath}_1 \\ \hat{\jmath}_1 \end{Bmatrix} = \begin{bmatrix} cos\theta_1 & sin\theta_1 \\ -sin\theta_1 & cos\theta_1 \end{bmatrix} \begin{Bmatrix} \hat{I} \\ \hat{J} \end{Bmatrix} \tag{3.2}$$

The global motion of the arms is composed of rigid motion and elastic motion. Elastic motions of each arm are represented in the local coordinate systems as shown in

Figure 3.1 and given by

$$\vec{p}_1 = w_1\hat{i}_1 - r_1\hat{j}_1 \tag{3.3}$$

$$\vec{p}_2 = w_2\hat{i}_2 - r_2\hat{j}_2 \tag{3.4}$$

where w_1 is an elastic deflection at a point p_1 on the upper arm along the local coordinate $\hat{i}_1$ and w_2 is an elastic deflection at a point p_2 on the lower arm along the local coordinate $\hat{i}_2$.

3.2 Equations of Motion

This section derives the equations of motion for the elastic two arms robot using two different methods. The equations are derived for the continuous model using the extended Hamilton's principle. Discrete equations are generated using the assumed modes method. Both schemes require kinetic and potential energy expressions which are developed in the following two sections.

3.2.1 Kinetic Energy

The angular velocities for mass m_1, m_a, m_b, and m_p are found using the addition theorem of angular velocity.

$$\vec{\omega}_{m_1} = \dot{\theta}_1\hat{k} \tag{3.5}$$

$$\vec{\omega}_1 = \dot{\theta}_1\hat{k} \tag{3.6}$$

$$\vec{\omega}_{m_a} = \dot{\theta}_1\hat{k} + \left(\dot{w}\right)'_{\ell_1}\hat{k} \tag{3.7}$$

$$\vec{\omega}_{m_b} = \dot{\theta}_1\hat{k} + \dot{\theta}_2\hat{k} \tag{3.8}$$

$$\vec{\omega}_2 = \dot{\theta}_1\hat{k} + \dot{\theta}_2\hat{k} \tag{3.9}$$

$$\vec{\omega}_{m_p} = \dot{\theta}_1\hat{k} + \dot{\theta}_2\hat{k} + (\dot{w})'_{\ell_2}\hat{k} \tag{3.10}$$

Where $(\dot{w})'_{\ell_1}$ and $(\dot{w})'_{\ell_2}$ are the angular velocities due to the flexible deformations of the end masses at the end of each arm. The linear velocity at a point on the upper arm is given by

$$\vec{V}_{p_1} = (\vec{\omega}_1 \times \vec{p}_1) + \dot{w}_1\hat{i}_1 \tag{3.11}$$

Substituting Equations 3.6 and 3.3, and performing the vector cross product, the velocity in the local coordinate system $(\hat{i}_1\hat{j}_1\hat{k})$ is given by

$$\vec{V}_{p_1} = (r_1\dot{\theta}_1 + \dot{w}_1)\,\hat{i}_1 + (w_1\dot{\theta}_1)\,\hat{j}_1 \tag{3.12}$$

The velocity at the second joint is defined as

$$\vec{V}_{\ell_1} = (\ell_1\dot{\theta}_1 + \dot{w}_{\ell_1})\,\hat{i}_1 + (w_{\ell_1}\dot{\theta}_1)\,\hat{j}_1 \tag{3.13}$$

Similarly, the velocity at a point on the lower arm is found by adding the velocity $\vec{V}_{\ell_1}$ of the origin of the local coordinate system $(\hat{i}_2\hat{j}_2\hat{k})$ and the velocity of a point on the second arm with respect to that local coordinate system.

$$\vec{V}_{p_2} = \vec{V}_{\ell_1} + \vec{\omega}_2 \times \vec{p}_2 + \dot{w}_2\hat{i}_2 \tag{3.14}$$

Substituting Equations 3.13, 3.9 and 3.4 and using the transformation defined in Equation 3.1 yields the expression for the velocity of a point on the lower arm in the local $(\hat{i}_1\hat{j}_1\hat{k})$ coordinate system.

$$\begin{aligned}\vec{V}_{p_2} = {} & \left\{\ell_1\dot{\theta}_1 + \dot{w}_{\ell_1} - (\dot{\theta}_1 + \dot{\theta}_2)(w_2 sin\theta_2 - r_2 cos\theta_2) + \dot{w}_2 cos\theta_2\right\}\hat{i}_1 \\ & + \left\{w_{\ell_1}\dot{\theta}_1 + (\dot{\theta}_1 + \dot{\theta}_2)(r_2 sin\theta_2 + w_2 cos\theta_2) + \dot{w}_2 sin\theta_2\right\}\hat{j}_1\end{aligned} \tag{3.15}$$

The velocity at the end of the lower arm is found by substituting ℓ_2 for r_2 in Equation 3.15.

$$\begin{aligned}\vec{V}_{\ell_2} &= \left\{\ell_1\dot{\theta}_1 + \dot{w}_{\ell_1} - \left(\dot{\theta}_1+\dot{\theta}_2\right)\left(w_{\ell_2}sin\theta_2 - \ell_2 cos\theta_2\right) + \dot{w}_{\ell_2}cos\theta_2\right\}\hat{\imath}_1 \\ &+ \left\{w_{\ell_1}\dot{\theta}_1 + \left(\dot{\theta}_1+\dot{\theta}_2\right)\left(\ell_2 sin\theta_2 + w_{\ell_2}cos\theta_2\right) + \dot{w}_{\ell_2}sin\theta_2\right\}\hat{\jmath}_1\end{aligned} \tag{3.16}$$

The mass m_1 has no translational motion, therefore the kinetic energy for mass m_1 is

$$T_{m_1} = \frac{1}{2}J_1\left(\dot{\theta}_1\right)^2. \tag{3.17}$$

The kinetic energy of the upper arm is given by

$$T_1 = \frac{1}{2}\int_0^{\ell_1}\left(\vec{V}_{p1}\cdot\vec{V}_{p1}\right)dm_1 \tag{3.18}$$

where $dm_1 = (\rho A)_1 dr_1$. Substituting Equation 3.12, and performing the vector dot product, the kinetic energy for the upper arm is given by

$$T_1 = \frac{1}{2}\int_0^{\ell_1}(\rho A)_1\left[\left(r_1\dot{\theta}_1\right)^2 + 2r_1\dot{\theta}_1\dot{w}_1 + (\dot{w}_1)^2 + \left(w_1\dot{\theta}_1\right)^2\right]dr_1 \tag{3.19}$$

The mass m_a undergoes both rotational and translational motion. The kinetic energy for mass m_a is given by

$$T_{ma} = \frac{1}{2}m_a\left(\vec{V}_{\ell_1}\cdot\vec{V}_{\ell_1}\right) + \frac{1}{2}J_a\left(\vec{\omega}_{ma}\cdot\vec{\omega}_{ma}\right) \tag{3.20}$$

Substituting Equations 3.13 and 3.7 and performing the vector dot products yields the kinetic energy for mass m_a as

$$\begin{aligned}T_{ma} &= \frac{1}{2}m_a\left[\left(\ell_1\dot{\theta}_1\right)^2 + 2\ell_1\dot{\theta}_1\dot{w}_{\ell_1} + \left(\dot{w}_{\ell_1}\right)^2 + \left(w_{\ell_1}\dot{\theta}_1\right)^2\right] \\ &+ \frac{1}{2}J_a\left(\dot{\theta}_1 + \dot{w}'_{\ell_1}\right)^2\end{aligned} \tag{3.21}$$

Similarly, the kinetic energy for mass m_b is given by

$$T_{m_b} = \frac{1}{2}m_b\left(\vec{V}_{\ell_1}\cdot\vec{V}_{\ell_1}\right)+\frac{1}{2}J_b\left(\vec{\omega}_{m_b}\cdot\vec{\omega}_{m_b}\right) \tag{3.22}$$

$$\begin{aligned} T_{m_b} &= \frac{1}{2}m_b\left[\left(\ell_1\dot{\theta}_1\right)^2+2\ell_1\dot{\theta}_1\dot{w}_{\ell_1}+\left(\dot{w}_{\ell_1}\right)^2+\left(w_{\ell_1}\dot{\theta}_1\right)^2\right] \\ &\quad +\frac{1}{2}J_b\left(\dot{\theta}_1+\dot{\theta}_2\right)^2 \end{aligned} \tag{3.23}$$

The kinetic energy for the lower arm is given by

$$T_2=\frac{1}{2}\int_0^{\ell_2}\left(\vec{V}_{p_2}\cdot\vec{V}_{p_2}\right)dm_2 \tag{3.24}$$

where $dm_2=(\rho A)_2 dr_2$. Substituting Equation 3.15 and performing the vector dot product, the kinetic energy for the lower arm is given by

$$\begin{aligned} T_2 &= \frac{1}{2}\int_0^{\ell_2}(\rho A)_2\left[\left(\ell_1\dot{\theta}_1\right)^2+2\ell_1\dot{\theta}_1\dot{w}_{\ell_1}+(\dot{w}_2)^2\right. \\ &\quad +\left(\dot{w}_{\ell_1}\right)^2+\left(w_{\ell_1}\dot{\theta}_1\right)^2+2\dot{w}_{\ell_1}\dot{w}_2 cos\theta_2+2\ell_1\dot{\theta}_1\dot{w}_2 cos\theta_2 \\ &\quad +2w_{\ell_1}\dot{\theta}_1\dot{w}_2 sin\theta_2+\left(\dot{\theta}_1+\dot{\theta}_2\right)^2\left(w_2^2+r_2^2\right) \\ &\quad +2\left(\dot{\theta}_1+\dot{\theta}_2\right)\left\{\dot{w}_2 r_2+\left(\ell_1\dot{\theta}_1+\dot{w}_{\ell_1}\right)\left(r_2 cos\theta_2-w_2 sin\theta_2\right)\right. \\ &\quad \left.\left.+w_{\ell_1}\dot{\theta}_1\left(r_2 sin\theta_2+w_2 cos\theta_2\right)\right\}\right]dr_2 \end{aligned} \tag{3.25}$$

The kinetic energy for the end mass m_p is defined as

$$T_{m_p}=\frac{1}{2}m_p\left(\vec{V}_{\ell_2}\cdot\vec{V}_{\ell_2}\right)+\frac{1}{2}J_p\left(\vec{\omega}_{m_p}\cdot\vec{\omega}_{m_p}\right) \tag{3.26}$$

Substituting Equations 3.16 and 3.10 into Equation 3.26 and performing the vector dot products yields the kinetic energy for mass m_p.

$$\begin{aligned} T_{m_p} &= \frac{1}{2}m_p\left[2\ell_1\dot{\theta}_1\dot{w}_{\ell_1}+2\dot{w}_{\ell_1}\dot{w}_{\ell_2}cos\theta_2+2\ell_1\dot{\theta}_1\dot{w}_{\ell_2}cos\theta_2\right. \\ &\quad \left.+\left(\ell_1\dot{\theta}_1\right)^2+\left(\dot{w}_{\ell_2}\right)^2+\left(\dot{w}_{\ell_1}\right)^2+\left(w_{\ell_1}\dot{\theta}_1\right)^2\right. \end{aligned} \tag{3.27}$$

$$
\begin{aligned}
&+2w_{\ell_1}\dot{\theta}_1\dot{w}_{\ell_2}sin\theta_2+\left(\dot{\theta}_1+\dot{\theta}_2\right)^2\left(w_{\ell_2}^2+\ell_2^2\right)\\
&+2\left(\dot{\theta}_1+\dot{\theta}_2\right)\left\{\dot{w}_{\ell_2}\ell_2+\left(\ell_1\dot{\theta}_1+\dot{w}_{\ell_1}\right)\left(\ell_2cos\theta_2-w_{\ell_2}sin\theta_2\right)\right.\\
&\qquad\left.+w_{\ell_1}\dot{\theta}_1\left(\ell_2sin\theta_2+w_{\ell_2}cos\theta_2\right)\right\}\Big]\\
&+\frac{1}{2}J_p\left(\dot{\theta}_1+\dot{\theta}_1+\dot{w}'_{\ell_2}\right)^2
\end{aligned}
$$

The total kinetic energy for the system is the sum of all the kinetic energy terms.

$$T = T_{m_1}+T_1+T_{m_a}+T_{m_b}+T_2+T_{m_p} \tag{3.28}$$

$$
\begin{aligned}
T = \;& \frac{1}{2}J_1\left(\dot{\theta}_1\right)^2 \qquad (3.29)\\
&+\frac{1}{2}\int_0^{\ell_1}(\rho A)_1\left[\left(r_1\dot{\theta}_1\right)^2+2r_1\dot{\theta}_1\dot{w}_1+\left(\dot{w}_1\right)^2+\left(w_1\dot{\theta}_1\right)^2\right]dr_1\\
&+\frac{1}{2}m_a\left[\left(\ell_1\dot{\theta}_1\right)^2+2\ell_1\dot{\theta}_1\dot{w}_{\ell_1}+\left(\dot{w}_{\ell_1}\right)^2+\left(w_{\ell_1}\dot{\theta}_1\right)^2\right]\\
&+\frac{1}{2}J_a\left(\dot{\theta}_1+\dot{w}'_{\ell_1}\right)^2\\
&+\frac{1}{2}m_b\left[\left(\ell_1\dot{\theta}_1\right)^2+2\ell_1\dot{\theta}_1\dot{w}_{\ell_1}+\left(\dot{w}_{\ell_1}\right)^2+\left(w_{\ell_1}\dot{\theta}_1\right)^2\right]\\
&+\frac{1}{2}J_b\left(\dot{\theta}_1+\dot{\theta}_2\right)^2\\
&+\frac{1}{2}\int_0^{\ell_2}(\rho A)_2\left[\left(\ell_1\dot{\theta}_1\right)^2+2\ell_1\dot{\theta}_1\dot{w}_{\ell_1}+\left(\dot{w}_2\right)^2\right.\\
&\quad+\left(\dot{w}_{\ell_1}\right)^2+\left(w_{\ell_1}\dot{\theta}_1\right)^2+2\dot{w}_{\ell_1}\dot{w}_2cos\theta_2+2\ell_1\dot{\theta}_1\dot{w}_2cos\theta_2\\
&\quad+2w_{\ell_1}\dot{\theta}_1\dot{w}_2sin\theta_2+\left(\dot{\theta}_1+\dot{\theta}_2\right)^2\left(w_2^2+r_2^2\right)\\
&\quad+2\left(\dot{\theta}_1+\dot{\theta}_2\right)\left\{\dot{w}_2r_2+\left(\ell_1\dot{\theta}_1+\dot{w}_{\ell_1}\right)\left(r_2cos\theta_2-w_2sin\theta_2\right)\right.\\
&\qquad\left.\left.+w_{\ell_1}\dot{\theta}_1\left(r_2sin\theta_2+w_2cos\theta_2\right)\right\}\right]dr_2\\
&+\frac{1}{2}m_p\left[2\ell_1\dot{\theta}_1\dot{w}_{\ell_1}+2\dot{w}_{\ell_1}\dot{w}_{\ell_2}cos\theta_2+2\ell_1\dot{\theta}_1\dot{w}_{\ell_2}cos\theta_2\right.\\
&\quad\left.+\left(\ell_1\dot{\theta}_1\right)^2+\left(\dot{w}_{\ell_2}\right)^2+\left(\dot{w}_{\ell_1}\right)^2+\left(w_{\ell_1}\dot{\theta}_1\right)^2\right.
\end{aligned}
$$

$$+2w_{\ell_1}\dot{\theta}_1\dot{w}_{\ell_2}sin\theta_2+\left(\dot{\theta}_1+\dot{\theta}_2\right)^2\left(w_{\ell_2}^2+\ell_2^2\right)$$
$$+2\left(\dot{\theta}_1+\dot{\theta}_2\right)\left\{\dot{w}_{\ell_2}\ell_2+\left(\ell_1\dot{\theta}_1+\dot{w}_{\ell_1}\right)\left(\ell_2cos\theta_2-w_{\ell_2}sin\theta_2\right)\right.$$
$$\left.+w_{\ell_1}\dot{\theta}_1\left(\ell_2sin\theta_2+w_{\ell_2}cos\theta_2\right)\right\}\Big]$$
$$+\frac{1}{2}J_p\left(\dot{\theta}_1+\dot{\theta}_2+\dot{w}'_{\ell_2}\right)^2$$

3.2.2 Potential Energy

Potential energy is stored by the gravitational field, in the torsional springs, and in elastic deformations of the flexible arms. The potential energy from the torsional springs is given by

$$\Pi_1=\frac{1}{2}K_{t_1}\theta_1^2+\frac{1}{2}K_{t_2}\left[\left(\frac{\partial w_1}{\partial r_1}\right)_{r_1=\ell_1}-\theta_2\right]^2 \tag{3.30}$$

Using the coordinate transforms, the global coordinate of a point on the upper arm is expressed by

$$\vec{p}_1=\left(w_1cos\theta_1+r_1sin\theta_1\right)\hat{I}+\left(w_1sin\theta_1-r_1cos\theta_1\right)\hat{J} \tag{3.31}$$

The global coordinate at the lower end of the upper arm is found by substituting ℓ_1 for r_1.

$$\vec{p}_{\ell_1}=\left(w_{\ell_1}cos\theta_1+\ell_1sin\theta_1\right)\hat{I}+\left(w_{\ell_1}sin\theta_1-\ell_1cos\theta_1\right)\hat{J} \tag{3.32}$$

Similarly, the global coordinates of a point on the lower arm and at the end of the lower arm are given by

$$\vec{p}_2 = \Big[\left(w_{\ell_1}cos\theta_1+\ell_1sin\theta_1\right)+\left(w_2cos\theta_2+r_2sin\theta_2\right)cos\theta_1 \tag{3.33}$$
$$-\left(w_2sin\theta_2-r_2cos\theta_2\right)sin\theta_1\Big]\hat{I}$$

$$+\Big[\Big(w_{\ell_1}sin\theta_1 - \ell_1 cos\theta_1\Big) + \Big(w_2 cos\theta_2 + r_2 sin\theta_2\Big)sin\theta_1$$
$$+\Big(w_2 sin\theta_2 - r_2 cos\theta_2\Big)cos\theta_1\Big]\hat{J}$$

$$\vec{p}_{\ell_2} = \Big[\Big(w_{\ell_1}cos\theta_1 + \ell_1 sin\theta_1\Big) + \Big(w_{\ell_2}cos\theta_2 + \ell_2 sin\theta_2\Big)cos\theta_1 \qquad (3.34)$$
$$-\Big(w_{\ell_2}sin\theta_2 - \ell_2 cos\theta_2\Big)sin\theta_1\Big]\hat{I}$$
$$+\Big[\Big(w_{\ell_1}sin\theta_1 - \ell_1 cos\theta_1\Big) + \Big(w_{\ell_2}cos\theta_2 + \ell_2 sin\theta_2\Big)sin\theta_1$$
$$+\Big(w_{\ell_2}sin\theta_2 - \ell_2 cos\theta_2\Big)cos\theta_1\Big]\hat{J}$$

The global coordinate axis $\hat{I}$ is set as the reference for the potential energy due to gravity. The potential energy of two elastic arms due to gravity is given by

$$\Pi_2 = \int_0^{\ell_1}(\rho A)_1 g\Big(w_1 sin\theta_1 - r_1 cos\theta_1\Big)\,dr_1 \qquad (3.35)$$
$$+\int_0^{\ell_2}(\rho A)_2 g\Big[w_{\ell_1}sin\theta_1 - \ell_1 cos\theta_1 + \Big(w_2 cos\theta_2 + r_2 sin\theta_2\Big)sin\theta_1$$
$$+\Big(w_2 sin\theta_2 - r_2 cos\theta_2\Big)cos\theta_1\Big]\,dr_2$$

The potential energy due to gravity of mass $m_2(= m_a + m_b)$ and mass m_p is given by

$$\Pi_3 = m_2 g\Big(w_{\ell_1}sin\theta_1 - \ell_1 cos\theta_1\Big) \qquad (3.36)$$
$$+m_p g\Big[\Big(w_{\ell_1}sin\theta_1 - \ell_1 cos\theta_1\Big) + \Big(w_{\ell_2}cos\theta_2 + \ell_2 sin\theta_2\Big)sin\theta_1$$
$$+\Big(w_{\ell_2}sin\theta_2 - \ell_2 cos\theta_2\Big)cos\theta_1\Big]$$

The potential energy due to elastic deformations of the upper and lower arms is defined as

$$\Pi_4 = \frac{1}{2}\int_0^{\ell_1}(EI)_1\left(w_1''\right)^2 dr_1 + \frac{1}{2}\int_0^{\ell_2}(EI)_2\left(w_2''\right)^2 dr_2 \qquad (3.37)$$

3.2.2.1 The Shortening Effect Figure 3.2 shows the shortening effect of the arm due to elastic deflection. If there is elastic deflection in the arm, it is not valid to assume that the location of a point p on the arm in the local coordinate $\hat{j}$ is the same as the distance along the arm to point p. The length of a small section of the deflected arm (ds) is given by

$$ds^2 = dr^2 + dw^2 \tag{3.38}$$

$$ds = \left[1 + \left(\frac{dw}{dr}\right)^2\right]^{\frac{1}{2}} dr \tag{3.39}$$

where dw is the deflection of a small section dr along the local coordinate $\hat{\imath}$. For a given point p, its distance from the hub along the arm is given by

$$s = \int_0^{r-h} \left[1 + \left(\frac{dw}{dr}\right)^2\right]^{\frac{1}{2}} dr \tag{3.40}$$

where h indicates the shortened length of the local $\hat{j}$ coordinate of the point p. The square bracket term in Equation 3.40 is expanded using a binomial series and all but the first two terms are assumed to be negligible. The $\hat{j}$ component of the arm at the point p is approximately

$$s \cong \int_0^{r-h} \left[1 + \frac{1}{2}\left(\frac{dw}{dr}\right)^2\right] dr \tag{3.41}$$

Note that $s = r$ from Figure 3.2.

$$r = (r-h) + \int_0^{r-h} \frac{1}{2}\left(\frac{dw}{dr}\right)^2 dr \tag{3.42}$$

The reduction in the local $\hat{j}$ coordinate due to deformation for the point p is given as

$$h \cong \int_0^{r-h} \frac{1}{2}\left(\frac{dw}{dr}\right)^2 dr \tag{3.43}$$

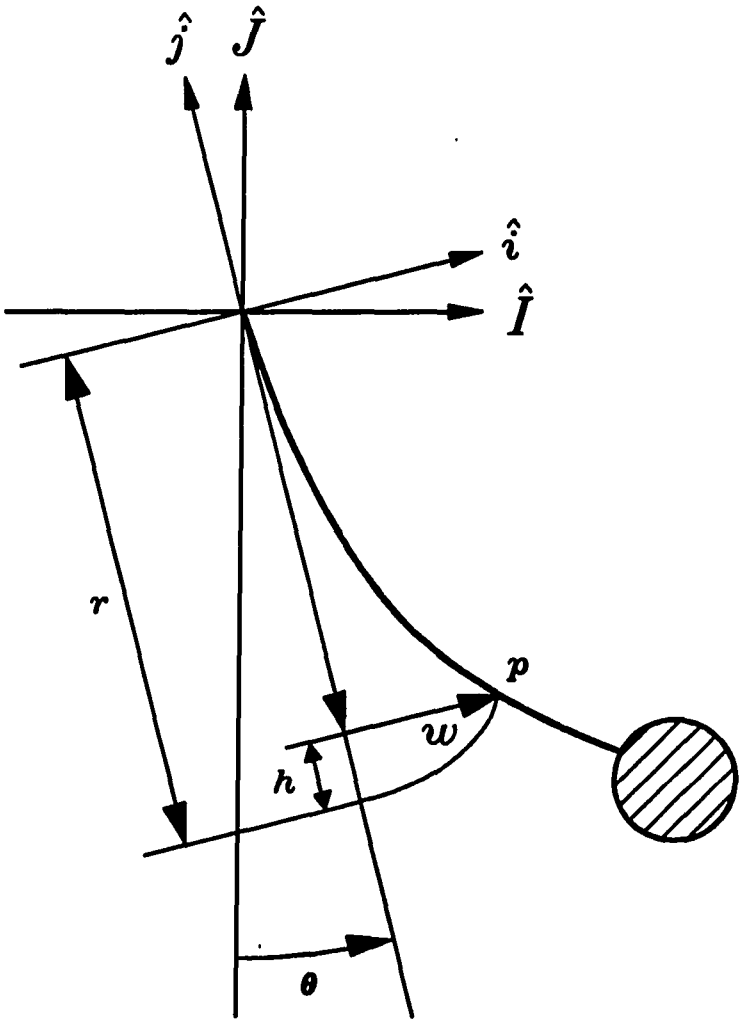

Figure 3.2: A schematic diagram to show the shortening effect

In Equation 3.43, the upper limit of the integral is approximated as r. Then, Equation 3.43 is represented as

$$h \cong \int_0^r \frac{1}{2}\left(\frac{dw}{dr}\right)^2 dr \tag{3.44}$$

Thus, the location of the point p in the local $\hat{j}$ coordinate is given as $\left(-r+h\right)$.

It is necessary to consider the shortening effect when deriving the kinetic energy. The shortening effect appears in kinetic energy in two forms. One is in the velocities along the local axes $\hat{i}_1$ and $\hat{i}_2$ because the radius for calculating the tangential velocity is reduced. The other is in the velocities along the local axes $\hat{j}_1$ and $\hat{j}_2$ because the shortening of the arm requires a velocity along the length of the arm ($\dot{h}$). If a system is operated about a vertical position, the shortening effect is small in kinetic energy. Thus, all kinetic energy terms from the shortening effect disappear during the linearization process. However, when the system is operated off of vertical position, the shortening terms will remain in the linearization.

The shortening effect is also considered in the calculation of potential energy due to gravity. Considering the shortening effect in Equations 3.35 and 3.36 yields the following two equations for potential energy.

$$\begin{aligned}
\left[\Pi_2\right]_s \;=\; & \int_0^{\ell_1} (\rho A)_1 g\left(w_1 sin\theta_1 - r_1 cos\theta_1\right) dr_1 \\
& + \frac{1}{2}\int_0^{\ell_1} (\rho A)_1 g\left[cos\theta_1 \int_0^{r_1} \left(w_1'\right)^2 d\xi_1\right] dr_1 \\
& + \int_0^{\ell_2} (\rho A)_2 g\Big[w_{\ell_1} sin\theta_1 - \ell_1 cos\theta_1 + \left(w_2 cos\theta_2 + r_2 sin\theta_2\right) sin\theta_1 \\
& \qquad + \left(w_2 sin\theta_2 - r_2 cos\theta_2\right) cos\theta_1\Big] dr_2 \\
& + \frac{1}{2}\int_0^{\ell_2} (\rho A)_2 g\left[cos\theta_1 \int_0^{\ell_1} \left(w_1'\right)^2 dr_1\right] dr_2
\end{aligned} \tag{3.45}$$

$$
\begin{aligned}
&+\frac{1}{2}\int_0^{\ell_2}(\rho A)_2 g\left[\left(-sin\theta_2 sin\theta_1+cos\theta_2 cos\theta_1\right)\int_0^{r_2}\left(w_2'\right)^2\,d\xi_2\right]dr_2\\
\left[\Pi_3\right]_s &= m_2 g\left(w_{\ell_1}sin\theta_1-\ell_1 cos\theta_1\right) \qquad (3.46)\\
&+\frac{1}{2}m_2 g cos\theta_1\int_0^{\ell_1}\left(w_1'\right)^2\,dr_1\\
&+m_p g\Big[\left(w_{\ell_1}sin\theta_1-\ell_1 cos\theta_1\right)+\left(w_{\ell_2}cos\theta_2+\ell_2 sin\theta_2\right)sin\theta_1\\
&\qquad+\left(w_{\ell_2}sin\theta_2-\ell_2 cos\theta_2\right)cos\theta_1\Big]\\
&+\frac{1}{2}m_p g cos\theta_1\int_0^{\ell_1}\left(w_1'\right)^2\,dr_1\\
&+\frac{1}{2}m_p g\left(-sin\theta_2 sin\theta_1+cos\theta_2 cos\theta_1\right)\int_0^{\ell_2}\left(w_2'\right)^2\,dr_2
\end{aligned}
$$

3.2.2.2 Total Potential Energy The total potential energy including the shortening effect is the sum of all potential energy terms and is given by

$$\Pi = \Pi_1+\left[\Pi_2\right]_s+\left[\Pi_3\right]_s+\Pi_4 \qquad (3.47)$$

$$
\begin{aligned}
\Pi &= \frac{1}{2}K_{t_1}\theta_1^2+\frac{1}{2}K_{t_2}\left[\left(\frac{\partial w_1}{\partial r_1}\right)_{r_1=\ell_1}-\theta_2\right]^2 \qquad (3.48)\\
&+\int_0^{\ell_1}(\rho A)_1 g\left(w_1 sin\theta_1-r_1 cos\theta_1\right)dr_1\\
&+\frac{1}{2}\int_0^{\ell_1}(\rho A)_1 g\left[cos\theta_1\int_0^{r_1}\left(w_1'\right)^2 d\xi_1\right]dr_1\\
&+\int_0^{\ell_2}(\rho A)_2 g\Big[w_{\ell_1}sin\theta_1-\ell_1 cos\theta_1+\left(w_2 cos\theta_2+r_2 sin\theta_2\right)sin\theta_1\\
&\qquad+\left(w_2 sin\theta_2-r_2 cos\theta_2\right)cos\theta_1\Big]\,dr_2\\
&+\frac{1}{2}\int_0^{\ell_2}(\rho A)_2 g\left[cos\theta_1\int_0^{\ell_1}\left(w_1'\right)^2\,dr_1\right]dr_2\\
&+\frac{1}{2}\int_0^{\ell_2}(\rho A)_2 g\left[\left(-sin\theta_2 sin\theta_1+cos\theta_2 cos\theta_1\right)\int_0^{r_2}\left(w_2'\right)^2\,d\xi_2\right]dr_2\\
&+m_2 g\left(w_{\ell_1}sin\theta_1-\ell_1 cos\theta_1\right)
\end{aligned}
$$

$$+\frac{1}{2}m_2 g cos\theta_1 \int_0^{\ell_1} \left(w_1'\right)^2 \, dr_1$$
$$+m_p g\Big[\Big(w_{\ell_1} sin\theta_1 - \ell_1 cos\theta_1\Big) + \Big(w_{\ell_2} cos\theta_2 + \ell_2 sin\theta_2\Big) sin\theta_1$$
$$+\Big(w_{\ell_2} sin\theta_2 - \ell_2 cos\theta_2\Big) cos\theta_1\Big]$$
$$+\frac{1}{2}m_p g cos\theta_1 \int_0^{\ell_1} \left(w_1'\right)^2 \, dr_1$$
$$+\frac{1}{2}m_p g\big(-sin\theta_2 sin\theta_1 + cos\theta_2 cos\theta_1\big) \int_0^{\ell_2} \left(w_2'\right)^2 \, dr_2$$
$$+\frac{1}{2}\int_0^{\ell_1} (EI)_1 \left(w_1''\right)^2 dr_1 + \frac{1}{2}\int_0^{\ell_2} (EI)_2 \left(w_2''\right)^2 dr_2$$

3.2.3 Equations of Motion by the Extended Hamilton's Principle

This section derives the equations of motion for the continuous model of the two-elastic-arm robot system using the extended Hamilton's principle. The extended Hamilton's principle is developed based on D'Alambert's principle.

The extended Hamilton's principle is mathematically stated as

$$\int_{t_1}^{t_2} \big(\delta L + \delta W_{nc}\big) \, dt = 0 \tag{3.49}$$

where L is the Lagrangian ($L = T - \Pi$), T is the total kinetic energy, Π is the total potential energy, and W_{nc} is the work done by nonconservative forces.

If there is no work done by nonconservative force, the extended Hamilton's principle becomes Hamilton's principle, and it is mathematically defined as

$$\int_{t_1}^{t_2} \delta\big(T - \Pi\big) \, dt = 0 \tag{3.50}$$

In the following derivation of the equations of motion and their boundary conditions, it is assumed that all boundary terms evaluated at initial and final time, t_1 and t_2, are eliminated. That means that the true(actual) and varied paths coincide at initial and final time.

The Lagrangian L is decomposed into three parts for the convenience of derivation,

$$L = L_1 + L_2 + L_3 \tag{3.51}$$

where the first term L_1 is the collection of all terms which do not contain any integral signs, the second term L_2 is the collection of all terms integrated along the upper arm, and the last term L_3 is the collection of all terms integrated along the lower arm.

L_1 is implicitly defined as follow.

$$L_1 = L_1\left(\theta_1, \theta_2, \dot{\theta}_1, \dot{\theta}_2, w_{\ell_1}, w_{\ell_2}, w'_{\ell_1}, \dot{w}_{\ell_1}, \dot{w}_{\ell_2}, \dot{w}'_{\ell_1}, \dot{w}'_{\ell_2}\right) \tag{3.52}$$

The variational expression of L_1 is given by

$$\begin{aligned}\delta L_1 \;=\; & \frac{\partial L_1}{\partial \theta_1}\delta\theta_1 + \frac{\partial L_1}{\partial \theta_2}\delta\theta_2 + \frac{\partial L_1}{\partial \dot{\theta}_1}\delta\dot{\theta}_1 + \frac{\partial L_1}{\partial \dot{\theta}_2}\delta\dot{\theta}_2 + \frac{\partial L_1}{\partial w_{\ell_1}}\delta w_{\ell_1} \\ & + \frac{\partial L_1}{\partial w_{\ell_2}}\delta w_{\ell_2} + \frac{\partial L_1}{\partial w'_{\ell_1}}\delta w'_{\ell_1} + \frac{\partial L_1}{\partial \dot{w}_{\ell_1}}\delta \dot{w}_{\ell_1} + \frac{\partial L_1}{\partial \dot{w}_{\ell_2}}\delta \dot{w}_{\ell_2} \\ & + \frac{\partial L_1}{\partial \dot{w}'_{\ell_1}}\delta \dot{w}'_{\ell_1} + \frac{\partial L_1}{\partial \dot{w}'_{\ell_2}}\delta \dot{w}'_{\ell_2}.\end{aligned} \tag{3.53}$$

Expanding terms using integration by parts, the time integration of δL_1 is given by

$$\begin{aligned}\int_{t_1}^{t_2} \delta L_1 dt \;=\; & \int_{t_1}^{t_2}\left\{\left[\frac{\partial L_1}{\partial \theta_1} - \frac{d}{dt}\left(\frac{\partial L_1}{\partial \dot{\theta}_1}\right)\right]\delta\theta_1 + \left[\frac{\partial L_1}{\partial \theta_2} - \frac{d}{dt}\left(\frac{\partial L_1}{\partial \dot{\theta}_2}\right)\right]\delta\theta_2\right. \\ & + \left[\frac{\partial L_1}{\partial w_{\ell_1}} - \frac{d}{dt}\left(\frac{\partial L_1}{\partial \dot{w}_{\ell_1}}\right)\right]\delta w_{\ell_1} + \left[\frac{\partial L_1}{\partial w_{\ell_2}} - \frac{d}{dt}\left(\frac{\partial L_1}{\partial \dot{w}_{\ell_2}}\right)\right]\delta w_{\ell_2} \\ & \left. + \left[\frac{\partial L_1}{\partial w'_{\ell_1}} - \frac{d}{dt}\left(\frac{\partial L_1}{\partial \dot{w}'_{\ell_1}}\right)\right]\delta w'_{\ell_1} + \left[-\frac{d}{dt}\left(\frac{\partial L_1}{\partial \dot{w}'_{\ell_2}}\right)\right]\delta w'_{\ell_2}\right\} dt\end{aligned} \tag{3.54}$$

L_2 is implicitly defined as follow.

$$L_2 = \int_0^{\ell_1} g\left(\theta_1, \dot{\theta}_1, w_1, \dot{w}_1, w'_1, w''_1\right) dr_1 \tag{3.55}$$

The variational expression of L_2 is given by

$$\delta L_2 = \int_0^{\ell_1} \left[\frac{\partial g}{\partial \theta_1}\delta\theta_1 + \frac{\partial g}{\partial \dot{\theta}_1}\delta\dot{\theta}_1 + \frac{\partial g}{\partial w_1}\delta w_1 + \frac{\partial g}{\partial \dot{w}_1}\delta\dot{w}_1 + \frac{\partial g}{\partial w_1'}\delta w_1' + \frac{\partial g}{\partial w_1''}\delta w_1'' \right] dr_1 \tag{3.56}$$

Expanding terms using integration by parts, the time integration of δL_2 is given by

$$\begin{aligned} \int_{t_1}^{t_2} \delta L_2 dt = & \int_{t_1}^{t_2} \left\{ \left[\frac{\partial g}{\partial w_1''}\delta w_1' \right]_0^{\ell_1} \right. \\ & \left. + \left[\frac{\partial g}{\partial w_1'}\delta w_1 - \frac{d}{dr_1}\left(\frac{\partial g}{\partial w_1''} \right) \delta w_1 \right]_0^{\ell_1} \right\} dt \\ & + \int_{t_1}^{t_2} \int_0^{\ell_1} \left\{ \left[\frac{\partial g}{\partial \theta_1} - \frac{d}{dt}\left(\frac{\partial g}{\partial \dot{\theta}_1} \right) \right] \delta\theta_1 \right. \\ & + \left[\frac{\partial g}{\partial w_1} - \frac{d}{dt}\left(\frac{\partial g}{\partial \dot{w}_1} \right) \right] \delta w_1 \\ & \left. + \left[\frac{d^2}{dr_1^2}\left(\frac{\partial g}{\partial w_1''} \right) - \frac{d}{dr_1}\left(\frac{\partial g}{\partial w_1'} \right) \right] \delta w_1 \right\} dr_1\, dt \end{aligned} \tag{3.57}$$

Similarly, the implicit expression of L_3, the variational expression of L_3, and the time integration of the variational expression are given respectively as follows.

$$L_3 = \int_0^{\ell_2} h\left(\theta_1, \theta_2, \dot{\theta}_1, \dot{\theta}_2, w_2, w_{\ell_1}, \dot{w}_{\ell_1}, \dot{w}_2, w_2', w_2'' \right) dr_2 \tag{3.58}$$

$$\begin{aligned} \delta L_3 = & \int_0^{\ell_2} \left[\frac{\partial h}{\partial \theta_1}\delta\theta_1 + \frac{\partial h}{\partial \theta_2}\delta\theta_2 + \frac{\partial h}{\partial \dot{\theta}_1}\delta\dot{\theta}_1 + \frac{\partial h}{\partial \dot{\theta}_2}\delta\dot{\theta}_2 \right. \\ & + \frac{\partial h}{\partial w_2}\delta w_2 + \frac{\partial h}{\partial w_{\ell_1}}\delta w_{\ell_1} + \frac{\partial h}{\partial \dot{w}_{\ell_1}}\delta\dot{w}_{\ell_1} + \frac{\partial h}{\partial \dot{w}_2}\delta\dot{w}_2 \\ & \left. + \frac{\partial h}{\partial w_2'}\delta w_2' + \frac{\partial h}{\partial w_2''}\delta w_2'' \right] dr_2 \end{aligned} \tag{3.59}$$

$$\int_{t_1}^{t_2} \delta L_3 dt = \int_{t_1}^{t_2} \left\{ \left[\frac{\partial h}{\partial w_2'}\delta w_2 \right]_0^{\ell_2} - \left[\frac{d}{dr_2}\left(\frac{\partial h}{\partial w_2''} \right) \delta w_2 \right]_0^{\ell_2} \right. \tag{3.60}$$

$$+\left[\frac{\partial h}{\partial w_2''}\delta w_2'\right]_0^{\ell_2}\Bigg\}dt$$
$$+\int_{t_1}^{t_2}\int_0^{\ell_2}\Bigg\{\left[\frac{\partial h}{\partial \theta_1}-\frac{d}{dt}\left(\frac{\partial h}{\partial \dot{\theta}_1}\right)\right]\delta\theta_1$$
$$+\left[\frac{\partial h}{\partial \theta_2}-\frac{d}{dt}\left(\frac{\partial h}{\partial \dot{\theta}_2}\right)\right]\delta\theta_2$$
$$+\left[\frac{\partial h}{\partial w_{\ell_1}}-\frac{d}{dt}\left(\frac{\partial h}{\partial \dot{w}_{\ell_1}}\right)\right]\delta w_{\ell_1}$$
$$+\Bigg[\frac{\partial h}{\partial w_2}-\frac{d}{dt}\left(\frac{\partial h}{\partial \dot{w}_2}\right)-\frac{d}{dr_2}\left(\frac{\partial h}{\partial w_2'}\right)$$
$$+\frac{d^2}{dr_2^2}\left(\frac{\partial h}{\partial w_2''}\right)\Bigg]\delta w_2\Bigg\}\,dr_2\,dt$$

Adding Equations 3.54, 3.57, and 3.60, Hamilton's principle for the continuous model which does not have nonconservative forces is reduced to

$$\int_{t_1}^{t_2}\delta L dt=\int_{t_1}^{t_2}\left(\delta L_1+\delta L_2+\delta L_3\right)dt=0 \qquad (3.61)$$

$$\int_{t_1}^{t_2}\Bigg\langle\ \Bigg\{\left[\frac{\partial L_1}{\partial \theta_1}-\frac{d}{dt}\left(\frac{\partial L_1}{\partial \dot{\theta}_1}\right)\right]+\int_0^{\ell_1}\left[\frac{\partial g}{\partial \theta_1}-\frac{d}{dt}\left(\frac{\partial g}{\partial \dot{\theta}_1}\right)\right]dr_1 \qquad (3.62)$$
$$+\int_0^{\ell_2}\left[\frac{\partial h}{\partial \theta_1}-\frac{d}{dt}\left(\frac{\partial h}{\partial \dot{\theta}_1}\right)\right]dr_2\Bigg\}\delta\theta_1$$
$$+\Bigg\{\left[\frac{\partial L_1}{\partial \theta_2}-\frac{d}{dt}\left(\frac{\partial L_1}{\partial \dot{\theta}_2}\right)\right]+\int_0^{\ell_2}\left[\frac{\partial h}{\partial \theta_2}-\frac{d}{dt}\left(\frac{\partial h}{\partial \dot{\theta}_2}\right)\right]dr_2\Bigg\}\delta\theta_2$$
$$+\Bigg\{\int_0^{\ell_1}\left[\frac{\partial g}{\partial w_1}-\frac{d}{dt}\left(\frac{\partial g}{\partial \dot{w}_1}\right)+\frac{d^2}{dr_1^2}\left(\frac{\partial g}{\partial w_1''}\right)-\frac{d}{dr_1}\left(\frac{\partial g}{\partial w_1'}\right)\right]dr_1\Bigg\}\delta w_1$$
$$+\Bigg\{\int_0^{\ell_2}\left[\frac{\partial h}{\partial w_2}-\frac{d}{dt}\left(\frac{\partial h}{\partial \dot{w}_2}\right)-\frac{d}{dr_2}\left(\frac{\partial h}{\partial w_2'}\right)+\frac{d^2}{dr_2^2}\left(\frac{\partial h}{\partial w_2''}\right)\right]dr_2\Bigg\}\delta w_2$$
$$+\Bigg\{\left[\frac{\partial L_1}{\partial w_{\ell_1}}-\frac{d}{dt}\left(\frac{\partial L_1}{\partial \dot{w}_{\ell_1}}\right)\right]+\left[\frac{\partial g}{\partial w_1'}-\frac{d}{dr_1}\left(\frac{\partial g}{\partial w_1''}\right)\right]_{r_1=\ell_1}$$

$$
\begin{aligned}
&+\int_0^{\ell_2}\left[\frac{\partial h}{\partial w_{\ell_1}}-\frac{d}{dt}\left(\frac{\partial h}{\partial \dot{w}_{\ell_1}}\right)\right]dr_2\Bigg\}\delta w_1(\ell_1)\\
&+\left\{\left[-\frac{\partial g}{\partial w_1'}+\frac{d}{dr_1}\left(\frac{\partial g}{\partial w_1''}\right)\right]_{r_1=0}\right\}\delta w_1(0)\\
&+\left\{\left[\frac{\partial L_1}{\partial w'_{\ell_1}}-\frac{d}{dt}\left(\frac{\partial L_1}{\partial \dot{w}'_{\ell_1}}\right)\right]+\left[\frac{\partial g}{\partial w_1''}\right]_{r_1=\ell_1}\right\}\delta w_1'(\ell_1)\\
&+\left\{\left[-\frac{\partial g}{\partial w_1''}\right]_{r_1=0}\right\}\delta w_1'(0)\\
&+\left\{\left[\frac{\partial L_1}{\partial w_{\ell_2}}-\frac{d}{dt}\left(\frac{\partial L_1}{\partial \dot{w}_{\ell_2}}\right)\right]+\left[\frac{\partial h}{\partial w_2'}-\frac{d}{dr_2}\left(\frac{\partial h}{\partial w_2''}\right)\right]_{r_2=\ell_2}\right\}\delta w_2(\ell_2)\\
&+\left\{\left[-\frac{\partial h}{\partial w_2'}+\frac{d}{dr_2}\left(\frac{\partial h}{\partial w_2''}\right)\right]_{r_2=0}\right\}\delta w_2(0)\\
&+\left\{\left[-\frac{d}{dt}\left(\frac{\partial L_1}{\partial \dot{w}'_{\ell_2}}\right)\right]+\left[\frac{\partial h}{\partial w_2''}\right]_{r_2=\ell_2}\right\}\delta w_2'(\ell_2)\\
&+\left\{\left[-\frac{\partial h}{\partial w_2''}\right]_{r_2=0}\right\}\delta w_2'(0)\ \Bigg\rangle dt\\
&=0
\end{aligned}
$$

Since $\delta\theta_1, \delta\theta_2, \delta w_1$, and δw_2 are arbitrary and independent, all four terms multiplied by those must be zero for Equation 3.62 to be satisfied. Thus, the four nonlinear differential equations of motion including the shortening effect due to elastic deflection are given by

$$
\begin{aligned}
&K_{t_1}\theta_1+m_2g\left(w_{\ell_1}cos\theta_1+\ell_1 sin\theta_1\right) \qquad (3.63)\\
&+m_pg\Big[\left(w_{\ell_1}cos\theta_1+\ell_1 sin\theta_1\right)+\left(w_{\ell_2}cos\theta_2+\ell_2 sin\theta_2\right)cos\theta_1\\
&\qquad-\left(w_{\ell_2}sin\theta_2-\ell_2 cos\theta_2\right)sin\theta_1\Big]
\end{aligned}
$$

$$
\begin{aligned}
&+\left[\left(J_1+J_a+J_b+J_p\right)+\left(m_a+m_b\right)\left(\ell_1^2+w_{\ell_1}^2\right)\right.\\
&+m_p\left(\ell_1^2+w_{\ell_1}^2+\ell_2^2+w_{\ell_2}^2\right)+2m_p\ell_1\left(\ell_2 cos\theta_2-w_{\ell_2}sin\theta_2\right)\\
&\left.+2m_p w_{\ell_1}\left(\ell_2 sin\theta_2+w_{\ell_2}cos\theta_2\right)\right]\ddot{\theta}_1\\
&+\left[\left(J_b+J_p\right)+m_p\left(\ell_2^2+w_{\ell_2}^2\right)+m_p\ell_1\left(\ell_2 cos\theta_2-w_{\ell_2}sin\theta_2\right)\right.\\
&\left.+m_p w_{\ell_1}\left(\ell_2 sin\theta_2+w_{\ell_2}cos\theta_2\right)\right]\ddot{\theta}_2\\
&+\left[\left(m_a+m_b\right)\ell_1+m_p\left(\ell_1+\ell_2 cos\theta_2-w_{\ell_2}sin\theta_2\right)\right]\ddot{w}_{\ell_1}\\
&+m_p\left(\ell_1 cos\theta_2+w_{\ell_1}sin\theta_2+\ell_2\right)\ddot{w}_{\ell_2}+J_a\ddot{w}'_{\ell_1}\\
&+J_p\ddot{w}'_{\ell_2}+2\left(m_a+m_b\right)w_{\ell_1}\dot{w}_{\ell_1}\dot{\theta}_1\\
&+m_p\left[2w_{\ell_1}\dot{w}_{\ell_1}+2\ell_1\left(-\ell_2\dot{\theta}_2 sin\theta_2-\dot{w}_{\ell_2}sin\theta_2-w_{\ell_2}\dot{\theta}_2 cos\theta_2\right)\right.\\
&+2w_{\ell_2}\dot{w}_{\ell_2}+2\dot{w}_{\ell_1}\left(\ell_2 sin\theta_2+w_{\ell_2}cos\theta_2\right)\\
&\left.+2w_{\ell_1}\left(\ell_2\dot{\theta}_2 cos\theta_2+\dot{w}_{\ell_2}cos\theta_2-\dot{\theta}_2 w_{\ell_2}sin\theta_2\right)\right]\dot{\theta}_1\\
&+m_p\left[-2\ell_1\dot{w}_{\ell_2}sin\theta_2+2w_{\ell_1}\dot{w}_{\ell_2}cos\theta_2+2w_{\ell_2}\dot{w}_{\ell_2}\right.\\
&\left.+\ell_1\left(-\ell_2\dot{\theta}_2 sin\theta_2-w_{\ell_2}\dot{\theta}_2 cos\theta_2\right)+w_{\ell_1}\left(\ell_2\dot{\theta}_2 cos\theta_2-w_{\ell_2}\dot{\theta}_2 sin\theta_2\right)\right]\dot{\theta}_2\\
&+\int_0^{\ell_1}(\rho A)_1\left[g\left(w_1 cos\theta_1+r_1 sin\theta_1\right)+\left(r_1^2+w_1^2\right)\ddot{\theta}_1+r_1\ddot{w}_1+2w_1\dot{w}_1\dot{\theta}_1\right]dr_1\\
&+\int_0^{\ell_2}(\rho A)_2\left[g\left\{\left(w_{\ell_1}cos\theta_1+\ell_1 sin\theta_1\right)+\left(w_2 cos\theta_2+r_2 sin\theta_2\right)cos\theta_1\right.\right.\\
&\left.\left.-\left(w_2 sin\theta_2-r_2 cos\theta_2\right)sin\theta_1\right\}\right.\\
&+\left\{\ell_1^2+w_{\ell_1}^2+w_2^2+r_2^2+2\ell_1\left(r_2 cos\theta_2-w_2 sin\theta_2\right)\right.\\
&\left.+2w_{\ell_1}\left(r_2 sin\theta_2+w_2 cos\theta_2\right)\right\}\ddot{\theta}_1\\
&+\left\{w_2^2+r_2^2+\ell_1\left(r_2 cos\theta_2-w_2 sin\theta_2\right)+w_{\ell_1}\left(r_2 sin\theta_2+w_2 cos\theta_2\right)\right\}\ddot{\theta}_2\\
&+\left(\ell_1+r_2 cos\theta_2-w_2 sin\theta_2\right)\ddot{w}_{\ell_1}
\end{aligned}
$$

$$
\begin{aligned}
&+\left(\ell_1 cos\theta_2 + w_{\ell_1} sin\theta_2 + r_2\right)\ddot{w}_2 \\
&+\left\{2w_{\ell_1}\dot{w}_{\ell_1} + 2w_2\dot{w}_2 + 2\dot{w}_{\ell_1}\left(r_2 sin\theta_2 + w_2 cos\theta_2\right)\right. \\
&\quad +2\ell_1\left(-r_2\dot{\theta}_2 sin\theta_2 - \dot{w}_2 sin\theta_2 - w_2\dot{\theta}_2 cos\theta_2\right) \\
&\quad \left.+2w_{\ell_1}\left(r_2\dot{\theta}_2 cos\theta_2 + \dot{w}_2 cos\theta_2 - w_2\dot{\theta}_2 sin\theta_2\right)\right\}\dot{\theta}_1 \\
&+\left\{2w_2\dot{w}_2 + \ell_1\left(-r_2\dot{\theta}_2 sin\theta_2 - 2\dot{w}_2 sin\theta_2 - w_2\dot{\theta}_2 cos\theta_2\right)\right. \\
&\quad \left.+w_{\ell_1}\left(r_2\dot{\theta}_2 cos\theta_2 + 2\dot{w}_2 cos\theta_2 - w_2\dot{\theta}_2 sin\theta_2\right)\right\}\dot{\theta}_2\Big] dr_2 \\
&+\frac{1}{2}\int_0^{\ell_1}\Big[(\rho A)_1 g\int_0^{r_1} sin\theta_1\left(w_1'\right)^2 d\xi_1 + \left(m_2 + m_p\right)g\left(w_1'\right)^2 sin\theta_1 \\
&\quad +(\rho A)_2 g sin\theta_1\int_0^{\ell_2}\left(w_1'\right)^2 dr_2\Big] dr_1 \\
&+\frac{1}{2}\int_0^{\ell_2}\left(sin\theta_2 cos\theta_1 + cos\theta_2 sin\theta_1\right) \\
&\quad \Big[m_p g\left(w_2'\right)^2 + (\rho A)_2 g\int_0^{r_2}\left(w_2'\right)^2 d\xi_2\Big] dr_2 \\
&\quad = 0
\end{aligned}
$$

$$
\begin{aligned}
&m_p\left(-\dot{w}_{\ell_1}\dot{w}_{\ell_2} sin\theta_2 - \ell_1\dot{\theta}_1\dot{w}_{\ell_2} sin\theta_2 + w_{\ell_1}\dot{\theta}_1\dot{w}_{\ell_2} cos\theta_2\right) \qquad (3.64) \\
&+m_p\left(\dot{\theta}_1 + \dot{\theta}_2\right)\left\{\left(\ell_1\dot{\theta}_1 + \dot{w}_{\ell_1}\right)\left(-\ell_2 sin\theta_2 - w_{\ell_2} cos\theta_2\right)\right. \\
&\quad \left.+w_{\ell_1}\dot{\theta}_1\left(\ell_2 cos\theta_2 - w_{\ell_2} sin\theta_2\right)\right\} \\
&\quad +K_{t_2}\left(w'_{\ell_1} - \theta_2\right) \\
&-m_p g\left\{\left(-w_{\ell_2} sin\theta_2 + \ell_2 cos\theta_2\right) sin\theta_1 + \left(w_{\ell_2} cos\theta_2 + \ell_2 sin\theta_2\right) cos\theta_1\right\} \\
&-\left[\left(J_b + J_p\right) + m_p\left(w_{\ell_2}^2 + \ell_2^2\right) + m_p\ell_1\left(\ell_2 cos\theta_2 - w_{\ell_2} sin\theta_2\right)\right. \\
&\quad \left.+m_p w_{\ell_1}\left(\ell_2 sin\theta_2 + w_{\ell_2} cos\theta_2\right)\right]\ddot{\theta}_1 \\
&\quad -\left[\left(J_b + J_p\right) + m_p\left(w_{\ell_2}^2 + \ell_2^2\right)\right]\ddot{\theta}_2 \\
&\quad -\left[m_p\left(\ell_2 cos\theta_2 - w_{\ell_2} sin\theta_2\right)\right]\ddot{w}_{\ell_1} - m_p\ell_2\ddot{w}_{\ell_2} - J_p\ddot{w}'_{\ell_2}
\end{aligned}
$$

$$
\begin{aligned}
&-m_p\Big[2w_{\ell_2}\dot{w}_{\ell_2}+\ell_1\Big(-\ell_2\dot{\theta}_2 sin\theta_2-\dot{w}_{\ell_2}sin\theta_2-w_{\ell_2}\dot{\theta}_2 cos\theta_2\Big)\\
&\qquad+\dot{w}_{\ell_1}\Big(\ell_2 sin\theta_2+w_{\ell_2}cos\theta_2\Big)\\
&\qquad+w_{\ell_1}\Big(\ell_2\dot{\theta}_2 cos\theta_2+\dot{w}_{\ell_2}cos\theta_2-w_{\ell_2}\dot{\theta}_2 sin\theta_2\Big)\Big]\dot{\theta}_1\\
&-2m_p\dot{\theta}_2 w_{\ell_2}\dot{w}_{\ell_2}-m_p\dot{w}_{\ell_1}\Big(-\ell_2\dot{\theta}_2 sin\theta_2-\dot{w}_{\ell_2}sin\theta_2-w_{\ell_2}\dot{\theta}_2 cos\theta_2\Big)\\
&+\int_0^{\ell_2}(\rho A)_2\Big[\Big\{-\dot{w}_{\ell_1}\dot{w}_2 sin\theta_2-\ell_1\dot{\theta}_1\dot{w}_2 sin\theta_2+w_{\ell_1}\dot{\theta}_1\dot{w}_2 cos\theta_2\\
&\qquad+\big(\dot{\theta}_1+\dot{\theta}_2\big)\Big(\ell_1\dot{\theta}_1+\dot{w}_{\ell_1}\Big)\big(-r_2 sin\theta_2-w_2 cos\theta_2\big)\\
&\qquad+\big(\dot{\theta}_1+\dot{\theta}_2\big)w_{\ell_1}\dot{\theta}_1\big(r_2 cos\theta_2-w_2 sin\theta_2\big)\Big\}\\
&-g\Big\{\big(-w_2 sin\theta_2+r_2 cos\theta_2\big)sin\theta_1+\big(w_2 cos\theta_2+r_2 sin\theta_2\big)cos\theta_1\Big\}\\
&-\Big\{w_2^2+r_2^2+\ell_1\big(r_2 cos\theta_2-w_2 sin\theta_2\big)+w_{\ell_1}\big(r_2 sin\theta_2+w_2 cos\theta_2\big)\Big\}\ddot{\theta}_1\\
&-\big(w_2^2+r_2^2\big)\ddot{\theta}_2-r_2\ddot{w}_2-\big(r_2 cos\theta_2-w_2 sin\theta_2\big)\ddot{w}_{\ell_1}\\
&-\Big\{2w_2\dot{w}_2+\dot{w}_{\ell_1}\big(r_2 sin\theta_2+w_2 cos\theta_2\big)\\
&+\ell_1\big(-r_2\dot{\theta}_2 sin\theta_2-\dot{w}_2 sin\theta_2-w_2\dot{\theta}_2 cos\theta_2\big)\\
&+w_{\ell_1}\big(r_2\dot{\theta}_2 cos\theta_2+\dot{w}_2 cos\theta_2-w_2\dot{\theta}_2 sin\theta_2\big)\Big\}\dot{\theta}_1\\
&-\Big\{2w_2\dot{\theta}_2\dot{w}_2+\dot{w}_{\ell_1}\big(-r_2\dot{\theta}_2 sin\theta_2-\dot{w}_2 sin\theta_2-w_2\dot{\theta}_2 cos\theta_2\big)\Big\}\Big]dr_2\\
&+\frac{1}{2}\int_0^{\ell_2}\big(cos\theta_2 sin\theta_1+sin\theta_2 cos\theta_1\big)\Big[m_p g\big(w_2'\big)^2+(\rho A)_2 g\int_0^{r_2}\big(w_2'\big)^2 d\xi_2\Big]dr_2\\
&\qquad=0
\end{aligned}
$$

$$
\begin{aligned}
&\int_0^{\ell_1}\Big[(\rho A)_1\big\{\dot{\theta}_1^2 w_1-g sin\theta_1-r_1\ddot{\theta}_1-\ddot{w}_1\big\}-(EI)_1 w_1^{iv}\Big]dr_1 \qquad (3.65)\\
&+\int_0^{\ell_1}\Big[(\rho A)_1 g cos\theta_1\Big\{w_1'+\int_0^{r_1}\big(w_1''\big)d\xi_1\Big\}+\big(m_2+m_p\big)g\big(w_1''\big)cos\theta_1\\
&\qquad+(\rho A)_2 g cos\theta_1\int_0^{\ell_2}\big(w_1''\big)dr_2\Big]dr_1\\
&\qquad=0
\end{aligned}
$$

$$\int_0^{\ell_2}\Big[(\rho A)_2\Big\{\big(\dot\theta_1+\dot\theta_2\big)^2 w_2-\big(\dot\theta_1+\dot\theta_2\big)\big(\ell_1\dot\theta_1+\dot w_{\ell_1}\big)sin\theta_2 \\ +\big(\dot\theta_1+\dot\theta_2\big)w_{\ell_1}\dot\theta_1 cos\theta_2\Big\} \\ -(\rho A)_2 g\big(cos\theta_2 sin\theta_1+sin\theta_2 cos\theta_1\big) \\ -(\rho A)_2\Big\{\big(\ell_1 cos\theta_2+w_{\ell_1}sin\theta_2+r_2\big)\ddot\theta_1+r_2\ddot\theta_2+\ddot w_2+cos\theta_2\ddot w_{\ell_1}\Big\} \\ -(\rho A)_2\Big\{\big(-\ell_1\dot\theta_2 sin\theta_2+\dot w_{\ell_1}sin\theta_2+w_{\ell_1}\dot\theta_2 cos\theta_2\big)\dot\theta_1-\dot w_{\ell_1}\dot\theta_2 sin\theta_2\Big\} \\ -(EI)_2 w_2^{iv}\Big]\,dr_2 \\ +\int_0^{\ell_2}\big(-sin\theta_2 sin\theta_1+cos\theta_2 cos\theta_1\big) \\ \Big[m_p g\big(w_2''\big)+(\rho A)_2 g\Big\{w_2'+\int_0^{r_2}\big(w_2''\big)d\xi_2\Big\}\Big]dr_2 \\ =0 \tag{3.66}$$

Since the elastic arms have zero displacements and slopes at the joints, the four geometric boundary conditions are given by

$$w_{r_1=0} = 0 \tag{3.67}$$

$$w_{r_2=0} = 0 \tag{3.68}$$

$$w'_{r_1=0} = 0 \tag{3.69}$$

$$w'_{r_2=0} = 0 \tag{3.70}$$

However, since the elastic arms have displacements and slopes at the ends of the arms, all four terms multiplied by $\delta w_1(\ell_1), \delta w_1'(\ell_1), \delta w_2(\ell_2)$ and $\delta w_2'(\ell_2)$ must be zero for Equation 3.62 to be satisfied. Thus, the four natural boundary conditions are given by

$$\big(m_a+m_b+m_p\big)\big(\dot\theta_1^2 w_{\ell_1}\big)+m_p\dot\theta_1\dot w_{\ell_2}sin\theta_2 \tag{3.71}$$

$$
\begin{aligned}
&+m_p\dot{\theta}_1\left(\dot{\theta}_1+\dot{\theta}_2\right)\left(\ell_2 sin\theta_2+w_{\ell_2}cos\theta_2\right)-\left(m_a+m_b+m_p\right)gsin\theta_1\\
&-\left\{\left(m_a+m_b+m_p\right)\ell_1+m_p\left(\ell_2 cos\theta_2-w_{\ell_2}sin\theta_2\right)\right\}\ddot{\theta}_1\\
&-m_p\left(\ell_2 cos\theta_2-w_{\ell_2}sin\theta_2\right)\ddot{\theta}_2-\left(m_a+m_b+m_p\right)\ddot{w}_{\ell_1}\\
&-m_p cos\theta_2\ddot{w}_{\ell_2}+m_p\left(\ell_2\dot{\theta}_2 sin\theta_2+\dot{w}_{\ell_2}sin\theta_2+w_{\ell_2}\dot{\theta}_2 cos\theta_2\right)\dot{\theta}_1\\
&+m_p\left(\ell_2\dot{\theta}_2 sin\theta_2+2\dot{w}_{\ell_2}sin\theta_2+w_{\ell_2}\dot{\theta}_2 cos\theta_2\right)\dot{\theta}_2+(EI)_1\left(w_1'''\right)_{r_1=\ell_1}\\
&+\int_0^{\ell_2}(\rho A)_2\left[\dot{\theta}_1\dot{w}_2 sin\theta_2+\left(\dot{\theta}_1+\dot{\theta}_2\right)\dot{\theta}_1\left(r_2 sin\theta_2+w_2 cos\theta_2\right)\right.\\
&+\dot{\theta}_1^2 w_{\ell_1}-\left(\ell_1+r_2 cos\theta_2-w_2 sin\theta_2\right)\ddot{\theta}_1-\left(r_2 cos\theta_2-w_2 sin\theta_2\right)\ddot{\theta}_2\\
&-\ddot{w}_{\ell_1}-cos\theta_2\ddot{w}_2+\left(r_2\dot{\theta}_2 sin\theta_2+\dot{w}_2 sin\theta_2+w_2\dot{\theta}_2 cos\theta_2\right)\dot{\theta}_1\\
&\left.-gsin\theta_1+\left(r_2\dot{\theta}_2 sin\theta_2+2\dot{w}_2 sin\theta_2+w_2\dot{\theta}_2 cos\theta_2\right)\dot{\theta}_2\right]dr_2\\
&-\left[(\rho A)_1 gcos\theta_1\int_0^{r_1}\left(w_1'\right)dr_1+\left(m_2+m_p\right)gcos\theta_1\left(w_1'\right)\right.\\
&\left.+(\rho A)_2 gcos\theta_1\int_0^{\ell_2}\left(w_1'\right)dr_2\right]_{r_1=\ell_1}\\
&=0
\end{aligned}
$$

$$
\begin{aligned}
&m_p\left(\dot{\theta}_1+\dot{\theta}_2\right)\left\{-\left(\ell_1\dot{\theta}_1+\dot{w}_{\ell_1}\right)sin\theta_2+w_{\ell_1}\dot{\theta}_1 cos\theta_2\right\} \quad (3.72)\\
&-m_p g\left(cos\theta_2 sin\theta_1+sin\theta_2 cos\theta_1\right)-m_p\left(\ell_1 cos\theta_2+w_{\ell_1}sin\theta_2+\ell_2\right)\ddot{\theta}_1\\
&-m_p\left\{cos\theta_2\ddot{w}_{\ell_1}+\ddot{w}_{\ell_2}+\left(-\ell_1\dot{\theta}_2 sin\theta_2+\dot{w}_{\ell_1}sin\theta_2+w_{\ell_1}\dot{\theta}_2 cos\theta_2\right)\dot{\theta}_1\right\}\\
&+m_p\left(\dot{\theta}_1+\dot{\theta}_2\right)^2 w_{\ell_2}-m_p\ell_2\ddot{\theta}_2+m_p\dot{w}_{\ell_1}\dot{\theta}_2 sin\theta_2+(EI)_2\left(w_2'''\right)_{r_2=\ell_2}\\
&+\left[\left(sin\theta_2 sin\theta_1-cos\theta_2 cos\theta_1\right)\left\{m_p g\left(w_2'\right)+(\rho A)_2 g\int_0^{r_2}\left(w_2'\right)d\xi_2\right\}\right]_{r_2=\ell_2}\\
&=0
\end{aligned}
$$

$$
K_{t_2}\left(w_{\ell_1}'-\theta_2\right)+J_a\left(\ddot{\theta}_1+\ddot{w}_{\ell_1}'\right)+(EI)_1\left(w_1''\right)_{r_1=\ell_1}=0 \quad (3.73)
$$

$$
J_p\left(\ddot{\theta}_1+\ddot{\theta}_2+\ddot{w}_{\ell_2}'\right)+(EI)_2\left(w_2''\right)_{r_2=\ell_2}=0 \quad (3.74)
$$

3.2.4 Equations of Motion by the Assumed Modes Method

This section derives the discrete equations of motion for elastic two arms robot system using the assumed modes method. The assumed modes method is a popular formulation methods because it reduces an infinite degree of freedom problem to a finite one with a relatively small number of generalized coordinates.

This method approximates a continuous displacement field having infinite degrees of freedom with a linear combination of n basis functions and n generalized coordinates resulting in an n-degree of freedom system. The number of basis functions n is determined based on how accurately the continuous system must be represented. The degrees of freedom become the generalized coordinates of the basis functions.

An approximate solution of a dynamic system converges to the exact solution as the number of degrees of freedom increases to infinity when the assumed mode shapes for the approximate solution are selected to satisfy the certain conditions such as linear independency, continuity and p times differentiability (p is the highest order of the governing partial differential equations), satisfaction of the geometric boundary conditions, and completeness. Thus, the assumed mode shapes are usually used as the basis functions to approximate a continuous displacement. The elastic deformations of the arms are given by a linear combination of basis functions and generalized coordinates.

$$w_1(r_1,t) = \sum_{i=1}^{n} \phi_i(r_1) a_i(t) = \boldsymbol{\phi}^T \mathbf{a} \tag{3.75}$$

$$w_2(r_2,t) = \sum_{j=1}^{m} \psi_j(r_2) c_j(t) = \boldsymbol{\psi}^T \mathbf{c} \tag{3.76}$$

Where the superscript T means the transpose of a matrix. $\phi_i(r_1)$ is the i^{th} basis

function for the upper arm, and $a_i(t)$ is its i^{th} time dependent the generalized coordinate. Similarly, $\psi_j(r_2)$ is the j^{th} basis function for the lower arm and $c_j(t)$ is its j^{th} time dependent the generalized coordinate.

$\dot{w}_1$ and $\dot{w}_2$ represent time derivatives of w_1 and w_2 and are defined as

$$\dot{w}_1 = \boldsymbol{\phi}^T \dot{\mathbf{a}} \tag{3.77}$$

$$\dot{w}_2 = \boldsymbol{\psi}^T \dot{\mathbf{c}} \tag{3.78}$$

w_1' and w_2' represent spatial derivatives of w_1 and w_2 with respect to r_1 and r_2 and are defined as

$$w_1' = (\boldsymbol{\phi}')^T \mathbf{a} \tag{3.79}$$

$$w_2' = (\boldsymbol{\psi}')^T \mathbf{c} \tag{3.80}$$

The kinetic and potential energy expressions are rederived using the discrete formulation. The kinetic energy is given as

$$\begin{aligned} T \;=\; & \frac{1}{2} J_1 \dot{\theta}_1^2 \\ & + \frac{1}{2} \int_0^{\ell_1} (\rho A)_1 \left[\left(r_1 \dot{\theta}_1 \right)^2 + 2 r_1 \dot{\theta}_1 \left(\boldsymbol{\phi}^T \dot{\mathbf{a}} \right) \right. \\ & \qquad \left. + \left(\dot{\mathbf{a}}^T \boldsymbol{\phi} \boldsymbol{\phi}^T \dot{\mathbf{a}} \right) + \left(\mathbf{a}^T \boldsymbol{\phi} \boldsymbol{\phi}^T \mathbf{a} \right) \dot{\theta}_1^2 \right] dr_1 \\ & + \frac{1}{2} m_a \left[\left(\ell_1 \dot{\theta}_1 \right)^2 + 2 \ell_1 \dot{\theta}_1 \left(\boldsymbol{\phi}_{\ell_1}^T \dot{\mathbf{a}} \right) + \left(\dot{\mathbf{a}}^T \boldsymbol{\phi}_{\ell_1} \boldsymbol{\phi}_{\ell_1}^T \dot{\mathbf{a}} \right) + \left(\mathbf{a}^T \boldsymbol{\phi}_{\ell_1} \boldsymbol{\phi}_{\ell_1}^T \mathbf{a} \right) \dot{\theta}_1^2 \right] \\ & + \frac{1}{2} J_a \left[\dot{\theta}_1^2 + 2 \dot{\theta}_1 \left(\boldsymbol{\phi}_{\ell_1}'^T \dot{\mathbf{a}} \right) + \left(\dot{\mathbf{a}}^T \boldsymbol{\phi}_{\ell_1}' \boldsymbol{\phi}_{\ell_1}'^T \dot{\mathbf{a}} \right) \right] \\ & + \frac{1}{2} m_b \left[\left(\ell_1 \dot{\theta}_1 \right)^2 + 2 \ell_1 \dot{\theta}_1 \left(\boldsymbol{\phi}_{\ell_1}^T \dot{\mathbf{a}} \right) + \left(\dot{\mathbf{a}}^T \boldsymbol{\phi}_{\ell_1} \boldsymbol{\phi}_{\ell_1}^T \dot{\mathbf{a}} \right) + \left(\mathbf{a}^T \boldsymbol{\phi}_{\ell_1} \boldsymbol{\phi}_{\ell_1}^T \mathbf{a} \right) \dot{\theta}_1^2 \right] \\ & + \frac{1}{2} J_b \left(\dot{\theta}_1 + \dot{\theta}_2 \right)^2 \\ & + \frac{1}{2} \int_0^{\ell_2} (\rho A)_2 \left[\left(\ell_1 \dot{\theta}_1 \right)^2 + \left(\dot{\mathbf{a}}^T \boldsymbol{\phi}_{\ell_1} \boldsymbol{\phi}_{\ell_1}^T \dot{\mathbf{a}} \right) + \left(\dot{\mathbf{c}}^T \boldsymbol{\psi} \boldsymbol{\psi}^T \dot{\mathbf{c}} \right) \right. \end{aligned} \tag{3.81}$$

$$
\begin{aligned}
&+\left(\mathbf{a}^T\phi_{\ell_1}\phi_{\ell_1}^T\mathbf{a}\right)\dot{\theta}_1^2+2\ell_1\dot{\theta}_1\left(\phi_{\ell_1}^T\dot{\mathbf{a}}\right)+2\left(\phi_{\ell_1}^T\dot{\mathbf{a}}\right)\left(\psi^T\dot{\mathbf{c}}\right)cos\theta_2\\
&+2\ell_1\dot{\theta}_1\left(\psi^T\dot{\mathbf{c}}\right)cos\theta_2+2\dot{\theta}_1\left(\phi_{\ell_1}^T\mathbf{a}\right)\left(\psi^T\dot{\mathbf{c}}\right)sin\theta_2\\
&+\left(\dot{\theta}_1+\dot{\theta}_2\right)^2\left(\mathbf{c}^T\psi\psi^T\mathbf{c}+r_2^2\right)\\
&+2\left(\dot{\theta}_1+\dot{\theta}_2\right)\left\{\left(\ell_1\dot{\theta}_1+\phi_{\ell_1}^T\dot{\mathbf{a}}\right)\left(r_2cos\theta_2-\left(\psi^T\mathbf{c}\right)sin\theta_2\right)\right.\\
&\quad\left.+r_2\left(\psi^T\dot{\mathbf{c}}\right)+\dot{\theta}_1\left(\phi_{\ell_1}^T\mathbf{a}\right)\left(r_2sin\theta_2+\left(\psi^T\mathbf{c}\right)cos\theta_2\right)\right\}\Big]\,dr_2\\
&+\frac{1}{2}m_p\Big[\left(\ell_1\dot{\theta}_1\right)^2+\left(\dot{\mathbf{a}}^T\phi_{\ell_1}\phi_{\ell_1}^T\dot{\mathbf{a}}\right)+\left(\dot{\mathbf{c}}^T\psi_{\ell_2}\psi_{\ell_2}^T\dot{\mathbf{c}}\right)+\left(\mathbf{a}^T\phi_{\ell_1}\phi_{\ell_1}^T\mathbf{a}\right)\dot{\theta}_1^2\\
&+2\ell_1\dot{\theta}_1\left(\phi_{\ell_1}^T\dot{\mathbf{a}}\right)+2\left(\phi_{\ell_1}^T\dot{\mathbf{a}}\right)\left(\psi_{\ell_2}^T\dot{\mathbf{c}}\right)cos\theta_2+2\ell_1\dot{\theta}_1\left(\psi_{\ell_2}^T\dot{\mathbf{c}}\right)cos\theta_2\\
&+2\dot{\theta}_1\left(\phi_{\ell_1}^T\mathbf{a}\right)\left(\psi_{\ell_2}^T\dot{\mathbf{c}}\right)sin\theta_2+\left(\dot{\theta}_1+\dot{\theta}_2\right)^2\left(\mathbf{c}^T\psi_{\ell_2}\psi_{\ell_2}^T\mathbf{c}+\ell_2^2\right)\\
&+2\left(\dot{\theta}_1+\dot{\theta}_2\right)\left\{\left(\ell_1\dot{\theta}_1+\phi_{\ell_1}^T\dot{\mathbf{a}}\right)\left(\ell_2cos\theta_2-\left(\psi_{\ell_2}^T\mathbf{c}\right)sin\theta_2\right)\right.\\
&\quad\left.+\ell_2\left(\psi_{\ell_2}^T\dot{\mathbf{c}}\right)+\dot{\theta}_1\left(\phi_{\ell_1}^T\mathbf{a}\right)\left(\ell_2sin\theta_2+\left(\psi_{\ell_2}^T\mathbf{c}\right)cos\theta_2\right)\right\}\Big]\\
&+\frac{1}{2}J_p\left[\left(\dot{\theta}_1+\dot{\theta}_2\right)^2+2\left(\dot{\theta}_1+\dot{\theta}_2\right)\left(\psi_{\ell_2}'^T\dot{\mathbf{c}}\right)+\left(\dot{\mathbf{c}}^T\psi_{\ell_2}'\psi_{\ell_2}'^T\dot{\mathbf{c}}\right)\right]
\end{aligned}
$$

Similarly, the potential energy including the shortening effect due to elastic deflection of the system is given as

$$
\begin{aligned}
\Pi\;=\;&\frac{1}{2}K_{t_1}\theta_1^2+\frac{1}{2}K_{t_2}\left[\mathbf{a}^T\phi_{\ell_1}'\phi_{\ell_1}'^T\mathbf{a}-2\theta_2\phi_{\ell_1}'^T\mathbf{a}+\theta_2^2\right] \qquad (3.82)\\
&+\frac{1}{2}\int_0^{\ell_1}(EI)_1\left(\mathbf{a}^T\phi''\phi''^T\mathbf{a}\right)dr_1\\
&+\frac{1}{2}\int_0^{\ell_2}(EI)_2\left(\mathbf{c}^T\psi''\psi''^T\mathbf{c}\right)dr_2\\
&+\int_0^{\ell_1}(\rho A)_1g\left[\left(\phi^T\mathbf{a}\right)sin\theta_1-r_1cos\theta_1\right]dr_1\\
&+\frac{1}{2}\int_0^{\ell_1}(\rho A)_1gcos\theta_1\left[\int_0^{r_1}\left(\mathbf{a}^T\phi'\phi'^T\mathbf{a}\right)d\xi_1\right]dr_1\\
&+\left(m_a+m_b\right)g\left[\left(\phi_{\ell_1}^T\mathbf{a}\right)sin\theta_1-\ell_1cos\theta_1\right]
\end{aligned}
$$

$$
\begin{aligned}
&+\frac{1}{2}\int_0^{\ell_1}(m_a+m_b)g\cos\theta_1\left(\mathbf{a}^T\phi'\phi'^T\mathbf{a}\right)dr_1\\
&+\int_0^{\ell_2}(\rho A)_2 g\left[\left\{\left(\phi_{\ell_1}^T\mathbf{a}\right)\sin\theta_1-\ell_1\cos\theta_1\right\}\right.\\
&\qquad+\left\{\left(\psi^T\mathbf{c}\right)\cos\theta_2+r_2\sin\theta_2\right\}\sin\theta_1\\
&\qquad\left.+\left\{\left(\psi^T\mathbf{c}\right)\sin\theta_2-r_2\cos\theta_2\right\}\cos\theta_1\right]dr_2\\
&+\frac{1}{2}\int_0^{\ell_2}(\rho A)_2 g\cos\theta_1\left[\int_0^{\ell_1}\left(\mathbf{a}^T\phi'\phi'^T\mathbf{a}\right)dr_1\right]dr_2\\
&+\frac{1}{2}\int_0^{\ell_2}(\rho A)_2 g\left(-\sin\theta_2\sin\theta_1+\cos\theta_2\cos\theta_1\right)\left[\int_0^{r_2}\left(\mathbf{c}^T\psi'\psi'^T\mathbf{c}\right)d\xi_2\right]dr_2\\
&+m_p g\left[\left\{\left(\phi_{\ell_1}^T\mathbf{a}\right)\sin\theta_1-\ell_1\cos\theta_1\right\}\right.\\
&\qquad+\left\{\left(\psi_{\ell_2}^T\mathbf{c}\right)\cos\theta_2+\ell_2\sin\theta_2\right\}\sin\theta_1\\
&\qquad\left.+\left\{\left(\psi_{\ell_2}^T\mathbf{c}\right)\sin\theta_2-\ell_2\cos\theta_2\right\}\cos\theta_1\right]\\
&+\frac{1}{2}m_p g\cos\theta_1\int_0^{\ell_1}\left(\mathbf{a}^T\phi'\phi'^T\mathbf{a}\right)dr_1\\
&+\frac{1}{2}m_p g\left(-\sin\theta_2\sin\theta_1+\cos\theta_2\cos\theta_1\right)\int_0^{\ell_2}\left(\mathbf{c}^T\psi'\psi'^T\mathbf{c}\right)dr_2
\end{aligned}
$$

Lagrange's equation for a finite degree of freedom system is derived from Equation 3.49.

$$\frac{d}{dt}\left(\frac{\partial T}{\partial\dot{q}_i}\right)-\frac{\partial T}{\partial q_i}+\frac{\partial \Pi}{\partial q_i}=\left(Q_{nc}\right)_i \qquad i=1,2,\cdots,n+m+2 \tag{3.83}$$

where q_i represents the generalized coordinates $\theta_1,\theta_2,a_{i=1,\cdots,n}$ and $c_{i=1,\cdots,m}$ (n and m are the number of basis functions used to approximate the elastic deformation of each arm) and Q_{nc} represents the generalized nonconservative force. If there is no nonconservative force, the right hand side of Equation 3.83 becomes zero.

The generalized coordinate vector $\mathbf{q}$ and velocity vector $\dot{\mathbf{q}}$ are defined as

$$\mathbf{q}=\left(\theta_1,a_1,a_2,\cdots,a_n,\theta_2,c_1,c_2,\cdots,c_m\right)^T \tag{3.84}$$

$$\dot{\mathbf{q}} = \left(\dot{\theta}_1, \dot{a}_1, \dot{a}_2, \cdots, \dot{a}_n, \dot{\theta}_2, \dot{c}_1, \dot{c}_2, \cdots, \dot{c}_m\right)^T \tag{3.85}$$

Substituting Equations 3.81 and 3.82 into Equation 3.83 and performing the necessary partial and total derivatives, the discrete differential equations of motion including the shortening effect for a conservative system are given in the following matrix form.

$$\begin{bmatrix} P_{11} & \mathbf{P}_{12} & P_{13} & \mathbf{P}_{14} \\ \mathbf{P}_{21} & \mathbf{P}_{22} & \mathbf{P}_{23} & \mathbf{P}_{24} \\ P_{31} & \mathbf{P}_{32} & P_{33} & \mathbf{P}_{34} \\ \mathbf{P}_{41} & \mathbf{P}_{42} & \mathbf{P}_{43} & \mathbf{P}_{44} \end{bmatrix} \begin{Bmatrix} \ddot{\theta}_1 \\ \ddot{\mathbf{a}} \\ \ddot{\theta}_2 \\ \ddot{\mathbf{c}} \end{Bmatrix} = \begin{Bmatrix} f_1(\mathbf{q}, \dot{\mathbf{q}}) \\ \mathbf{f}_2(\mathbf{q}, \dot{\mathbf{q}}) \\ f_3(\mathbf{q}, \dot{\mathbf{q}}) \\ \mathbf{f}_4(\mathbf{q}, \dot{\mathbf{q}}) \end{Bmatrix} \tag{3.86}$$

Upper triangular elements of the matrix $\left[P_{ij}\right]$ because of the symmetry of the matrix and the right hand side vector in Equation 3.86 are given in Appendix A.

4. EXACT SOLUTION OF LINEARIZED MODEL

The solution of the complete nonlinear differential equations of motion describing the physical system is difficult if not impossible to find. Therefore, this chapter will first linearize the nonlinear equations of motion and their geometric and natural boundary conditions with respect to an equilibrium point of $\theta_1 = 0, w_1 = 0, \theta_2 = 0,$ and $w_2 = 0$. The linearized equations of motion and their boundary conditions for the exact solution do not include the shortening effect due to elastic deflection. Generally, the nonlinear differential equations of motion can be given in the following implicit form

$$\mathbf{S}(\mathbf{q}, \dot{\mathbf{q}})\ddot{\mathbf{q}} + \mathbf{h}(\mathbf{q}, \dot{\mathbf{q}}) = \mathbf{0} \tag{4.1}$$

The perturbation variable vector around an equilibrium point is defined as

$$\tilde{\mathbf{q}} = \mathbf{q} - (\mathbf{q})_{eq} \tag{4.2}$$

$$\dot{\tilde{\mathbf{q}}} = \dot{\mathbf{q}} - (\dot{\mathbf{q}})_{eq} = \dot{\mathbf{q}} \tag{4.3}$$

$$\ddot{\tilde{\mathbf{q}}} = \ddot{\mathbf{q}} - (\ddot{\mathbf{q}})_{eq} = \ddot{\mathbf{q}} \tag{4.4}$$

where the subscription *eq* means that a variable vector is evaluated at an equilibrium point.

Equation 4.1 is expanded using Taylor series around an equilibrium point, and

zero and first order terms of the expansion are taken. Then, Equation 4.1 becomes

$$\begin{aligned}
&\left[\mathbf{S}(\mathbf{q},\dot{\mathbf{q}})\ddot{\mathbf{q}}+\mathbf{h}(\mathbf{q},\dot{\mathbf{q}})\right]_{eq} \\
&+\left[\frac{\partial \mathbf{S}(\mathbf{q},\dot{\mathbf{q}})}{\partial \mathbf{q}}\ddot{\mathbf{q}}\right]_{eq}(\mathbf{q}-\mathbf{q}_{eq}) \\
&+\left[\frac{\partial \mathbf{S}(\mathbf{q},\dot{\mathbf{q}})}{\partial \dot{\mathbf{q}}}\ddot{\mathbf{q}}\right]_{eq}(\dot{\mathbf{q}}-\dot{\mathbf{q}}_{eq}) \\
&+\left[\mathbf{S}(\mathbf{q},\dot{\mathbf{q}})\right]_{eq}(\ddot{\mathbf{q}}-(\ddot{\mathbf{q}})_{eq}) \\
&+\left[\frac{\partial \mathbf{h}(\mathbf{q},\dot{\mathbf{q}})}{\partial \mathbf{q}}\right]_{eq}(\mathbf{q}-\mathbf{q}_{eq}) \\
&+\left[\frac{\partial \mathbf{h}(\mathbf{q},\dot{\mathbf{q}})}{\partial \dot{\mathbf{q}}}\right]_{eq}(\dot{\mathbf{q}}-\dot{\mathbf{q}}_{eq}) \cong \mathbf{0}
\end{aligned} \tag{4.5}$$

Since $\dot{\mathbf{q}}_{eq}$ and $\ddot{\mathbf{q}}_{eq}$ are zero, Equation 4.5 is given as

$$\left[\mathbf{S}(\mathbf{q},\dot{\mathbf{q}})\right]_{eq}\ddot{\tilde{\mathbf{q}}}+\left[\frac{\partial \mathbf{h}(\mathbf{q},\dot{\mathbf{q}})}{\partial \dot{\mathbf{q}}}\right]_{eq}\dot{\tilde{\mathbf{q}}}+\left[\frac{\partial \mathbf{h}(\mathbf{q},\dot{\mathbf{q}})}{\partial \mathbf{q}}\right]_{eq}\tilde{\mathbf{q}} \cong \mathbf{0} \tag{4.6}$$

If an equilibrium point $\mathbf{q}_{eq}$ is equal to zero, the perturbation variable vector $\tilde{\mathbf{q}}$ is the same as $\mathbf{q}$. The four linearized equations of motion which do not include the shortening effect are given by

$$\begin{aligned}
&K_{t_1}\theta_1+m_2g\left(w_{\ell_1}+\ell_1\theta_1\right)+m_pg\left(w_{\ell_1}+\ell_1\theta_1+w_{\ell_2}+\ell_2\theta_2+\ell_2\theta_1\right) \\
&+\left[\left(J_1+J_a+J_b+J_p\right)+\left(m_a+m_b\right)\ell_1^2+m_p\left(\ell_1^2+\ell_2^2\right)+2m_p\ell_1\ell_2\right]\ddot{\theta}_1 \\
&+\left[\left(J_b+J_p\right)+m_p\left(\ell_2^2+\ell_1\ell_2\right)\right]\ddot{\theta}_2+\left[\left(m_a+m_b\right)\ell_1+m_p\left(\ell_1+\ell_2\right)\right]\ddot{w}_{\ell_1} \\
&+m_p\left(\ell_1+\ell_2\right)\ddot{w}_{\ell_2}+J_a\ddot{w}'_{\ell_1}+J_p\ddot{w}'_{\ell_2} \\
&+\int_0^{\ell_1}(\rho A)_1\left[g\left(w_1+r_1\theta_1\right)+\left(r_1^2\ddot{\theta}_1+r_1\ddot{w}_1\right)\right]dr_1
\end{aligned} \tag{4.7}$$

$$+\int_0^{\ell_2}(\rho A)_2\Big[g\left(w_{\ell_1}+\ell_1\theta_1+w_2+r_2\theta_2+r_2\theta_1\right)$$
$$+\left(\ell_1+r_2\right)\ddot{w}_{\ell_1}+\left(\ell_1+r_2\right)\ddot{w}_2$$
$$+\left(\ell_1^2+r_2^2+2\ell_1 r_2\right)\ddot{\theta}_1+\left(r_2^2+\ell_1 r_2\right)\ddot{\theta}_2\Big]dr_2$$
$$=0$$

$$K_{t_2}\left(\theta_2-w'_{\ell_1}\right)+m_p g\left(\ell_2\theta_1+w_{\ell_2}+\ell_2\theta_2\right) \quad (4.8)$$
$$+\left[\left(J_b+J_p\right)+m_p\left(\ell_2^2+\ell_1\ell_2\right)\right]\ddot{\theta}_1+\left[\left(J_b+J_p\right)+m_p\ell_2^2\right]\ddot{\theta}_2$$
$$+m_p\ell_2\ddot{w}_{\ell_1}+m_p\ell_2\ddot{w}_{\ell_2}+J_p\ddot{w}'_{\ell_2}$$
$$+\int_0^{\ell_2}(\rho A)_2\Big[g\left(r_2\theta_1+w_2+r_2\theta_2\right)+\left(r_2^2+\ell_1 r_2\right)\ddot{\theta}_1$$
$$+r_2^2\ddot{\theta}_2+r_2\ddot{w}_2+r_2\ddot{w}_{\ell_1}\Big]dr_2$$
$$=0$$

$$(\rho A)_1\left(g\theta_1+r_1\ddot{\theta}_1+\ddot{w}_1\right)+(EI)_1 w_1^{iv} = 0 \quad (4.9)$$

$$(\rho A)_2\left[g\left(\theta_1+\theta_2\right)+\left(\ell_1+r_2\right)\ddot{\theta}_1+r_2\ddot{\theta}_2+\left(\ddot{w}_2+\ddot{w}_{\ell_1}\right)\right]+(EI)_2 w_2^{iv} = 0 \quad (4.10)$$

The geometric boundary conditions (Equations 3.67 - 3.70) are linear. However, the natural boundary conditions are nonlinear and are linearized to yield.

$$\left(m_a+m_b+m_p\right)g\theta_1-(EI)_1\left(w_1'''\right)_{r_1=\ell_1} \quad (4.11)$$
$$+\left[\left(m_a+m_b+m_p\right)\ell_1+m_p\ell_2\right]\ddot{\theta}_1+m_p\ell_2\ddot{\theta}_2$$
$$+\left(m_a+m_b+m_p\right)\ddot{w}_{\ell_1}+m_p\ddot{w}_{\ell_2}$$
$$+\int_0^{\ell_2}(\rho A)_2\left[g\theta_1+\left(\ell_1+r_2\right)\ddot{\theta}_1+r_2\ddot{\theta}_2+\ddot{w}_{\ell_1}+\ddot{w}_2\right]dr_2$$
$$=0$$

$$m_p\left[g\left(\theta_1+\theta_2\right)+\left(\ell_1+\ell_2\right)\ddot{\theta}_1+\ell_2\ddot{\theta}_2+\ddot{w}_{\ell_1}+\ddot{w}_{\ell_2}\right]-(EI)_2\left(w_2'''\right)_{r_2=\ell_2} \quad (4.12)$$
$$=0$$

$$K_{t_2}\left(w'_{\ell_1}-\theta_2\right)+J_a\left(\ddot{\theta}_1+\ddot{w}'_{\ell_1}\right)+(EI)_1\left(w''_1\right)_{r_1=\ell_1} = 0 \quad (4.13)$$

$$J_p\left(\ddot{\theta}_1+\ddot{\theta}_2+\ddot{w}'_{\ell_2}\right)+(EI)_2\left(w''_2\right)_{r_2=\ell_2} = 0 \quad (4.14)$$

Now that a linear system has been defined, an exact solution can be found. In order to simplify the derivation, the following four parameters are defined

$$\nu_1^2 = \frac{(EI)_1}{(\rho A)_1} \quad (4.15)$$

$$\alpha^4 = \frac{\omega^2}{\nu_1^2} \quad (4.16)$$

$$\nu_2^2 = \frac{(EI)_2}{(\rho A)_2} \quad (4.17)$$

$$\beta^4 = \frac{\omega^2}{\nu_2^2} \quad (4.18)$$

The flexible and rigid modes of the upper arm are expressed in separated form as

$$w_1(r_1,t) = W_1(r_1)e^{j\omega t} \quad (4.19)$$

$$\theta_1(t) = \Theta_1 e^{j\omega t} \quad (4.20)$$

Substituting Equations 4.19 and 4.20 into Equation 4.9 and rearranging yields the following fourth order ordinary differential equation.

$$\frac{d^4W_1}{dr_1^4}-\frac{\omega^2}{\nu_1^2}W_1=\frac{\Theta_1}{\nu_1^2}\left(r_1\omega^2-g\right) \quad (4.21)$$

The particular solution of Equation 4.21 is

$$(W_1)_p=\Theta_1\left(\frac{g}{\omega^2}-r_1\right) \quad (4.22)$$

And, the homogeneous solution is

$$(W_1)_h = b_1 cosh(\alpha r_1)+b_2 sinh(\alpha r_1)+b_3 cos(\alpha r_1)+b_4 sin(\alpha r_1) \quad (4.23)$$

The general solution of Equation 4.11 is obtained by summing Equations 4.22 and 4.23.

$$W_1(r_1) = b_1 cosh(\alpha r_1) + b_2 sinh(\alpha r_1) + b_3 cos(\alpha r_1) + b_4 sin(\alpha r_1) + \Theta_1\left(\frac{g}{\omega^2} - r_1\right) \tag{4.24}$$

Similarly, for the lower arm, the rigid and flexible modes are given in separated form as

$$w_2(r_2,t) = W_2(r_2)e^{j\omega t} \tag{4.25}$$

$$\theta_2(t) = \Theta_2 e^{j\omega t} \tag{4.26}$$

Substituting Equations 4.25 and 4.26 into Equation 4.10 and rearranging yields the following fourth order ordinary differential equation.

$$\frac{d^4W_2}{dr_2^4} - \frac{\omega^2}{\nu_2^2}W_2 = \frac{1}{\nu_2^2}\Big[-g\big(\Theta_1+\Theta_2\big) + \omega^2\ell_1\Theta_1 + \omega^2 W_{\ell_1} + \omega^2\big(\Theta_1+\Theta_2\big)r_2\Big] \tag{4.27}$$

The particular solution of Equation 4.27 is given by

$$(W_2)_p = -\big(\Theta_1+\Theta_2\big)r_2 + \frac{g}{\omega^2}\Theta_2 - b_1 cosh(\alpha\ell_1) - b_2 sinh(\alpha\ell_1) - b_3 cos(\alpha\ell_1) - b_4 sin(\alpha\ell_1) \tag{4.28}$$

And, the homogeneous solution is given by

$$(W_2)_h = d_1 cosh(\beta r_2) + d_2 sinh(\beta r_2) + d_3 cos(\beta r_2) + d_4 sin(\beta r_2) \tag{4.29}$$

The general solution of Equation 4.27 is obtained by summing Equations 4.28 and 4.29.

$$W_2(r_2) = d_1 cosh(\beta r_2) + d_2 sinh(\beta r_2) + d_3 cos(\beta r_2) + d_4 sin(\beta r_2) - \big(\Theta_1+\Theta_2\big)r_2 + \frac{g}{\omega^2}\Theta_2 - b_1 cosh(\alpha\ell_1) - b_2 sinh(\alpha\ell_1) - b_3 cos(\alpha\ell_1) - b_4 sin(\alpha\ell_1) \tag{4.30}$$

Substituting Equations 4.24 and 4.30 into the four geometric boundary conditions (Equations 3.67 - 3.70), the four linearized natural boundary conditions (Equations 4.11 - 4.14), and the other two linearized equations of motion (Equations 4.7 and 4.8) yields ten equations which can be arranged in the following homogeneous matrix system.

$$\begin{bmatrix} S_{11} & 1 & 0 & 1 & 0 & 0 & 0 & 0 & 0 & 0 \\ -1 & 0 & S_{23} & 0 & S_{25} & 0 & 0 & 0 & 0 & 0 \\ 0 & S_{32} & S_{33} & S_{34} & S_{35} & S_{36} & 1 & 0 & 1 & 0 \\ -1 & 0 & 0 & 0 & 0 & -1 & 0 & S_{48} & 0 & S_{410} \\ 0 & S_{52} & S_{53} & S_{54} & S_{55} & S_{56} & S_{57} & S_{58} & S_{59} & S_{510} \\ S_{61} & S_{62} & S_{63} & S_{64} & S_{65} & S_{66} & 0 & 0 & 0 & 0 \\ 0 & 0 & 0 & 0 & 0 & 0 & S_{77} & S_{78} & S_{79} & S_{710} \\ 0 & 0 & 0 & 0 & 0 & 0 & S_{87} & S_{88} & S_{89} & S_{810} \\ S_{91} & S_{92} & S_{93} & S_{94} & S_{95} & S_{96} & S_{97} & S_{98} & S_{99} & S_{910} \\ S_{101} & S_{102} & S_{103} & S_{104} & S_{105} & S_{106} & S_{107} & S_{108} & S_{109} & S_{1010} \end{bmatrix} \begin{Bmatrix} \Theta_1 \\ b_1 \\ b_2 \\ b_3 \\ b_4 \\ \Theta_2 \\ d_1 \\ d_2 \\ d_3 \\ d_4 \end{Bmatrix} = 0 \tag{4.31}$$

Nonzero elements of the matrix $[S_{ij}]$ are given in Appendix B.

In order to have a nontrivial solution of the unknowns (Θ_1, b_1, b_2, b_3, b_4,Θ_2, d_1, d_2, d_3, d_4), the determinant of the characteristic matrix $[S_{ij}]$ must be zero.

$$det\,[S_{ij}] = 0 \tag{4.32}$$

This yields the nonlinear algebraic characteristic equation. The eigenvalues are found by solving the nonlinear algebraic characteristic equation. Since the characteristic equation is a highly nonlinear algebraic equation, it is almost impossible to get an

explicit analytical solution for the system eigenvalues. Thus, the solution of the nonlinear characteristic equation is found numerically. Two methods for finding the eigenvectors are presented in Appendix C.

5. DEVELOPMENT OF ASSUMED MODE SHAPES

Approximate solutions using the Rayleigh-Ritz method and a finite set of basis functions, often referred to as assumed mode shapes are used because exact solutions are unavailable. The accuracy of the approximate solution is greatly dependent on the assumed mode shapes used to approximate the elastic behavior of elastic arms. Ideally, exact mode shapes (eigenfunctions) which satisfy governing partial differential equations of motion and their geometric and natural boundary conditions should be used to represent the elastic behavior. However, it is not always possible to find exact mode shapes as the analytical model is often complicate. Thus, assumed mode shapes are used instead of exact mode shapes. Even though assumed mode shapes are required to satisfy the geometric boundary conditions as a minimum, the selection of assumed mode shapes directly affects the accuracy of the model.

This chapter develops a set of assumed mode shapes which satisfies all geometric and natural boundary conditions for a single cantilever beam with end mass. In this thesis, these assumed mode shapes are referred to as modified comparison function. The modified comparison functions consider each elastic arm separately. These shapes are used twice once each for the top and bottom arms. When finding the upper arm mode shapes however, the end mass and end mass moment of inertia are modified to approximate the mass contribution from the lower arm. Each arm is assumed

to be fixed at one end with the other end having end mass. Geometric boundary conditions for one arm are easily derived from Equations 3.67 - 3.70 by eliminating terms from the lower arm. The linearized natural boundary conditions are obtained from Equations 4.11 - 4.14 by eliminating terms and conditions corresponding to the lower arm.

The boundary conditions of the one arm model are given as :

$$w_{r=0} = 0 \tag{5.1}$$

$$w'_{r=0} = 0 \tag{5.2}$$

$$EI\left(w''\right)_{r=\ell} + J_a\left(\ddot{w}'\right)_{r=\ell} = 0 \tag{5.3}$$

$$EI\left(w'''\right)_{r=\ell} - m_a\left(\ddot{w}\right)_{r=\ell} = 0 \tag{5.4}$$

The flexible mode of each arm is expressed in separated form as

$$w\left(r,t\right) = \phi(r)e^{j\omega t} \tag{5.5}$$

The mode shape $\phi(r)$ is assumed as

$$\phi(r) = D_1 cosh\left(\beta r\right) + D_2 sinh\left(\beta r\right) + D_3 cos\left(\beta r\right) + D_4 sin\left(\beta r\right) \tag{5.6}$$

where β is defined as

$$\beta^4 = \rho A\left(\frac{\omega^2}{EI}\right) \tag{5.7}$$

Substituting Equations 5.5 and 5.6 into boundary conditions given in Equations 5.1 - 5.4 yields the following nonlinear algebraic characteristic equation.

$$\left(\frac{m_a}{\rho A\ell}\right)\left[tan\left(\beta\ell\right) - tanh\left(\beta\ell\right)\right] + \left(\frac{J_a}{\rho A\ell^3}\right)\left(\beta\ell\right)^2\left[tan\left(\beta\ell\right) + tanh\left(\beta\ell\right)\right] \tag{5.8}$$

$$-\left(\frac{m_a}{\rho A\ell}\right)\left(\frac{J_a}{\rho A\ell^3}\right)(\beta\ell)^3\left[\frac{1}{\cosh(\beta\ell)\cos(\beta\ell)}-1\right]$$
$$-\left(\frac{1}{\beta\ell}\right)\left[\frac{1}{\cosh(\beta\ell)\cos(\beta\ell)}+1\right]$$
$$=0$$

First, the characteristic value β is found by solving the nonlinear algebraic Equation 5.8. Then, the coefficients (D_1, D_2, D_3 and D_4) are found by the following relationships given from Equations 5.1 - 5.4 after assigning a value for any one unknown arbitrarily.

$$D_1 = -D_3 \tag{5.9}$$

$$D_2 = -D_4 \tag{5.10}$$

$$D_1 = \frac{\left[-\left(\sinh\beta\ell+\sin\beta\ell\right)+\left(\frac{J_a}{\rho A\ell^3}\right)(\beta\ell)^3\left(\cosh\beta\ell-\cos\beta\ell\right)\right]}{\left[\left(\cosh\beta\ell+\cos\beta\ell\right)-\left(\frac{J_a}{\rho A\ell^3}\right)(\beta\ell)^3\left(\sinh\beta\ell+\sin\beta\ell\right)\right]}D_2 \tag{5.11}$$

In the development of an mode shape for the upper arm, end mass of the upper arm adds mass of the lower arm to approximate lower arm.

$$\bar{m}_a = m_a + m_b + (\rho A)_2\,\ell_2 + m_p \tag{5.12}$$

The radius of gyration of end mass m_a before mass of the lower arm is added is defined as

$$r_g^2 = \frac{J_a}{m_a} \tag{5.13}$$

End mass moment of inertia of the upper arm is modified according to new end mass given in Equation 5.12 and it is given as

$$\bar{J}_a = r_g^2 \times \bar{m}_a \tag{5.14}$$

where r_g^2 is defined in Equation 5.13.

The modified end mass $\bar{m}_a$ and end mass moment of inertia $\bar{J}_a$ are used in place of m_a and J_a in Equations 5.8 and 5.11 to derive assumed mode shapes for the upper arm. For the derivation of assumed mode shapes of the lower arm, the lower arm's end mass m_p and end mass moment of inertia J_p are used in place of m_a and J_a in Equations 5.8 and 5.11. If two arms have different physical and mechanical properties, in equations given in the above development, the different values of ρ, A, ℓ, E and I must be used in each arm.

6. EIGENVALUE ANALYSIS

This chapter compares eigenvalues calculated using the exact solution presented in Chapter 4 with eigenvalues calculated using the assumed modes method. The primary objective of this chapter is to determine the number of mode shapes required to accurately model the system. Therefore, eigenvalues are computed for the assumed modes model for 2, 4 and 6 assumed mode shapes.

In order to find eigenvalues using the assumed modes method, Equation 3.86 is linearized at the vertical equilibrium position which corresponds to zero generalized coordinates($\mathbf{q} = 0$) where $\mathbf{q}$ is defined in Equation 3.84. The general form of the linearized equations of motion is given by the following matrix equation.

$$\mathbf{M}\,\ddot{\mathbf{q}} + \mathbf{K}\,\mathbf{q} = \mathbf{0} \tag{6.1}$$

$\mathbf{M}$ and $\mathbf{K}$ are symmetric, and the upper triangular elements including the shortening effect due to elastic deflection are given in Appendix D. The modified comparison functions developed in Chapter 5 are used as the assumed mode shapes in Equation 6.1.

Eigenvalues are found from Equation 6.1 for three models with 2, 4 and 6 assumed mode shapes. For the comparison, six sets of the upper and lower torsion springs given in Table 6.1 and four different end masses given in Table 6.2 are used. The other physical and mechanical properties of the two elastic arm system are given in

Table 6.1: Six sets of torsional springs

unit : lb_f-in-rad^{-1}

	UPPER (K_{t_1})	LOWER (K_{t_2})
Set 1	10.0000	10.0000
Set 2	60.0000	60.0000
Set 3	120.0000	120.0000
Set 4	180.0000	180.0000
Set 5	60.0000	120.0000
Set 6	120.0000	60.0000

Table 6.3.

Tables 6.4 - 6.15 present the comparisons of the eigenvalues. The eigenvalues from the assumed modes method are calculated with three cases which have three, two and one flexible modes for each arm. For these comparisons, the shortening effect is not included. The eigenvalues given in parentheses in the three mode frequency column represent eigenvalues calculated using the assumed modes method including the shortening effect.

Relative error is calculated using the following equations.

$$\text{ABS. ERROR(Hz)} = \text{EXACT FREQ.} - \text{ASSUMED MODE FREQ.} \quad (6.2)$$

$$\text{REL. ERROR(\%)} = \frac{\text{ABSOLUTE ERROR}}{\text{EXACT FREQ.}} \times 100 \quad (6.3)$$

As the tables indicate, when three assumed modes are used for each arm in the assumed modes method, there is good agreement between eigenvalues with a maximum relative error of 1.75% in the sixth eigenvalue for torsion spring set 4 and end mass 4. Up through the third eigenvalue, the two methods yield almost identical

Table 6.2: Four end masses

unit : $m_p = lb_f\text{-}in^{-1}\text{-}sec^2$
$J_p = lb_f\text{-}in\text{-}sec^2$

END MASS	MASS (m_p)	MASS MOMENT OF INERTIA (J_p)
Mass 1	1.051×10^{-4}	1.110×10^{-5}
Mass 2	4.482×10^{-4}	1.078×10^{-4}
Mass 3	5.761×10^{-4}	1.385×10^{-4}
Mass 4	7.475×10^{-4}	1.783×10^{-4}

Table 6.3: Dimensions and mechanical properties of an elastic two-arm system

PROPERTY	UPPER ARM	LOWER ARM	UNIT
Length	$L_1 = 9.0$	$L_2 = 19.0$	in
Density	$\rho_1 = 2.538 \times 10^{-4}$	$\rho_2 = 2.538 \times 10^{-4}$	$lb_f\text{-}sec^2\text{-}in^{-4}$
Modulus of Elasticity	$E_1 = 1.000 \times 10^7$	$E_2 = 1.000 \times 10^7$	$lb_f\text{-}in^{-2}$
Area Moment of Inertia	$I_1 = 1.501 \times 10^{-5}$	$I_2 = 1.505 \times 10^{-5}$	in^4
Area	$A_1 = 4.656 \times 10^{-2}$	$A_2 = 4.668 \times 10^{-2}$	in^2
Mass Moment of Inertia	$J_a = 2.1854 \times 10^{-4}$	$J_b = 2.3937 \times 10^{-4}$	$lb_f\text{-}in\text{-}sec^2$
Mass	$m_a = 1.8395 \times 10^{-4}$	$m_b = 2.1861 \times 10^{-4}$	$lb_f\text{-}in^{-1}\text{-}sec^2$
Mass Moment of Inertia	$J_1 = 1.743 \times 10^{-3}$	$J_p = 1.110 \times 10^{-5}$	$lb_f\text{-}in\text{-}sec^2$
Mass		$m_p = 1.051 \times 10^{-4}$	$lb_f\text{-}in^{-1}\text{-}sec^2$

results with almost zero relative error. Larger end mass results in more error between the two methods in most cases.

When two assumed mode shapes are used for each arm, six eigenvalues are found. Up through the third eigenvalue, there is good agreement between eigenvalues with a maximum relative error of 0.04%. The fourth eigenvalue from the assumed modes method has a maximum relative error of 4.17%. As it is expected, the last two eigenvalues have large errors.

When one assumed mode shape is used for each arm, four eigenvalues are found. The assumed modes method has a maximum relative error of 3.15% in the first eigenvalue and has a maximum relative error of 7.71% in the second eigenvalue. The last two eigenvalues (third and fourth eigenvalues) have large errors compared to eigenvalues calculated using the exact solution. In the first two eigenvalues, smaller end mass results in more error between the two methods in all cases.

In general, eigenvalues calculated using the assumed modes method show slightly larger values than those calculated using the exact solution. The last two eigenvalues from the assumed modes method are not reliable. Eigenvalues are increased by including the shortening effect due to elastic deflection.

Table 6.4: Comparison of the first natural frequency with torsional spring set 1, 2 and 3

Torsion spring set 1

END MASS	EXACT FREQ. (Hz)	THREE MODE FREQ. (HZ)	REL. ERR. (%)	TWO MODE (Hz)	REL. ERR. (%)	ONE MODE (HZ)	REL. ERR. (%)
Mass 1	1.0949	1.0949 (1.1005)	0.00	1.0949	0.00	1.1030	-0.74
Mass 2	0.8283	0.8283 (0.8341)	0.00	0.8283	0.00	0.8324	-0.49
Mass 3	0.7912	0.7912 (0.7971)	0.00	0.7912	0.00	0.7945	-0.42
Mass 4	0.7573	0.7573 (0.7632)	0.00	0.7573	0.00	0.7598	-0.33

Torsion spring set 2

END MASS	EXACT FREQ. (Hz)	THREE MODE FREQ. (HZ)	REL. ERR. (%)	TWO MODE (Hz)	REL. ERR. (%)	ONE MODE (HZ)	REL. ERR. (%)
Mass 1	1.5073	1.5073 (1.5331)	0.00	1.5075	-0.01	1.5442	-2.45
Mass 2	1.0306	1.0306 (1.0580)	0.00	1.0307	-0.01	1.0500	-1.88
Mass 3	0.9624	0.9624 (0.9906)	0.00	0.9624	0.00	0.9784	-1.66
Mass 4	0.8992	0.8992 (0.9283)	0.00	0.8992	0.00	0.9117	-1.39

Torsion spring set 3

END MASS	EXACT FREQ. (Hz)	THREE MODE FREQ. (HZ)	REL. ERR. (%)	TWO MODE (Hz)	REL. ERR. (%)	ONE MODE (HZ)	REL. ERR. (%)
Mass 1	1.6088	1.6088 (1.6425)	0.00	1.6091	-0.01	1.6572	-3.01
Mass 2	1.0797	1.0797 (1.1152)	0.00	1.0798	-0.01	1.1050	-2.34
Mass 3	1.0039	1.0039 (1.0405)	0.00	1.0039	0.00	1.0246	-2.06
Mass 4	0.9334	0.9334 (0.9714)	0.00	0.9334	0.00	0.9497	-1.75

Table 6.5: Comparison of the first natural frequency with torsional spring set 4, 5 and 6

Torsion spring set 4

END MASS	EXACT FREQ. (Hz)	THREE MODE FREQ. (HZ)	REL. ERR. (%)	TWO MODE (Hz)	REL. ERR. (%)	ONE MODE (HZ)	REL. ERR. (%)
Mass 1	1.6492	1.6492 (1.6864)	0.00	1.6495	-0.02	1.7028	-3.25
Mass 2	1.0991	1.0991 (1.1382)	0.00	1.0992	-0.01	1.1269	-2.53
Mass 3	1.0202	1.0202 (1.0606)	0.00	1.0203	-0.01	1.0431	-2.24
Mass 4	0.9469	0.9469 (0.9888)	0.00	0.9469	0.00	0.9648	-1.89

Torsion spring set 5

END MASS	EXACT FREQ. (Hz)	THREE MODE FREQ. (HZ)	REL. ERR. (%)	TWO MODE (Hz)	REL. ERR. (%)	ONE MODE (HZ)	REL. ERR. (%)
Mass 1	1.5290	1.5290 (1.5564)	0.00	1.5292	-0.01	1.5681	-2.56
Mass 2	1.0421	1.0421 (1.0714)	0.00	1.0421	0.00	1.0631	-2.02
Mass 3	0.9718	0.9718 (1.0021)	0.00	0.9719	-0.01	0.9891	-1.78
Mass 4	0.9066	0.9066 (0.9380)	0.00	0.9066	0.00	0.9202	-1.50

Torsion spring set 6

END MASS	EXACT FREQ. (Hz)	THREE MODE FREQ. (HZ)	REL. ERR. (%)	TWO MODE (Hz)	REL. ERR. (%)	ONE MODE (HZ)	REL. ERR. (%)
Mass 1	1.5823	1.5823 (1.6138)	0.00	1.5825	-0.01	1.6275	-2.86
Mass 2	1.0660	1.0660 (1.0989)	0.00	1.0661	-0.01	1.0893	-2.19
Mass 3	0.9926	0.9926 (1.0265)	0.00	0.9927	-0.01	1.0117	-1.92
Mass 4	0.9246	0.9246 (0.9597)	0.00	0.9246	0.00	0.9394	-1.60

Table 6.6: Comparison of the second natural frequency with torsional spring set 1, 2 and 3

Torsion spring set 1

END MASS	EXACT FREQ. (Hz)	THREE MODE FREQ. (HZ)	REL. ERR. (%)	TWO MODE (Hz)	REL. ERR. (%)	ONE MODE (HZ)	REL. ERR. (%)
Mass 1	4.2473	4.2474 (4.2763)	0.00	4.2480	-0.02	4.3855	-3.25
Mass 2	4.0326	4.0327 (4.1171)	0.00	4.0330	-0.01	4.1355	-2.55
Mass 3	4.0290	4.0290 (4.1358)	0.00	4.0293	-0.01	4.1255	-2.40
Mass 4	4.0354	4.0355 (4.1741)	0.00	4.0357	-0.01	4.1246	-2.21

Torsion spring set 2

END MASS	EXACT FREQ. (Hz)	THREE MODE FREQ. (HZ)	REL. ERR. (%)	TWO MODE (Hz)	REL. ERR. (%)	ONE MODE (HZ)	REL. ERR. (%)
Mass 1	6.6039	6.6041 (6.7168)	0.00	6.6063	-0.04	7.0476	-6.72
Mass 2	6.0497	6.0498 (6.3449)	0.00	6.0509	-0.02	6.3465	-4.91
Mass 3	5.9698	5.9699 (6.3354)	0.00	5.9709	-0.02	6.2404	-4.53
Mass 4	5.8816	5.8817 (6.3447)	0.00	5.8826	-0.02	6.1221	-4.09

Torsion spring set 3

END MASS	EXACT FREQ. (Hz)	THREE MODE FREQ. (HZ)	REL. ERR. (%)	TWO MODE (Hz)	REL. ERR. (%)	ONE MODE (HZ)	REL. ERR. (%)
Mass 1	7.2508	7.2510 (7.4037)	0.00	7.2538	-0.04	7.7839	-7.35
Mass 2	6.6016	6.6017 (6.9819)	0.00	6.6032	-0.02	6.9496	-5.27
Mass 3	6.5001	6.5003 (6.9674)	0.00	6.5016	-0.02	6.8155	-4.85
Mass 4	6.3852	6.3854 (6.9722)	0.00	6.3866	-0.02	6.6634	-4.36

Table 6.7: Comparison of the second natural frequency with torsional spring set 4, 5 and 6

Torsion spring set 4

END MASS	EXACT FREQ. (Hz)	THREE MODE FREQ. (HZ)	REL. ERR. (%)	TWO MODE (Hz)	REL. ERR. (%)	ONE MODE (HZ)	REL. ERR. (%)
Mass 1	7.5236	7.5238 (7.6967)	0.00	7.5269	-0.04	8.0931	-7.57
Mass 2	6.8334	6.8336 (7.2540)	0.00	6.8351	-0.02	7.2018	-5.39
Mass 3	6.7226	6.7228 (7.2376)	0.00	6.7242	-0.02	7.0588	-4.96
Mass 4	6.5962	6.5965 (7.2408)	0.00	6.5978	-0.02	6.8893	-4.44

Torsion spring set 5

END MASS	EXACT FREQ. (Hz)	THREE MODE FREQ. (HZ)	REL. ERR. (%)	TWO MODE (Hz)	REL. ERR. (%)	ONE MODE (HZ)	REL. ERR. (%)
Mass 1	6.8054	6.8055 (6.9329)	0.00	6.8081	-0.04	7.3306	-7.71
Mass 2	6.1761	6.1763 (6.5089)	0.00	6.1775	-0.02	6.5180	-5.54
Mass 3	6.0831	6.0832 (6.4947)	0.00	6.0843	-0.02	6.3926	-5.09
Mass 4	5.9799	5.9800 (6.5003)	0.00	5.9810	-0.02	6.2524	-4.56

Torsion spring set 6

END MASS	EXACT FREQ. (Hz)	THREE MODE FREQ. (HZ)	REL. ERR. (%)	TWO MODE (Hz)	REL. ERR. (%)	ONE MODE (HZ)	REL. ERR. (%)
Mass 1	7.0533	7.0535 (7.1922)	0.00	7.0559	-0.04	7.5041	-6.39
Mass 2	6.4797	6.4799 (6.8226)	0.00	6.4812	-0.02	6.7829	-4.68
Mass 3	6.3913	6.3915 (6.8126)	0.00	6.3927	-0.02	6.6682	-4.33
Mass 4	6.2914	6.2916 (6.8210)	0.00	6.2927	-0.02	6.5379	-3.92

Table 6.8: Comparison of the third natural frequency with torsional spring set 1, 2 and 3

Torsion spring set 1

END MASS	EXACT FREQ. (Hz)	THREE MODE FREQ. (HZ)	REL. ERR. (%)	TWO MODE (Hz)	REL. ERR. (%)	ONE MODE (HZ)	REL. ERR. (%)
Mass 1	19.326	19.326 (19.677)	0.00	19.334	-0.04	24.471	-26.62
Mass 2	17.270	17.270 (18.195)	0.00	17.277	-0.04	21.916	-26.90
Mass 3	16.936	16.937 (18.083)	-0.01	16.943	-0.04	21.420	-26.48
Mass 4	16.553	16.553 (18.000)	0.00	16.560	-0.04	20.830	-25.84

Torsion spring set 2

END MASS	EXACT FREQ. (Hz)	THREE MODE FREQ. (HZ)	REL. ERR. (%)	TWO MODE (Hz)	REL. ERR. (%)	ONE MODE (HZ)	REL. ERR. (%)
Mass 1	22.413	22.414 (22.628)	0.00	22.416	-0.01	33.461	-49.29
Mass 2	20.612	20.612 (21.140)	0.00	20.614	-0.01	31.923	-54.88
Mass 3	20.363	20.363 (21.008)	0.00	20.364	0.00	31.639	-55.37
Mass 4	20.094	20.094 (20.894)	0.00	20.096	-0.01	31.311	-55.82

Torsion spring set 3

END MASS	EXACT FREQ. (Hz)	THREE MODE FREQ. (HZ)	REL. ERR. (%)	TWO MODE (Hz)	REL. ERR. (%)	ONE MODE (HZ)	REL. ERR. (%)
Mass 1	23.638	23.638 (23.810)	0.00	23.640	-0.01	41.639	-76.15
Mass 2	21.855	21.855 (22.281)	0.00	21.856	0.00	40.255	-84.19
Mass 3	21.618	21.618 (22.137)	0.00	21.619	0.00	40.016	-85.11
Mass 4	21.366	21.367 (22.008)	0.00	21.367	0.00	39.748	-86.03

Table 6.9: Comparison of the third natural frequency with torsional spring set 4, 5 and 6

Torsion spring set 4

END MASS	EXACT FREQ. (Hz)	THREE MODE FREQ. (HZ)	REL. ERR. (%)	TWO MODE (Hz)	REL. ERR. (%)	ONE MODE (HZ)	REL. ERR. (%)
Mass 1	24.199	24.199 (24.357)	0.00	24.201	-0.01	48.480	-100.34
Mass 2	22.416	22.416 (22.806)	0.00	22.417	0.00	47.109	-110.16
Mass 3	22.182	22.182 (22.657)	0.00	22.182	0.00	46.884	-111.36
Mass 4	21.934	21.934 (22.520)	0.00	21.934	0.00	46.637	-112.62

Torsion spring set 5

END MASS	EXACT FREQ. (Hz)	THREE MODE FREQ. (HZ)	REL. ERR. (%)	TWO MODE (Hz)	REL. ERR. (%)	ONE MODE (HZ)	REL. ERR. (%)
Mass 1	23.115	23.115 (23.314)	0.00	23.117	-0.01	34.430	-48.95
Mass 2	21.360	21.361 (21.830)	0.00	21.361	0.00	33.403	-56.38
Mass 3	21.123	21.123 (21.693)	0.00	21.124	0.00	33.201	-57.18
Mass 4	20.869	20.869 (21.572)	0.00	20.870	0.00	32.964	-57.96

Torsion spring set 6

END MASS	EXACT FREQ. (Hz)	THREE MODE FREQ. (HZ)	REL. ERR. (%)	TWO MODE (Hz)	REL. ERR. (%)	ONE MODE (HZ)	REL. ERR. (%)
Mass 1	22.818	22.818 (23.012)	0.00	22.821	-0.01	38.406	-68.31
Mass 2	21.004	21.004 (21.496)	0.00	21.005	0.00	36.101	-71.88
Mass 3	20.757	20.757 (21.359)	0.00	20.758	0.00	35.734	-72.15
Mass 4	20.492	20.492 (21.240)	0.00	20.493	0.00	35.325	-72.38

Table 6.10: Comparison of the fourth natural frequency with torsional spring set 1, 2 and 3

Torsion spring set 1

END MASS	EXACT FREQ. (Hz)	THREE MODE FREQ. (HZ)	REL. ERR. (%)	TWO MODE (Hz)	REL. ERR. (%)	ONE MODE (HZ)	REL. ERR. (%)
Mass 1	28.797	28.798 (29.534)	0.00	28.831	-0.12	30.167	-4.76
Mass 2	28.432	28.433 (29.516)	0.00	28.465	-0.12	29.318	-3.12
Mass 3	28.317	28.317 (29.528)	0.00	28.349	-0.11	29.156	-2.96
Mass 4	28.165	28.166 (29.549)	0.00	28.197	-0.11	28.957	-2.81

Torsion spring set 2

END MASS	EXACT FREQ. (Hz)	THREE MODE FREQ. (HZ)	REL. ERR. (%)	TWO MODE (Hz)	REL. ERR. (%)	ONE MODE (HZ)	REL. ERR. (%)
Mass 1	39.128	39.132 (39.684)	-0.01	39.269	-0.36	49.179	-25.69
Mass 2	38.655	38.663 (39.507)	-0.02	38.824	-0.44	47.300	-22.36
Mass 3	38.522	38.530 (39.485)	-0.02	38.698	-0.46	47.044	-22.12
Mass 4	38.347	38.358 (39.462)	-0.03	38.537	-0.50	46.765	-21.95

Torsion spring set 3

END MASS	EXACT FREQ. (Hz)	THREE MODE FREQ. (HZ)	REL. ERR. (%)	TWO MODE (Hz)	REL. ERR. (%)	ONE MODE (HZ)	REL. ERR. (%)
Mass 1	47.306	47.320 (47.793)	-0.03	47.720	-0.88	65.318	-38.08
Mass 2	46.582	46.609 (47.400)	-0.06	47.176	-1.28	62.896	-35.02
Mass 3	46.372	46.402 (47.318)	-0.06	47.022	-1.40	62.596	-34.99
Mass 4	46.086	46.126 (47.215)	-0.09	46.821	-1.59	62.283	-35.15

Table 6.11: Comparison of the fourth natural frequency with torsional spring set 4, 5 and 6

Torsion spring set 4

END MASS	EXACT FREQ. (Hz)	THREE MODE FREQ. (HZ)	REL. ERR. (%)	TWO MODE (Hz)	REL. ERR. (%)	ONE MODE (HZ)	REL. ERR. (%)
Mass 1	53.081	53.117 (53.558)	-0.07	54.164	-2.04	78.218	-47.36
Mass 2	51.704	51.769 (52.615)	-0.13	53.381	-3.24	75.377	-45.79
Mass 3	51.303	51.376 (52.381)	-0.14	53.161	-3.62	75.041	-46.27
Mass 4	50.757	50.847 (52.067)	-0.18	52.873	-4.17	74.699	-47.17

Torsion spring set 5

END MASS	EXACT FREQ. (Hz)	THREE MODE FREQ. (HZ)	REL. ERR. (%)	TWO MODE (Hz)	REL. ERR. (%)	ONE MODE (HZ)	REL. ERR. (%)
Mass 1	39.511	39.517 (40.065)	-0.02	39.676	-0.42	63.629	-61.04
Mass 2	38.949	38.959 (39.813)	-0.03	39.149	-0.51	60.775	-56.04
Mass 3	38.797	38.808 (39.778)	-0.03	39.007	-0.54	60.416	-55.72
Mass 4	38.599	38.613 (39.741)	-0.04	38.826	-0.59	60.042	-55.55

Torsion spring set 6

END MASS	EXACT FREQ. (Hz)	THREE MODE FREQ. (HZ)	REL. ERR. (%)	TWO MODE (Hz)	REL. ERR. (%)	ONE MODE (HZ)	REL. ERR. (%)
Mass 1	47.110	47.121 (47.591)	-0.02	47.469	-0.76	53.194	-12.91
Mass 2	46.483	46.506 (47.277)	-0.05	47.005	-1.12	52.156	-12.20
Mass 3	46.294	46.320 (47.210)	-0.06	46.869	-1.24	52.005	-12.33
Mass 4	46.033	46.068 (47.125)	-0.08	46.690	-1.43	51.836	-12.61

Table 6.12: Comparison of the fifth natural frequency with torsional spring set 1, 2 and 3

Torsion spring set 1

END MASS	EXACT FREQ. (Hz)	THREE MODE FREQ. (HZ)	REL. ERR. (%)	TWO MODE (Hz)	REL. ERR. (%)	ONE MODE (HZ)	REL. ERR. (%)
Mass 1	58.185	58.322 (58.846)	-0.24	65.284	-12.20	——	——
Mass 2	53.967	54.132 (55.406)	-0.31	61.487	-13.93	——	——
Mass 3	52.970	53.147 (54.678)	-0.33	60.550	-14.31	——	——
Mass 4	51.728	51.918 (53.775)	-0.37	59.362	-14.76	——	——

Torsion spring set 2

END MASS	EXACT FREQ. (Hz)	THREE MODE FREQ. (HZ)	REL. ERR. (%)	TWO MODE (Hz)	REL. ERR. (%)	ONE MODE (HZ)	REL. ERR. (%)
Mass 1	61.683	61.797 (62.228)	-0.18	68.609	-11.23	——	——
Mass 2	57.942	58.074 (59.040)	-0.23	65.992	-13.89	——	——
Mass 3	57.030	57.169 (58.312)	-0.24	65.336	-14.56	——	——
Mass 4	55.883	56.030 (57.389)	-0.26	64.496	-15.41	——	——

Torsion spring set 3

END MASS	EXACT FREQ. (Hz)	THREE MODE FREQ. (HZ)	REL. ERR. (%)	TWO MODE (Hz)	REL. ERR. (%)	ONE MODE (HZ)	REL. ERR. (%)
Mass 1	63.317	63.412 (63.808)	-0.15	69.832	-10.29	——	——
Mass 2	60.010	60.110 (60.923)	-0.17	67.626	-12.69	——	——
Mass 3	59.208	59.310 (60.251)	-0.17	67.081	-13.30	——	——
Mass 4	58.206	58.307 (59.398)	-0.17	66.387	-14.06	——	——

Table 6.13: Comparison of the fifth natural frequency with torsional spring set 4, 5 and 6

Torsion spring set 4

END MASS	EXACT FREQ. (Hz)	THREE MODE FREQ. (HZ)	REL. ERR. (%)	TWO MODE (Hz)	REL. ERR. (%)	ONE MODE (HZ)	REL. ERR. (%)
Mass 1	65.377	65.447 (65.809)	-0.11	71.258	-9.00	——	——
Mass 2	62.772	62.828 (63.475)	-0.09	69.415	-10.58	——	——
Mass 3	62.164	62.215 (62.942)	-0.08	68.970	-10.95	——	——
Mass 4	61.420	61.464 (62.276)	-0.07	68.409	-11.38	——	——

Torsion spring set 5

END MASS	EXACT FREQ. (Hz)	THREE MODE FREQ. (HZ)	REL. ERR. (%)	TWO MODE (Hz)	REL. ERR. (%)	ONE MODE (HZ)	REL. ERR. (%)
Mass 1	62.503	62.608 (63.016)	-0.17	69.130	-10.60	——	——
Mass 2	58.970	59.088 (59.971)	-0.20	66.805	-13.29	——	——
Mass 3	58.099	58.223 (59.260)	-0.21	66.227	-13.99	——	——
Mass 4	56.999	57.128 (58.352)	-0.23	65.488	-14.89	——	——

Torsion spring set 6

END MASS	EXACT FREQ. (Hz)	THREE MODE FREQ. (HZ)	REL. ERR. (%)	TWO MODE (Hz)	REL. ERR. (%)	ONE MODE (HZ)	REL. ERR. (%)
Mass 1	62.357	62.463 (62.883)	-0.17	69.231	-11.02	——	——
Mass 2	58.818	58.933 (59.833)	-0.20	66.712	-13.42	——	——
Mass 3	57.972	58.090 (59.141)	-0.20	66.085	-13.99	——	——
Mass 4	56.921	57.041 (58.269)	-0.21	65.284	-14.69	——	——

Table 6.14: Comparison of the sixth natural frequency with torsional spring set 1, 2 and 3

Torsion spring set 1

END MASS	EXACT FREQ. (Hz)	THREE MODE FREQ. (HZ)	REL. ERR. (%)	TWO MODE (Hz)	REL. ERR. (%)	ONE MODE (HZ)	REL. ERR. (%)
Mass 1	81.086	81.116 (81.340)	-0.04	83.370	-2.82	——	——
Mass 2	80.747	80.812 (81.144)	-0.08	83.460	-3.36	——	——
Mass 3	80.646	80.708 (81.085)	-0.08	83.495	-3.53	——	——
Mass 4	80.452	80.550 (80.996)	-0.12	83.531	-3.83	——	——

Torsion spring set 2

END MASS	EXACT FREQ. (Hz)	THREE MODE FREQ. (HZ)	REL. ERR. (%)	TWO MODE (Hz)	REL. ERR. (%)	ONE MODE (HZ)	REL. ERR. (%)
Mass 1	92.693	92.959 (93.183)	-0.29	117.84	-27.13	——	——
Mass 2	88.277	88.950 (89.499)	-0.76	117.02	-32.56	——	——
Mass 3	86.942	87.795 (88.493)	-0.98	116.84	-34.39	——	——
Mass 4	85.200	86.311 (87.234)	-1.30	116.62	-36.88	——	——

Torsion spring set 3

END MASS	EXACT FREQ. (Hz)	THREE MODE FREQ. (HZ)	REL. ERR. (%)	TWO MODE (Hz)	REL. ERR. (%)	ONE MODE (HZ)	REL. ERR. (%)
Mass 1	95.280	95.797 (96.053)	-0.54	151.03	-58.51	——	——
Mass 2	89.525	90.507 (91.164)	-1.10	149.91	-67.45	——	——
Mass 3	87.909	89.071 (89.897)	-1.32	149.66	-70.24	——	——
Mass 4	85.884	87.289 (88.359)	-1.64	149.34	-73.89	——	——

Table 6.15: Comparison of the sixth natural frequency with torsional spring set 4, 5 and 6

Torsion spring set 4

END MASS	EXACT FREQ. (Hz)	THREE MODE FREQ. (HZ)	REL. ERR. (%)	TWO MODE (Hz)	REL. ERR. (%)	ONE MODE (HZ)	REL. ERR. (%)
Mass 1	96.154	96.779 (97.049)	-0.65	178.38	-85.51	——	——
Mass 2	90.033	91.130 (91.826)	-1.22	177.06	-96.66	——	——
Mass 3	88.346	89.623 (90.492)	-1.45	176.77	-100.09	——	——
Mass 4	86.259	87.771 (88.889)	-1.75	176.40	-104.50	——	——

Torsion spring set 5

END MASS	EXACT FREQ. (Hz)	THREE MODE FREQ. (HZ)	REL. ERR. (%)	TWO MODE (Hz)	REL. ERR. (%)	ONE MODE (HZ)	REL. ERR. (%)
Mass 1	95.147	95.658 (95.912)	-0.54	151.00	-58.70	——	——
Mass 2	89.362	90.330 (90.986)	-1.08	149.87	-67.71	——	——
Mass 3	87.737	88.883 (89.707)	-1.31	149.63	-70.54	——	——
Mass 4	85.700	87.086 (88.154)	-1.62	149.31	-74.22	——	——

Torsion spring set 6

END MASS	EXACT FREQ. (Hz)	THREE MODE FREQ. (HZ)	REL. ERR. (%)	TWO MODE (Hz)	REL. ERR. (%)	ONE MODE (HZ)	REL. ERR. (%)
Mass 1	92.905	93.179 (93.403)	-0.29	117.92	-26.93	——	——
Mass 2	88.505	89.196 (89.748)	-0.78	117.11	-32.32	——	——
Mass 3	87.173	88.047 (88.750)	-1.00	116.94	-34.15	——	——
Mass 4	85.434	86.572 (87.502)	-1.33	116.72	-36.62	——	——

7. EXPERIMENTAL TEST PROCEDURE AND MODEL VALIDATION

This chapter describes the experiment procedure used to measure the natural frequencies of the two elastic arm, and compare the experimentally measured natural frequencies to those predicted by the model.

7.1 Experimental Test Procedure

Figure 7.1 presents a photo of the experimental test equipment used to measure the frequency response of the two elastic arm. The arms are mounted on a rigid frame in which all translational and rotational motion are negligible.

A mounting rig for holding the upper arm is attached to the frame. The mounting rig contains two anti-friction bearings. A shaft passes through the bearings. At the middle of the shaft, a small block is attached which is used to fasten the flexible arm. An extended arm is also attached to the shaft which is used to measure rotational displacement. Two tension springs connect the block to the frame supplying a restoring torque to the block.

Two tension springs are used instead of a conventional torsion spring because torsion springs tend to have dry friction. The experimental procedure for measuring the torsion spring constant supplied by those two tension springs is explained

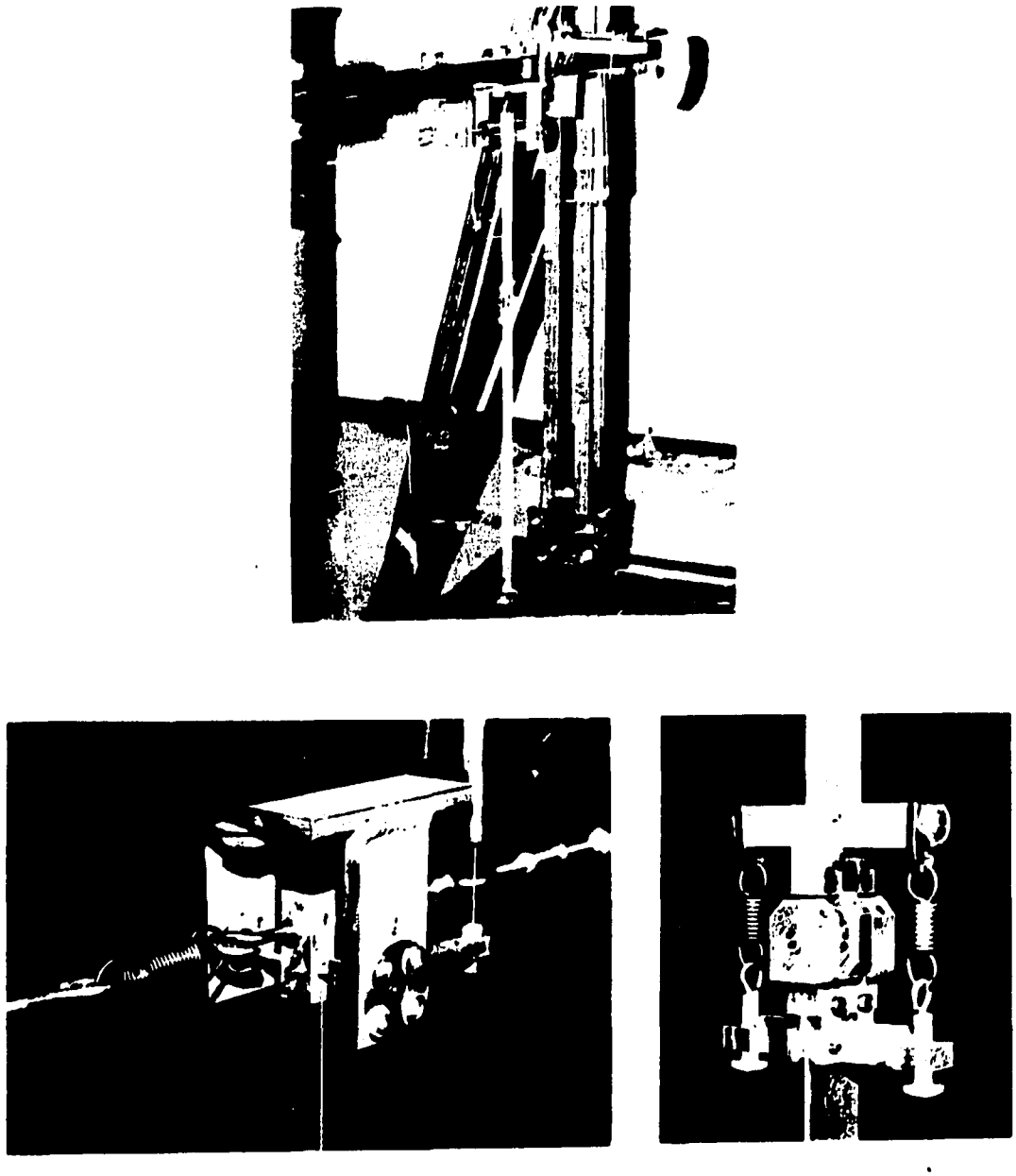

Figure 7.1: Experimental equipment

Table 7.1: Physical and mechanical properties of elastic arms

PROPERTY	UPPER ARM	LOWER ARM	UNIT
Length	$L_1 = 9.0$	$L_2 = 19.0$	in
Density	$\rho_1 = 2.538 \times 10^{-4}$	$\rho_2 = 2.538 \times 10^{-4}$	$lb_f\text{-}sec^2\text{-}in^{-4}$
Modulus of Elasticity	$E_1 = 1.000 \times 10^7$	$E_2 = 1.000 \times 10^7$	$lb_f\text{-}in^{-2}$
Area Moment of Inertia	$I_1 = 1.501 \times 10^{-5}$	$I_2 = 1.505 \times 10^{-5}$	in^4
Area	$A_1 = 4.656 \times 10^{-2}$	$A_2 = 4.668 \times 10^{-2}$	in^2

in detail in Appendix E. Two aluminum beams are used as elastic arms for the frequency response experiment and their physical and mechanical properties are given in Table 7.1.

The mass moment of inertia of the upper joint is difficult to estimate analytically because several components are involved in the rotational behavior such as the shaft, bearings, a mounting block, hooks to hold tension springs, the tension springs, an extended arm to hold a LVDT core and a LVDT core. Therefore, the mass moment of inertia of the upper joint is measured experimentally and the procedure is explained in detail in Appendix E.

A connector was designed to connect the upper and lower arm. The connection consists of an anti-friction bearing and two tension springs used to provide a restoring torque between the upper and lower arm. Again, two tension springs are used instead of a conventional torsion spring. The mass of the connector was measured, but the mass moment of inertia is calculated analytically. An end mass is attached at the lower end of the lower arm. The mass of the end mass is measured and the mass

moment of inertia is calculated analytically.

The natural frequencies of the system are found from the frequency response function. The system is excited with a soft impulse. Care was taken so that the impact did not induce warping or twisting of arms. In order to measure frequencies higher than the first two frequencies, the system must be excited so as not to induce a large rigid motions of two arm because the frequency response amplitudes of the higher modes are relatively weak if amplitudes of the first two frequencies prevail in the frequency response.

A schematic diagram of experimental test-bed with measurement instruments is shown in Figure 7.2. A dual spectrum analyzer is used for data acquisition and analysis of the frequency response. A LVDT is used to measure relatively low frequencies because the accelerations are too low for the accelerometer. In order to find higher frequencies, two accelerometers are used. One accelerometer is placed on the upper arm and the second accelerometer is placed on the lower arm. However, the analyzer is only two channel and only two of the three measurement instruments can be input. We found that using the LVDT at the upper arm and the accelerometer at the lower arm was the best combination for measuring the first four natural frequencies with the least amount of noise. The list of measurement instruments and a detailed explanation of the experimental set-up is given in Appendix E.

In order to reduce a resolution error of the analyzer in the lower frequency ranges, different frequency spans were used depending on the highest frequencies to be measured. For example, for the first two natural frequencies, a 6.25 or 12.5 Hz frequency span was used and, for the first four frequencies, a 50 Hz frequency span was used. The autospectral density (power spectral density) plot of the signals was

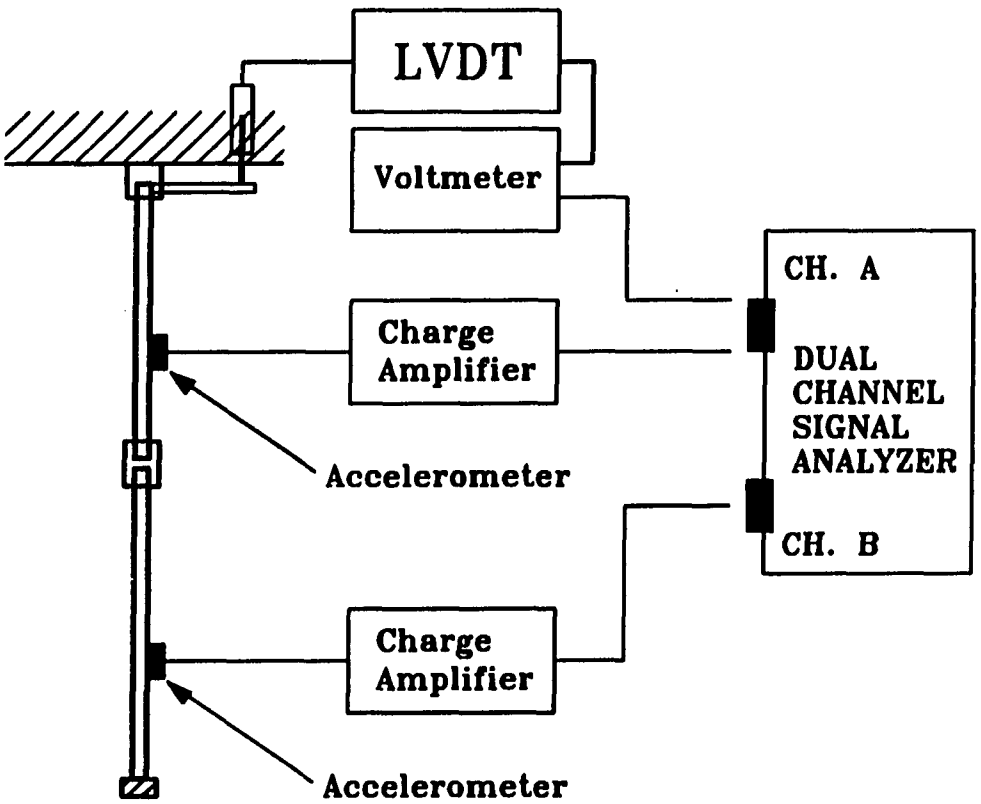

Figure 7.2: A schematic diagram of experimental test-bed with measurement instruments

Table 7.2: Three sets of torsional springs

unit : lb_f-in-rad^{-1}

	UPPER (K_{t_1})	LOWER (K_{t_2})
Set 1	15.4656	13.2480
Set 2	30.5566	22.5104
Set 3	52.3223	70.9744

used for the natural frequency measurement. A typical autospectral density plot is shown in Appendix E.

7.2 Model Validation

This section compares the natural frequency obtained from the analytical model to the experimentally measured frequency. Only, the first four natural frequencies are used because the first three flexible modes are considered from the model that yields an eight degree-of-freedom approximation.

Experiment results were obtained for three sets of torsion springs for the upper and lower joints. The torsion spring constants are given in Table 7.2. Four different end masses are used in the experiment and their masses and mass moments of inertia are given in Table 6.2. In Table 7.3, joint masses and mass moments of inertia used in the experiment are given.

Tables 7.4 - 7.7 compare the first four natural frequencies. For the analytically estimated natural frequencies, the modified comparison functions developed in Chapter 5 are used as the assumed modes, and the shortening effect due to an elas-

Table 7.3: Joint masses and mass moments of inertia

PARAMETER	UNIT	PARAMETER	UNIT
$J_1 = 1.743 \times 10^{-3}$	lb_f-in-sec^2		
$m_a = 1.8395 \times 10^{-4}$	lb_f-in^{-1}-sec^2	$m_b = 2.1861 \times 10^{-4}$	lb_f-in^{-1}-sec^2
$J_a = 2.1854 \times 10^{-4}$	lb_f-in-sec^2	$J_b = 2.3937 \times 10^{-4}$	lb_f-in-sec^2

tic deflection is included in the analytical model. In the tables, absolute error and relative error are calculated by the following formulas.

$$\text{ABS. ERROR(Hz)} = \text{MEAS. FREQ.} - \text{ESTI. FREQ.} \tag{7.1}$$

$$\text{REL. ERROR(\%)} = \frac{\text{MEAS. FREQ.} - \text{ESTI. FREQ.}}{\text{MEAS. FREQ.}} \times 100 \tag{7.2}$$

Tables 7.4 - 7.7 indicate that the measured first four natural frequencies are within $\pm 7\%$ of the frequencies predicted by the model with an average error of only 2.89%.

Table 7.4 shows that the analytical model gives a very good estimation of the first natural frequency of the system with the maximum relative error of 2.05% found in torsion spring set 3 with end mass 2. The analytical model underestimates the first natural frequency for most cases.

The comparison of the second natural frequency is shown in Table 7.5. The estimation of the second natural frequency is not as good as the first natural frequency, but the relative errors are within 5% for most cases. The second natural frequency is underestimated with torsion spring set 1 and set 2, and is overestimated with torsion spring set 3.

Table 7.4: Comparison of the first natural frequency

Torsion spring set 1

END MASS	MEASURED FREQ. (Hz)	ESTIMATED FREQ. (Hz)	ABS. ERROR (Hz)	REL. ERROR (%)
Mass 1	1.210	1.20	0.01	0.83
Mass 2	0.890	0.88	0.01	1.12
Mass 3	0.851	0.84	0.01	1.29
Mass 4	0.804	0.80	0.00	0.50

Torsion spring set 2

END MASS	MEASURED FREQ. (Hz)	ESTIMATED FREQ. (Hz)	ABS. ERROR (Hz)	REL. ERROR (%)
Mass 1	1.375	1.36	0.02	1.09
Mass 2	0.976	0.97	0.01	0.61
Mass 3	0.929	0.91	0.02	2.05
Mass 4	0.875	0.86	0.02	1.71

Torsion spring set 3

END MASS	MEASURED FREQ. (Hz)	ESTIMATED FREQ. (Hz)	ABS. ERROR (Hz)	REL. ERROR (%)
Mass 1	1.515	1.52	−0.01	−0.33
Mass 2	1.031	1.05	−0.02	−1.84
Mass 3	0.984	0.98	0.00	0.41
Mass 4	0.921	0.92	0.00	0.11

Table 7.5: Comparison of the second natural frequency

Torsion spring set 1

END MASS	MEASURED FREQ. (Hz)	ESTIMATED FREQ. (Hz)	ABS. ERROR (Hz)	REL. ERROR (%)
Mass 1	5.062	4.77	0.29	5.77
Mass 2	4.757	4.57	0.19	3.93
Mass 3	4.789	4.58	0.21	4.36
Mass 4	4.750	4.62	0.13	2.74

Torsion spring set 2

END MASS	MEASURED FREQ. (Hz)	ESTIMATED FREQ. (Hz)	ABS. ERROR (Hz)	REL. ERROR (%)
Mass 1	6.062	5.66	0.40	6.63
Mass 2	5.625	5.40	0.23	4.00
Mass 3	5.664	5.40	0.26	4.66
Mass 4	5.601	5.42	0.18	3.23

Torsion spring set 3

END MASS	MEASURED FREQ. (Hz)	ESTIMATED FREQ. (Hz)	ABS. ERROR (Hz)	REL. ERROR (%)
Mass 1	6.671	6.68	−0.01	−0.13
Mass 2	6.125	6.29	−0.17	−2.69
Mass 3	6.078	6.28	−0.20	−3.32
Mass 4	6.125	6.28	−0.16	−2.53

Table 7.6: Comparison of the third natural frequency

Torsion spring set 1

END MASS	MEASURED FREQ. (Hz)	ESTIMATED FREQ. (Hz)	ABS. ERROR (Hz)	REL. ERROR (%)
Mass 1	19.250	20.07	−0.82	−4.26
Mass 2	17.875	18.59	−0.72	−4.00
Mass 3	17.937	18.48	−0.54	−3.03
Mass 4	17.812	18.39	−0.58	−3.25

Torsion spring set 2

END MASS	MEASURED FREQ. (Hz)	ESTIMATED FREQ. (Hz)	ABS. ERROR (Hz)	REL. ERROR (%)
Mass 1	20.875	20.96	−0.09	−0.41
Mass 2	19.437	19.49	−0.05	−0.27
Mass 3	19.562	19.37	0.19	0.98
Mass 4	19.125	19.27	−0.15	−0.76

Torsion spring set 3

END MASS	MEASURED FREQ. (Hz)	ESTIMATED FREQ. (Hz)	ABS. ERROR (Hz)	REL. ERROR (%)
Mass 1	22.250	22.72	−0.47	−2.11
Mass 2	20.750	21.25	−0.50	−2.41
Mass 3	20.625	21.11	−0.49	−2.35
Mass 4	20.500	21.00	−0.50	−2.44

Table 7.7: Comparison of fourth natural frequency

Torsion spring set 1

END MASS	MEASURED FREQ. (Hz)	ESTIMATED FREQ. (Hz)	ABS. ERROR (Hz)	REL. ERROR (%)
Mass 1	29.187	30.86	−1.67	−5.73
Mass 2	29.125	30.83	−1.71	−5.85
Mass 3	29.062	30.84	−1.78	−6.12
Mass 4	28.875	30.85	−1.98	−6.84

Torsion spring set 2

END MASS	MEASURED FREQ. (Hz)	ESTIMATED FREQ. (Hz)	ABS. ERROR (Hz)	REL. ERROR (%)
Mass 1	32.000	34.13	−2.13	−6.66
Mass 2	32.000	34.06	−2.06	−6.44
Mass 3	32.250	34.06	−1.81	−5.61
Mass 4	32.125	34.07	−1.95	−6.05

Torsion spring set 3

END MASS	MEASURED FREQ. (Hz)	ESTIMATED FREQ. (Hz)	ABS. ERROR (Hz)	REL. ERROR (%)
Mass 1	38.375	38.65	−0.28	−0.72
Mass 2	37.625	38.45	−0.83	−2.19
Mass 3	37.875	38.42	−0.55	−1.44
Mass 4	37.375	38.40	−1.03	−2.74

In Table 7.6, the third natural frequency is predicted within 4.5% relative error. The third natural frequency is overestimated in all but one case.

Table 7.7 shows that the fourth natural frequency is predicted within 7% relative error. In all cases, the analytical model overestimates the fourth natural frequency.

The possible sources of the differences between the experimentally measured frequencies and the analytically estimated ones are as follows.

Experimental :

1. Masses of accelerometers may have a contribution on making the differences even though it was tried to avoid that additional mass effects by using accelerometers with as small masses as possible.

2. Friction in the joints and structural damping in arms may result in errors in the natural frequencies.

Analytical :

1. The error in the experimentally measured mass moment of inertia at the upper joint and the error in the analytical estimation of mass moment of inertia at the lower joint results in errors in the analytical model.

2. The error in the measurement of torsion spring constants will contribute to model differences especially, errors measuring the upper torsion spring constant because these are also used to measure the mass moment of inertia at the upper joint.

8. END POINT CONTROL

This chapter develops a control algorithm for end point control of a two arm elastic robot. First, an algorithm is developed to solve for the state variables as a function of end point position. This is used to determine a set of target state variables. A control algorithm is developed using a linear quadratic optimal control technique on an infinite time interval with the prescribed degree of stability method to control the movement of the end point from a specified initial end point position to a specified terminal end point position.

8.1 Static Deflection

In an elastic robot system, the end point location is not uniquely defined by the two joint angles in the presence of gravity or an external force. Instead, the elastic deflection must also be taken into account. This section describes the procedures used to find the state variables of an elastic two-arm robot system that results in a given end point location. Starting with the equations of motion for the two arm system (Equation 3.86) and assuming equilibrium, the terms including velocity and acceleration are eliminated yielding a set of nonlinear algebraic equations. The shortening effect is included in the nonlinear algebraic equations because an elastic deflection due to gravity may be considerable in some control positions. The nonlinear algebraic

equations including the shortening effect are given as follows.

$$\int_0^{\ell_1} (\rho A)_1 g \left\{ \left(\phi^T \mathbf{a} \right) cos\theta_1 + r_1 sin\theta_1 \right\} dr_1 \qquad (8.1)$$
$$+ (m_a + m_b) g \left\{ \left(\phi_{\ell_1}^T \mathbf{a} \right) cos\theta_1 + \ell_1 sin\theta_1 \right\}$$
$$+ \int_0^{\ell_2} (\rho A)_2 g \Big[\left(\phi_{\ell_1}^T \mathbf{a} \right) cos\theta_1 + \ell_1 sin\theta_1$$
$$+ \left\{ \left(\psi^T \mathbf{c} \right) cos\theta_2 + r_2 sin\theta_2 \right\} cos\theta_1$$
$$- \left\{ \left(\psi^T \mathbf{c} \right) sin\theta_2 - r_2 cos\theta_2 \right\} sin\theta_1 \Big] dr_2$$
$$+ m_p g \Big[\left(\phi_{\ell_1}^T \mathbf{a} \right) cos\theta_1 + \ell_1 sin\theta_1 + \left\{ \left(\psi_{\ell_2}^T \mathbf{c} \right) cos\theta_2 + \ell_2 sin\theta_2 \right\} cos\theta_1$$
$$- \left\{ \left(\psi_{\ell_2}^T \mathbf{c} \right) sin\theta_2 - \ell_2 cos\theta_2 \right\} sin\theta_1 \Big]$$
$$+ \frac{1}{2} \int_0^{\ell_1} (\rho A)_1 g \left[\int_0^{r_1} \left(\mathbf{a}^T \phi' \phi'^T \mathbf{a} \right) sin\theta_1 d\xi_1 \right] dr_1$$
$$+ \frac{1}{2} \int_0^{\ell_1} (m_a + m_b) \left(\mathbf{a}^T \phi' \phi'^T \mathbf{a} \right) sin\theta_1 \, dr_1$$
$$+ \frac{1}{2} \int_0^{\ell_2} (\rho A)_2 g \Big[\int_0^{\ell_1} \left(\mathbf{a}^T \phi' \phi'^T \mathbf{a} \right) sin\theta_1 \, dr_1$$
$$+ \left(sin\theta_2 cos\theta_1 + cos\theta_2 sin\theta_1 \right) \int_0^{r_2} \left(\mathbf{c}^T \psi' \psi'^T \mathbf{c} \right) d\xi_2 \Big] dr_2$$
$$+ \frac{1}{2} m_p g \Big[\int_0^{\ell_1} \left(\mathbf{a}^T \phi' \phi'^T \mathbf{a} \right) sin\theta_1 \, dr_1$$
$$+ \left(sin\theta_2 cos\theta_1 + cos\theta_2 sin\theta_1 \right) \int_0^{\ell_2} \left(\mathbf{c}^T \psi' \psi'^T \mathbf{c} \right) dr_2 \Big] = u_1$$
$$\int_0^{\ell_1} (EI)_1 \left(\phi'' \phi''^T \mathbf{a} \right) dr_1 \qquad (8.2)$$
$$+ \int_0^{\ell_1} (\rho A)_1 g \left(\phi sin\theta_1 \right) dr_1 + \left(m_a + m_b + m_p \right) g \left(\phi_{\ell_1} sin\theta_1 \right)$$
$$+ \int_0^{\ell_2} (\rho A)_2 g \left(\phi_{\ell_1} sin\theta_1 \right) dr_2$$
$$- \int_0^{\ell_1} (\rho A)_1 g \left[\int_0^{r_1} \left(\phi' \phi'^T \mathbf{a} \right) cos\theta_1 \, d\xi_1 \right] dr_1$$

$$
\begin{aligned}
&- \int_0^{\ell_1} (m_a + m_b) g \left(\phi' \phi'^T \mathbf{a} \right) cos\theta_1 \, dr_1 \\
&- \int_0^{\ell_2} (\rho A)_2 \, g \left[\int_0^{\ell_1} \left(\phi' \phi'^T \mathbf{a} \right) cos\theta_1 \, dr_1 \right] dr_2 \\
&- \int_0^{\ell_1} m_p g \left(\phi' \phi'^T \mathbf{a} \right) cos\theta_1 \, dr_1 \; = \; -u_2 \left(\phi' \right)_{\ell_1} \\
&\int_0^{\ell_2} (\rho A)_2 \, g \Big[\left(\psi^T \mathbf{c} \right) \left(cos\theta_2 cos\theta_1 - sin\theta_2 sin\theta_1 \right) \\
&\qquad + \left(r_2 \right) \left(cos\theta_2 sin\theta_1 + sin\theta_2 cos\theta_1 \right) \Big] \, dr_2 \\
&+ m_p g \Big[\left(\psi_{\ell_2}^T \mathbf{c} \right) \left(cos\theta_2 cos\theta_1 - sin\theta_2 sin\theta_1 \right) \\
&\qquad + \left(\ell_2 \right) \left(cos\theta_2 sin\theta_1 + sin\theta_2 cos\theta_1 \right) \Big] \\
&+ \frac{1}{2} \int_0^{\ell_2} (\rho A)_2 \, g \left[\left(cos\theta_2 sin\theta_1 + sin\theta_2 cos\theta_1 \right) \int_0^{r_2} \left(\mathbf{c}^T \psi' \psi'^T \mathbf{c} \right) d\xi_2 \right] dr_2 \\
&+ \frac{1}{2} \int_0^{\ell_2} \left(m_p \, g \right) \left(cos\theta_2 sin\theta_1 + sin\theta_2 cos\theta_1 \right) \left(\mathbf{c}^T \psi' \psi'^T \mathbf{c} \right) \, dr_2 \; = \; u_2 \\
&\qquad \int_0^{\ell_2} (EI)_2 \left(\psi'' \psi''^T \mathbf{c} \right) \, dr_2
\end{aligned}
\tag{8.3}
$$

$$
\begin{aligned}
&+ \int_0^{\ell_2} (\rho A)_2 \, g \left(\psi \right) \left(cos\theta_2 sin\theta_1 + sin\theta_2 cos\theta_1 \right) \, dr_2 \\
&+ m_p g \left(\psi_{\ell_2} \right) \left(cos\theta_2 sin\theta_1 + sin\theta_2 cos\theta_1 \right) \\
&- \int_0^{\ell_2} (\rho A)_2 \, g \left[\left(-sin\theta_2 sin\theta_1 + cos\theta_2 cos\theta_1 \right) \int_0^{r_2} \left(\psi' \psi'^T \mathbf{c} \right) \, d\xi_2 \right] dr_2 \\
&- \int_0^{\ell_2} \left(m_p \, g \right) \left(-sin\theta_2 sin\theta_1 + cos\theta_2 cos\theta_1 \right) \left(\psi' \psi'^T \mathbf{c} \right) \, dr_2 \; = \; 0
\end{aligned}
\tag{8.4}
$$

If two flexible modes are used to represent the elastic deflection of each arm, Equations 8.1 - 8.4 yield six equations. However, there are eight unknowns; two generalized coordinates for flexible behavior in each arm, two joint angles, and two joint torques to maintain the final configuration. Therefore, two more equations are necessary to solve the nonlinear equations. For control of the end point of the elastic

two-arm robot system, the two global coordinates of the end point are specified to supply two additional algebraic equations.

The global coordinates of end position which includes the shortening effect are calculated by the following procedures. The elastic deflection at the end of each arm is given as

$$w_{\ell_1} = \phi_{\ell_1}^T \mathbf{a} \tag{8.5}$$

$$w_{\ell_2} = \psi_{\ell_2}^T \mathbf{c} \tag{8.6}$$

The shortening effect is included as given by

$$r_{\ell_1} = \ell_1 - \frac{1}{2}\int_0^{\ell_1} \left(\mathbf{a}^T \phi' \phi'^T \mathbf{a}\right) dr_1 \tag{8.7}$$

$$r_{\ell_2} = \ell_2 - \frac{1}{2}\int_0^{\ell_2} \left(\mathbf{c}^T \psi' \psi'^T \mathbf{c}\right) dr_2 \tag{8.8}$$

Using Equations 8.5 - 8.8, the location of the end point of the lower arm is given in local coordinates as

$$\vec{p}_{\ell_2} = -r_{\ell_1}\hat{j}_1 + w_{\ell_1}\hat{i}_1 - r_{\ell_2}\hat{j}_2 + w_{\ell_2}\hat{i}_2 \tag{8.9}$$

Using Equations 3.1 - 3.2, the end point is given in global coordinates as

$$\begin{aligned}\vec{p}_{\ell_2} = &\left[\left\{w_{\ell_1} + r_{\ell_2} sin\theta_2 + w_{\ell_2} cos\theta_2\right\} cos\theta_1 \right. \\ &\left. -\left\{-r_{\ell_1} - r_{\ell_2} cos\theta_2 + w_{\ell_2} sin\theta_2\right\} sin\theta_1\right] \hat{I} \\ &+\left[\left\{w_{\ell_1} + r_{\ell_2} sin\theta_2 + w_{\ell_2} cos\theta_2\right\} sin\theta_1 \right. \\ &\left. +\left\{-r_{\ell_1} - r_{\ell_2} cos\theta_2 + w_{\ell_2} sin\theta_2\right\} cos\theta_1\right] \hat{J}\end{aligned} \tag{8.10}$$

For the end point control, if two global coordinates of the end point are specified, two residual functions are given as

$$\left[X_{end}\right]_{spec} - \left[\left\{w_{\ell_1} + r_{\ell_2} sin\theta_2 + w_{\ell_2} cos\theta_2\right\} cos\theta_1 \right. \tag{8.11}$$

$$
\begin{aligned}
&-\left\{-r_{\ell_1} - r_{\ell_2} cos\theta_2 + w_{\ell_2} sin\theta_2\right\} sin\theta_1\Big] \;=\; 0 \\
\left[Y_{end}\right]_{spec} - \Big[&\left\{w_{\ell_1} + r_{\ell_2} sin\theta_2 + w_{\ell_2} cos\theta_2\right\} sin\theta_1 \\
&+\left\{-r_{\ell_1} - r_{\ell_2} cos\theta_2 + w_{\ell_2} sin\theta_2\right\} cos\theta_1\Big] \;=\; 0
\end{aligned}
\tag{8.12}
$$

where $\left[X_{end}\right]_{spec}$ and $\left[Y_{end}\right]_{spec}$ represent specified global X and Y coordinates of the end point.

The unknowns (a_1, a_2, c_1, c_2, θ_1, θ_2, u_1 and u_2) can be found by solving eight nonlinear equations given in Equations 8.1- 8.4, Equation 8.11 and Equation 8.12. Generally, because these are nonlinear more than one solution may exist.

8.2 End Point Control

This section develops a scheme to control the end point of an elastic two-arm robot which moves from an initial position to a terminal position in a vertical plane. A linear quadratic optimal control technique on an infinite time interval with a prescribed degree of stability is used to define the control law. The prescribed degree of stability scheme [42] insures that all closed-loop eigenvalues of the system are less than $-\alpha$ where α is a positive real number known as the prescribed degree of stability. The objective of the control problem is to find an acceptable level of control inputs which minimize a performance index.

In general, the system dynamic equations are second order nonlinear differential equations including control torques. Since end point control moves from an initial position to a designated target position, it is reasonable to have the best dynamic model at the target position. Therefore, when defining the control law, the system is linearized with respect to the terminal position. The linearized equations of motion

including the shortening effect are given in Appendix F. The linearized system equations are put into first order yielding the following linear time-invariant state space form

$$\dot{\mathbf{x}}(t) = \mathbf{F}\mathbf{x}(t) + \mathbf{G}\mathbf{u}(t) \tag{8.13}$$

where $\mathbf{F}$ and $\mathbf{G}$ are time invariant matrices, $\mathbf{x}(t)$ is a state vector and $\mathbf{u}(t)$ is a control input vector. The state vector is given as

$$\mathbf{x} = \left[\theta_1, a_1, \cdots, a_n, \theta_2, c_1, \cdots, c_m, \dot{\theta}_1, \dot{a}_1, \cdots, \dot{a}_n, \dot{\theta}_2, \dot{c}_1, \cdots, \dot{c}_m\right]^T \tag{8.14}$$

where n is the number of flexible modes used to represent the deflection of the upper arm and m is the the number of flexible modes used to represent the deflection of the lower arm.

The higher frequency flexible modes have little contribution to the deflection at the end point compared with the lower modes. Therefore, we chose to use the first two flexible modes to express the deflection for both the upper and lower arms. This yields a 12^{th} order system with two control inputs(torques) at the upper and lower joints.

It is assumed that all states are measurable. Therefore, state estimator is not required to estimate any nonmeasurable states. The output equation for the system takes the form

$$\mathbf{y}(t) = \mathbf{C}\mathbf{x}(t) \tag{8.15}$$

where $\mathbf{C}$ is a constant matrix decided depending on the output.

The performance index chosen to bring the end point from initial position to a final position is

$$\mathbf{J} = \frac{1}{2}\int_0^\infty \left[\left(\mathbf{z}_{\ell_2} - \mathbf{z}^f_{\ell_2}\right)^T \mathbf{Q}_1 \left(\mathbf{z}_{\ell_2} - \mathbf{z}^f_{\ell_2}\right)\right. \tag{8.16}$$

$$+\left(\dot{z}_{\ell_2}-\dot{z}^f_{\ell_2}\right)^T Q_2\left(\dot{z}_{\ell_2}-\dot{z}^f_{\ell_2}\right)$$
$$+\left(\mathbf{u}-\mathbf{u}^f\right)^T \mathbf{B}\left(\mathbf{u}-\mathbf{u}^f\right)\Big]dt$$

where $z^f_{\ell_2}$ is a terminal end position, $\dot{z}^f_{\ell_2}$ is a velocity of the end point at a terminal position which we assume as zero, and $\mathbf{u}^f$ is a control input vector required to maintain a terminal position. Since the end position and velocity are functions of state variables, the above performance index can be rewritten as

$$\mathbf{J}=\frac{1}{2}\int_0^\infty \left[\left(\mathbf{x}-\mathbf{x}^f\right)^T \mathbf{A}\left(\mathbf{x}-\mathbf{x}^f\right)+\left(\mathbf{u}-\mathbf{u}^f\right)^T \mathbf{B}\left(\mathbf{u}-\mathbf{u}^f\right)\right]\,dt \qquad (8.17)$$

where $\mathbf{x}^f$ is the state vector at a terminal position resulting in $z^f_{\ell_2}$ and $\dot{z}^f_{\ell_2}$. Matrices **A** and **B** are weighting coefficients matrices. Matrix **A** must be a positive semi-definite symmetric matrix and matrix **B** must be a positive definite matrix.

As defined, the end point control problem has target state and control that are nonzero. Therefore, the state, control and output vector are shifted as follows

$$\mathbf{x}^\diamond(t) = \mathbf{x}(t)-\mathbf{x}^f \qquad (8.18)$$

$$\mathbf{u}^\diamond(t) = \mathbf{u}(t)-\mathbf{u}^f \qquad (8.19)$$

$$\mathbf{y}^\diamond(t) = \mathbf{y}(t)-\mathbf{y}^f \qquad (8.20)$$

By substituting Equations 8.18 - 8.20 into Equations 8.13, 8.15 and 8.17, the performance index, system dynamic equation and output equation are given

$$\mathbf{J} = \frac{1}{2}\int_0^\infty \left[\left(\mathbf{x}^\diamond\right)^T \mathbf{A}\left(\mathbf{x}^\diamond\right)+\left(\mathbf{u}^\diamond\right)^T \mathbf{B}\left(\mathbf{u}^\diamond\right)\right]\,dt \qquad (8.21)$$

$$\dot{\mathbf{x}}^\diamond(t) = \mathbf{F}\mathbf{x}^\diamond(t)+\mathbf{G}\mathbf{u}^\diamond(t) \qquad (8.22)$$

$$\mathbf{y}^\diamond(t) = \mathbf{C}\mathbf{x}^\diamond(t) \qquad (8.23)$$

Equations 8.21- 8.23 describe the optimal linear quadratic control problem with shifted inputs and outputs.

In order to introduce a prescribed degree of stability α into the above linear quadratic optimal control problem [42], the performance index given in Equation 8.21 is modified as

$$\hat{\mathbf{J}} = \frac{1}{2}\int_0^{tf} \left[\left(\mathbf{x}^{\diamond}\right)^T \mathbf{A}\left(\mathbf{x}^{\diamond}\right) + \left(\mathbf{u}^{\diamond}\right)^T \mathbf{B}\left(\mathbf{u}^{\diamond}\right)\right] e^{2\alpha t}\, dt \tag{8.24}$$

New state, control and output vector are defined as

$$\hat{\mathbf{x}} = \mathbf{x}^{\diamond} e^{\alpha t} \tag{8.25}$$

$$\hat{\mathbf{u}} = \mathbf{u}^{\diamond} e^{\alpha t} \tag{8.26}$$

$$\hat{\mathbf{y}} = \mathbf{y}^{\diamond} e^{\alpha t} \tag{8.27}$$

Using Equations 8.25- 8.26, a new performance index with a prescribed degree of stability α is given as

$$\hat{\mathbf{J}} = \frac{1}{2}\int_0^{\infty} \left[(\hat{\mathbf{x}})^T \mathbf{A}(\hat{\mathbf{x}}) + (\hat{\mathbf{u}})^T \mathbf{B}(\hat{\mathbf{u}})\right] dt \tag{8.28}$$

Differentiating Equation 8.25 with respect to time yields :

$$\dot{\hat{\mathbf{x}}} = \dot{\mathbf{x}}^{\diamond} e^{\alpha t} + \alpha \mathbf{x}^{\diamond} e^{\alpha t} \tag{8.29}$$

Multiplying Equation 8.22 by $e^{\alpha t}$ yields :

$$\dot{\mathbf{x}}^{\diamond}(t)\, e^{\alpha t} = \mathbf{F}\mathbf{x}^{\diamond}(t)\, e^{\alpha t} + \mathbf{G}\mathbf{u}^{\diamond}(t)\, e^{\alpha t} \tag{8.30}$$

Equations 8.25, 8.26 and 8.29 are substituted into Equation 8.30. Then, the new system dynamic equation is given as

$$\dot{\hat{\mathbf{x}}}(t) = (\mathbf{F} + \alpha \mathbf{I})\hat{\mathbf{x}}(t) + \mathbf{G}\hat{\mathbf{u}}(t) \tag{8.31}$$

The initial condition for the system is

$$\hat{\mathbf{x}}(0) = \mathbf{x}^{\diamond}(0) = \mathbf{x}(0) - \mathbf{x}^{f} \tag{8.32}$$

After multiplying Equation 8.23 by $e^{\alpha t}$ and substituting Equations 8.25 and 8.27, the new output equation is given by

$$\hat{\mathbf{y}}(t) = \mathbf{C}\hat{\mathbf{x}}(t) \tag{8.33}$$

Equations 8.28, 8.31 and 8.33 represent a linear optimal control problem with a prescribed degree of stability α. When Equations 8.28, 8.31 and 8.33 are compared with Equations 8.21, 8.22 and 8.23, it is obvious that Equations 8.28, 8.31 and 8.33 are an optimal linear quadratic control problem. Thus, acceptable levels of control inputs and state variables are obtained by minimizing the performance index (Equation 8.28) which is subjected to the system dynamic Equation 8.31. The acceptable levels are controlled by the choice of weighting matrices **A** and **B**.

A time invariant feedback gain matrix is given as

$$\mathbf{K}_{\alpha} = \mathbf{B}^{-1}\mathbf{G}^{T}\mathbf{S}^{\circ} \tag{8.34}$$

$\mathbf{S}^{\circ}$ is a unique positive definite matrix and the solution of the following nonlinear algebraic matrix Riccati equation.

$$0 = -\mathbf{S}^{\circ}(\mathbf{F} + \alpha\mathbf{I}) - (\mathbf{F} + \alpha\mathbf{I})^{T}\mathbf{S}^{\circ} + \mathbf{S}^{\circ}\mathbf{G}\mathbf{B}^{-1}\mathbf{G}^{T}\mathbf{S}^{\circ} - \mathbf{A} \tag{8.35}$$

The above linear quadratic optimal problem is solved using MATRIXx [41]. An optimal feedback control law is given as

$$\hat{\mathbf{u}}^{*} = -\mathbf{K}_{\alpha}\hat{\mathbf{x}} \tag{8.36}$$

Substituting Equation 8.36 into the system dynamic Equation 8.31, an optimal state vector $\hat{\mathbf{x}}^*$ is calculated by solving the following homogeneous initial value problem

$$\dot{\hat{\mathbf{x}}}(t) = (\mathbf{F} + \alpha\mathbf{I} - \mathbf{G}\mathbf{K}_\alpha)\hat{\mathbf{x}}(t) \tag{8.37}$$

$$\hat{\mathbf{x}}(0) = \mathbf{x}^\diamond(0) \tag{8.38}$$

Substituting the optimal state vector $\hat{\mathbf{x}}^*$ into Equation 8.36, the optimal feedback control law is given as

$$\hat{\mathbf{u}}^*(t) = -\mathbf{K}_\alpha\hat{\mathbf{x}}^*(t) \tag{8.39}$$

If Equations 8.25 and 8.26 are substituted into Equation 8.39, it is seen that Equation 8.39 is equivalent to

$$\mathbf{u}^{\diamond *}(t) = -\mathbf{K}_\alpha\mathbf{x}^{\diamond *}(t) \tag{8.40}$$

The system defined by Equations 8.31 and 8.39 is asymptotically stable [43]. From Equations 8.25 and 8.26, it can be seen that $\hat{\mathbf{x}}$ and $\hat{\mathbf{u}}$ are stable when $\mathbf{x}^\diamond$ and $\mathbf{u}^\diamond$ converge faster than $e^{-\alpha t}$. This means that all closed-loop eigenvalues of the system defined by Equations 8.22 and 8.40 have real parts less than $-\alpha$. Thus, the system has a degree of stability at a minimum α.

The optimal state and control vector are given in terms of original variables.

$$\mathbf{x}^*(t) = \hat{\mathbf{x}}^*(t)e^{-\alpha t} + \mathbf{x}^f \tag{8.41}$$

$$\mathbf{u}^*(t) = -\mathbf{K}_\alpha\left(\mathbf{x}^*(t) - \mathbf{x}^f\right) + \mathbf{u}^f \tag{8.42}$$

The control algorithm is tested in a simulation of the elastic two-arm system. The dimensions and properties of the elastic two-arm system used for the control simulation are given in Table 6.3 except that the length of the upper arm is 20 inches and the length of the lower arm is 30 inches.

Since the amplitudes of higher frequency modes are much smaller than the amplitudes of lower frequency modes, very few flexible modes are necessary. Two cases are investigated; one uses two flexible modes for each arm, and the second uses just one flexible mode for each arm. The modified comparison functions developed in Chapter 5 are used as assumed mode shapes.

Figures 8.2 - 8.12 show two seconds of simulation with the prescribed stability ($\alpha = 3$) and with the system dynamics linearized with respect to the terminal configurations. The simulation results with two flexible modes for each arm are given in solid line and those with one flexible mode for each arm are given in dashed line in the figures.

$$Diag(\mathbf{A}) = \begin{bmatrix} 0.00015 \\ 0.00015 \\ 0.00015 \\ 0.00015 \\ 0.00015 \\ 0.00015 \\ 0.00015 \\ 0.00015 \\ 0.015 \\ 0.00015 \\ 0.0015 \\ 0.015 \end{bmatrix} \tag{8.43}$$

Table 8.1: Initial and final configurations

	ONE FLEXIBLE MODE		TWO FLEXIBLE MODE	
MODE	INITIAL	FINAL	INITIAL	FINAL
θ_1(rad.)	1.2304	1.7593	1.2307	1.7580
a_1	8.6014	10.063	8.6150	10.049
a_2	———	———	0.0780	0.0999
θ_2(rad.)	−1.4979	−2.1521	−1.4986	−2.1514
c_1	−0.6400	−0.9330	−0.6415	−0.9351
c_2	———	———	−0.0103	−0.0148

$$Diag(\mathbf{B}) = \begin{bmatrix} 1.0 \\ 1.0 \end{bmatrix} \tag{8.44}$$

The X and Y coordinates are calculated using Equation 8.10. Diagonal matrices are used for the weighting coefficient matrices **A** and **B**. Diagonal elements of **A** and **B** are given in Equations 8.43 and 8.44.

This example uses an initial end point position of $X = 10''$ and $Y = -40''$. The final end point position is $X = 10''$ and $Y = -30''$. The corresponding initial and final states are calculated using Equations 8.1- 8.4 , 8.11 and 8.12 and given in Table 8.1. The initial and final end point positions are shown in Figure 8.1.

Figures 8.2 - 8.7 show the the time histories of rigid and flexible modes. Figure 8.2 shows a short hesitation in the upper joint angle before smoothly and quickly moving to the final upper joint angle with little overshoot. Figure 8.5 shows similar behavior for the lower joint angle. The responses of the flexible modes are given in Figures 8.3, 8.4, 8.6 and 8.7. These indicate that the second flexible modes in each arm will have a little contribution to the deflection because the second modes have much smaller

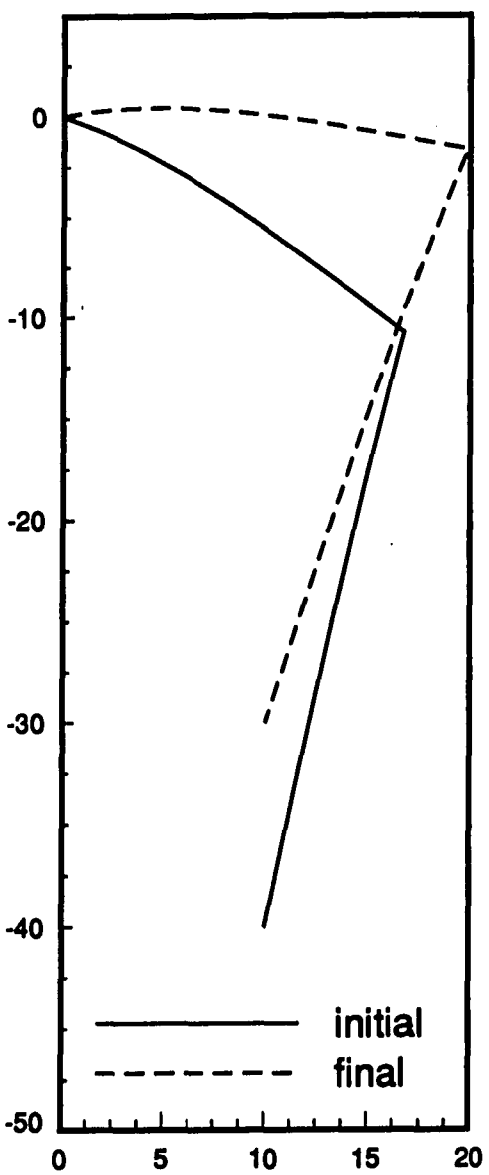

Figure 8.1: The initial and final end point positions

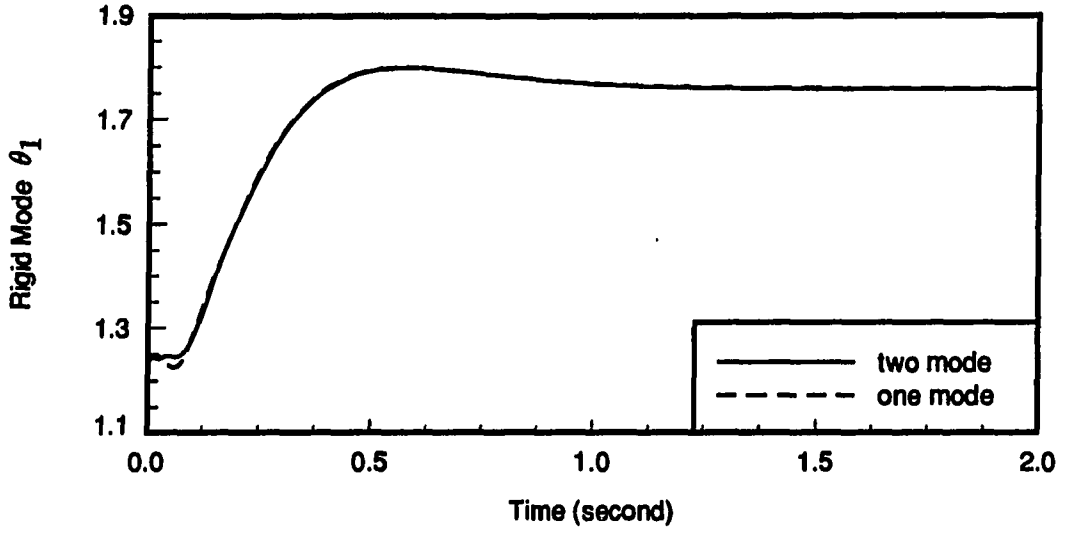

Figure 8.2: Time history of rigid mode θ_1 with prescribed stability ($\alpha = 3$)

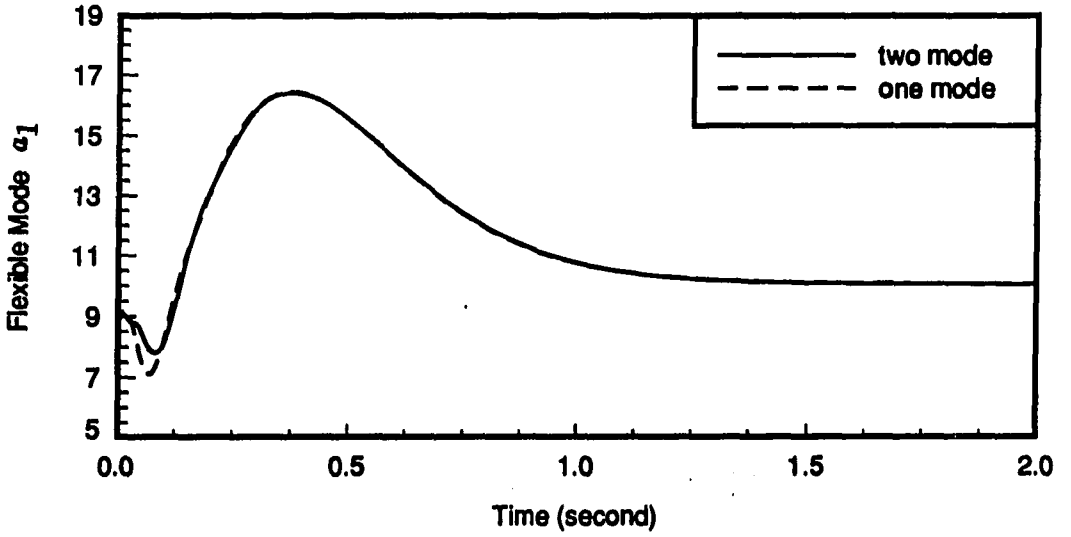

Figure 8.3: Time history of flexible mode a_1 with prescribed stability ($\alpha = 3$)

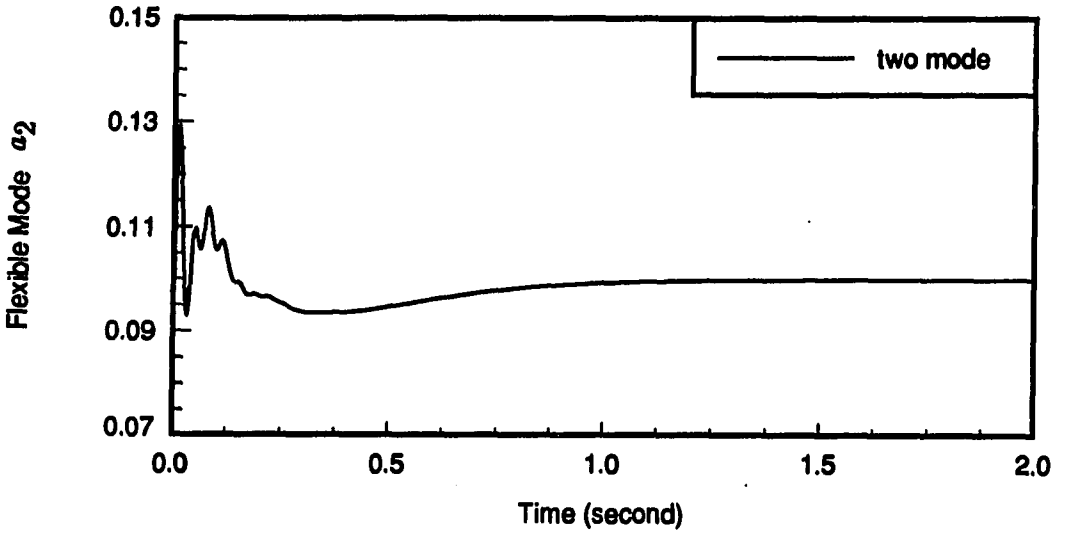

Figure 8.4: Time history of flexible mode a_2 with prescribed stability ($\alpha = 3$)

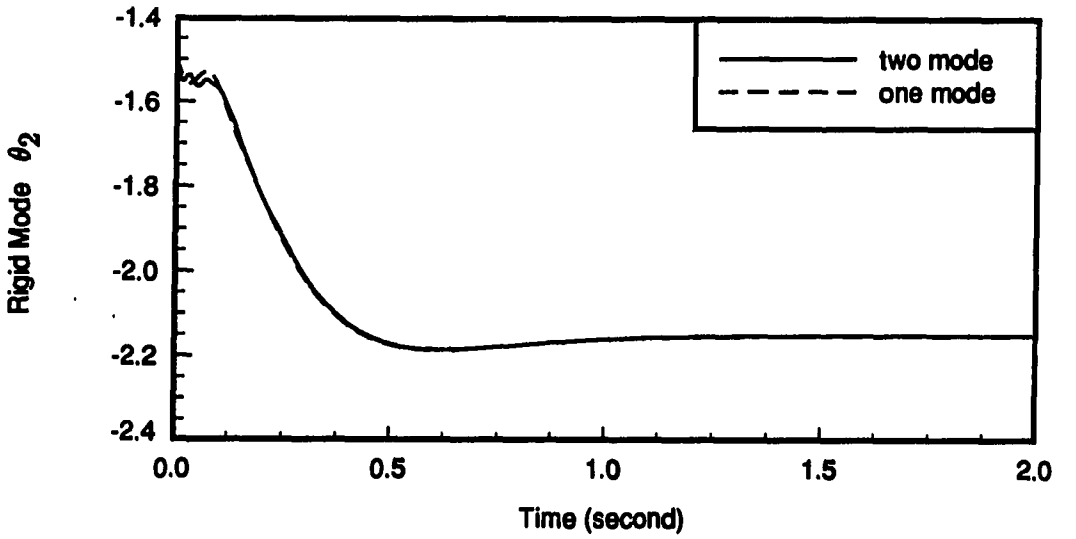

Figure 8.5: Time history of rigid mode θ_2 with prescribed stability ($\alpha = 3$)

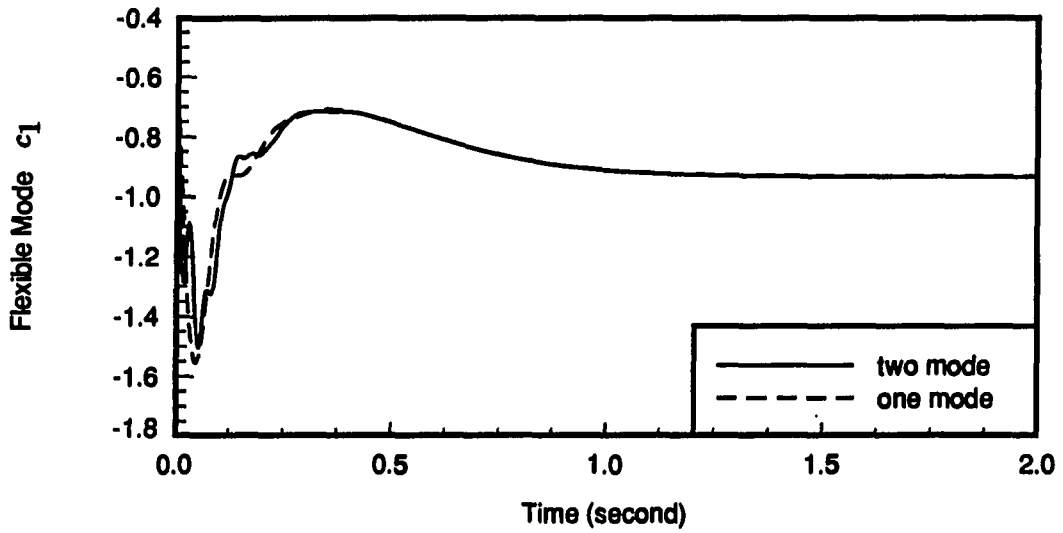

Figure 8.6: Time history of flexible mode c_1 with prescribed stability ($\alpha = 3$)

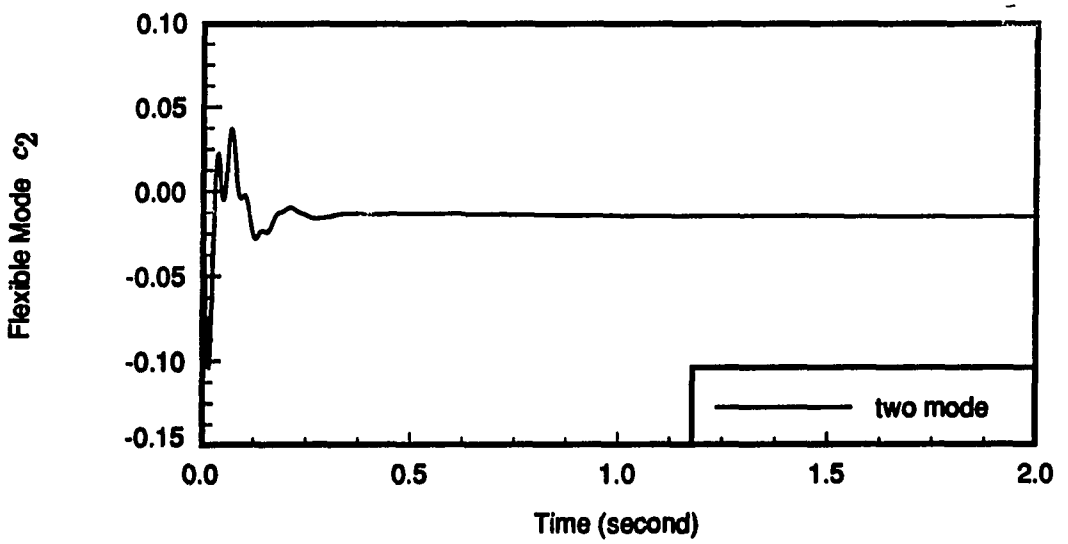

Figure 8.7: Time history of flexible mode c_2 with prescribed stability ($\alpha = 3$)

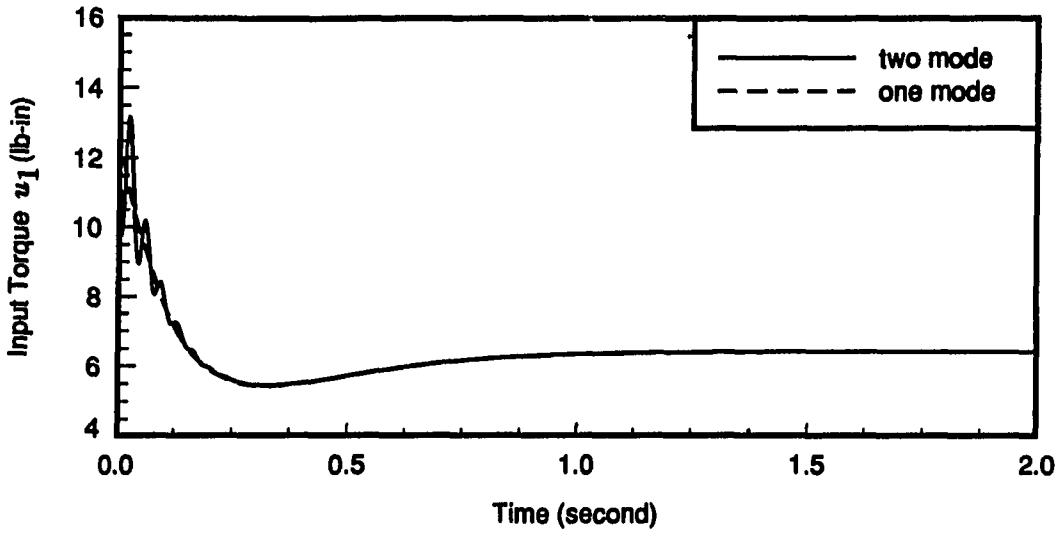

Figure 8.8: Time history of input torque of the upper joint (u_1) with prescribed stability ($\alpha = 3$)

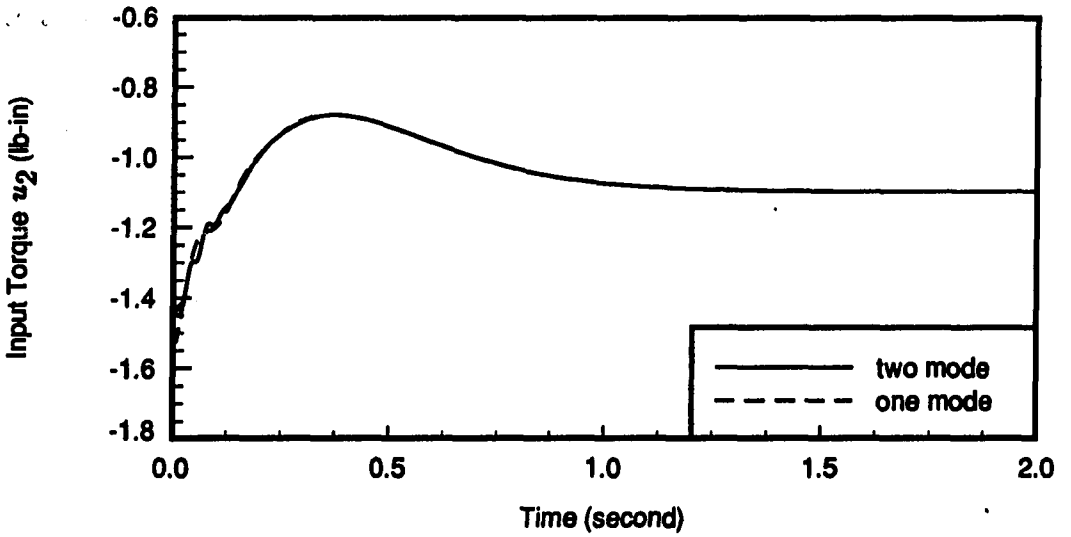

Figure 8.9: Time history of input torque of the lower joint (u_2) with prescribed stability ($\alpha = 3$)

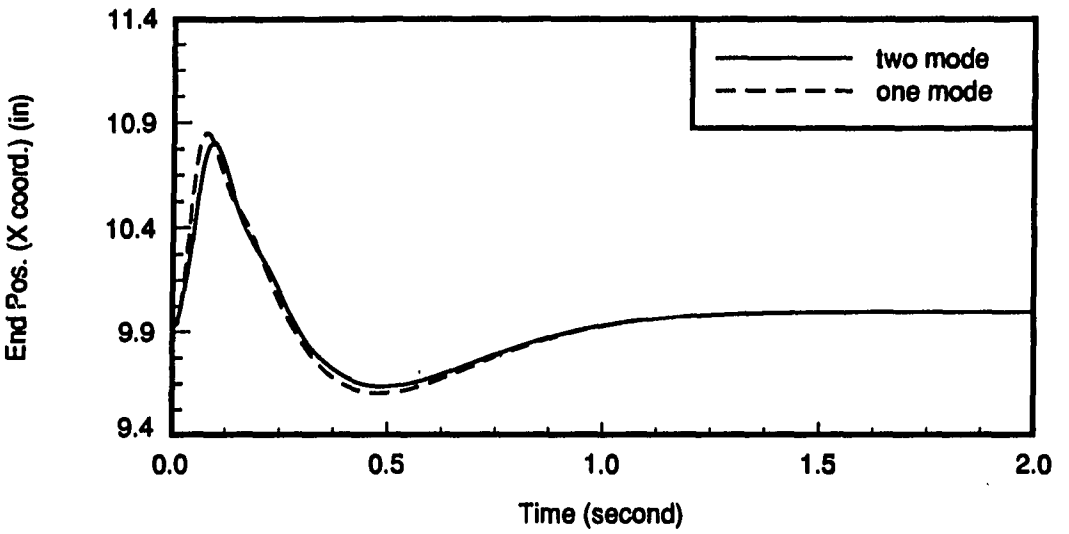

Figure 8.10: Time history of the global X coordinate of the end point with prescribed stability ($\alpha = 3$)

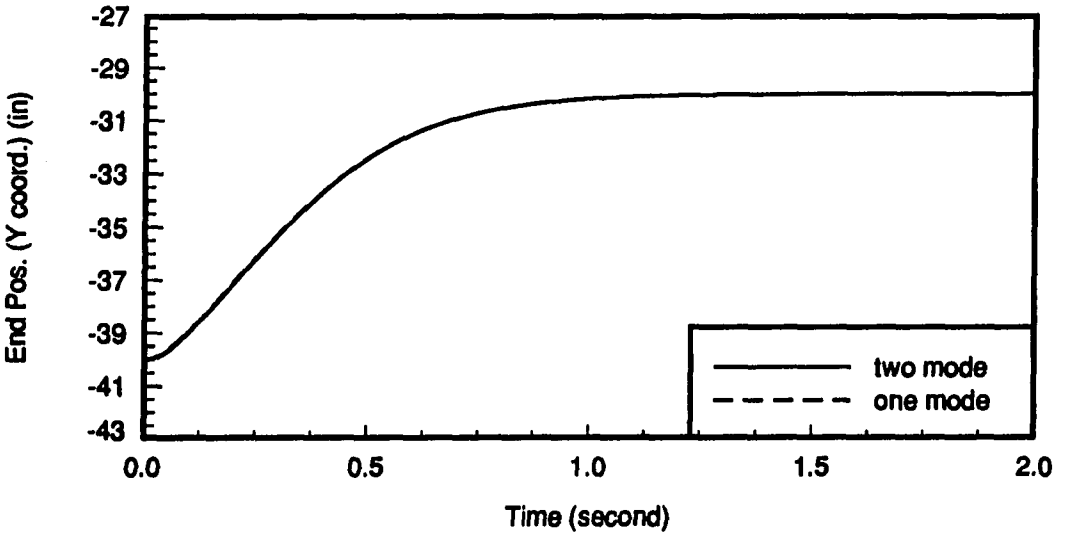

Figure 8.11: Time history of the global Y coordinate of the end point with prescribed stability ($\alpha = 3$)

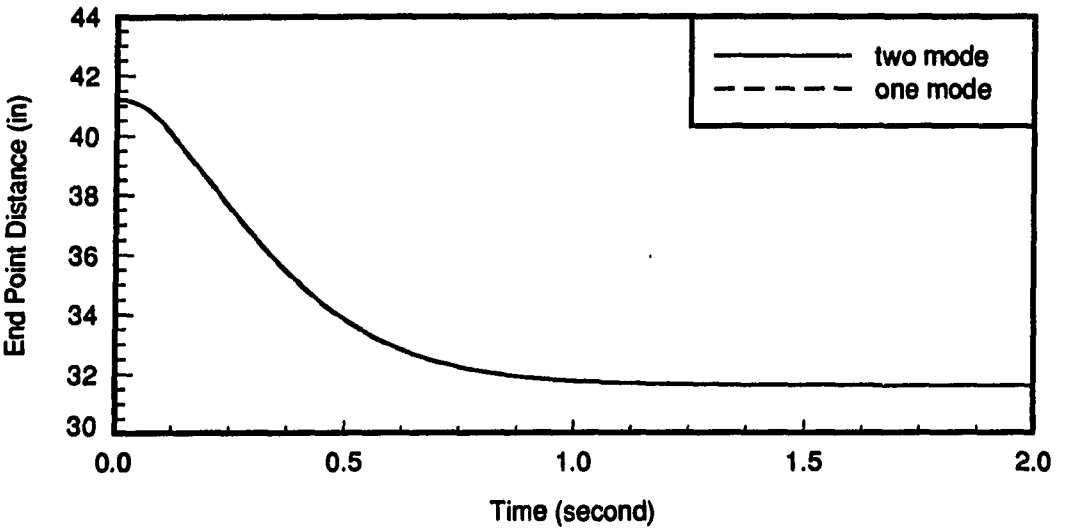

Figure 8.12: Time history of the distance of the end point from the origin with prescribed stability ($\alpha = 3$)

amplitudes than the first flexible modes.

Figures 8.8 and 8.9 show time histories of joint control torques. The upper joint control torque has small oscillations at first, but they quickly die out. The lower joint control torque has a smooth time history.

Figures 8.10 and 8.11 show the time histories of global X and Y position of the end point. The X coordinate of the end point, given in Figure 8.10, shows overshoot but returns smoothly to the final position. The Y coordinate of the end point, given in Figure 8.11, moves to the target point with no oscillation or overshoot. Figure 8.12 shows the time history of the distance of the end point measure from the origin of the global coordinate system and calculated by the following equation.

$$\text{Distance of the end point} = \sqrt{X^2 + Y^2} \tag{8.45}$$

The simulation results with one and two flexible modes for each arm have small differences in the early stage of the end point position control but the results are almost identical later in the simulation.

9. CONCLUSIONS

This thesis develops an analytical model of a two elastic arm robot system in a gravitational field. The model includes the shortening effect due to elastic deflection. The equations of motion are derived as a continuous system using the extended Hamilton's principle and as a discrete system using the assumed modes method.

The exact solution is found by solving the linearized differential equations of motion with their linearized boundary conditions. The eigenvalues are found by numerically solving the nonlinear algebraic characteristic equation. Two methods for finding the eigenvectors are presented.

A set of assumed mode shapes referred to as the modified comparison functions is developed in this thesis. The modified comparison functions satisfy all geometric and natural boundary conditions for a single cantilever beam with end mass and consider each elastic arm separately. When finding the upper arm mode shapes, the mass and mass moment of inertia of the end mass are modified to approximate the mass contribution from the lower arm. The accuracy of the modified comparison functions is given by comparing eigenvalues from the exact solution with those from the assumed modes method using the modified comparison functions as the assumed mode shapes. Different numbers of modes are used to evaluate how they affect accuracy. For the comparison, six sets of the upper and lower torsion springs and

four different end masses are used. When three assumed mode shapes are used for each arm, the comparison shows good agreement between eigenvalues in the first six eigenvalues with almost identical results up through the third eigenvalue and a maximum relative error of 1.75% in the sixth eigenvalue. Larger end mass results in more error between the two methods in most cases using three assumed mode shapes for each arm. When two assumed mode shapes are used for each arm, up through the third eigenvalue, there is good agreement between eigenvalues with a maximum relative error of 0.04%. The fourth eigenvalue from the assumed modes method has a maximum relative error of 4.17%. When one assumed mode shape is used for each arm, the first eigenvalue has a maximum relative error of 3.15% and the second eigenvalue has a maximum relative error of 7.71%. Smaller end mass results in more error between the two methods in all cases using one assumed mode shape for each arm. In general, eigenvalues calculated using the assumed modes method show slightly larger values than those calculated using the exact solution. The last two eigenvalues from the assumed modes method are not reliable. Eigenvalues are increased by including the shortening effect due to elastic deflection.

The analytical model developed in this thesis for a two elastic arm robot system in a gravitational field is validated by comparing the experimentally measured natural frequencies to those predicted by the model. The natural frequencies from the model which include the shortening effect are obtained using the assumed modes method with the modified comparison functions. The first four natural frequencies are used because the first three flexible modes are considered in the model. For the comparison, three sets of the upper and lower torsion springs and four different end masses are used. The comparison shows that the measured first four natural frequencies are

within ±7% of the frequencies predicted by the model and with an average error of only 2.89%. The model predicts the first natural frequency of the system with a maximum relative error of 2.05% and underestimates the first natural frequency for most cases. The second natural frequency is predicted within 5% relative error. It is underestimated with torsion spring set 1 and 2 but is overestimated with torsion spring set 3. The third natural frequency is predicted within 4.5% relative error and is overestimated in all but one case. The fourth natural frequency is predicted within 7% relative error and is overestimated in all cases.

An algorithm is developed to find the state variables as a function of a specified end point position. This is used to find a set of target state variables for the end position control. A control algorithm is developed using a linear quadratic optimal control technique on an infinite time interval with the prescribed degree of stability to control the movement of the end point from a specified initial end position to a specified terminal end position in a vertical plane. For the system dynamic equations, second order nonlinear differential equations including the shortening effect are linearized with respect to the terminal position and are put into first order.

Future work includes the implementation of this control scheme and others into an experimental test-bed.

10. BIBLIOGRAPHY

[1] L. Meirovitch. "Analytical Methods in Vibrations". *The Macmillan Company*, New York, 1967.

[2] W. J. Book, O. Maizza-Neto and D. E. Whitney. "Feedback Control of Two Beam, Two Joint Systems with Distributed Flexibility". *Journal of Dynamic Systems, Measurement, and Control*, 97 (December 1975): 424-431.

[3] R. H. Cannon, Jr. and E. Schmitz. "Initial Experiments on the End-Point Control of a Flexible One-Link Robot". *The International Journal of Robotics Research*, 3, No.3 (Fall 1984): 62-75.

[4] H. Krishnan and M. Vidyasagar. "Control of a Single-Link Flexible Beam Using a Hankel-Norm-Based Reduced order Model". *Proceedings 1988 IEEE International Conference on Robotics and Automation*, 1 (1988): 9-14.

[5] T. Tsujisawa and W. J. Book. "A Reduced Order Model Derivation for Lightweight Arms with a Parallel Mechanism". *Proceedings 1989 IEEE International Conference on Robotics and Automation*, 2 (1989): 728-735.

[6] C. M. Oakley and R. H. Cannon, Jr. "End-Point Control of a Two-Link Manipulator with a Very Flexible Forearm: Issues and Experiments". *Proceedings of the American Control Conference*, (1989): 1381-1388.

[7] R. Johanni. "On the Automatic Generation of the Equations of Motion for Robots with Elastically Deformable Arms". In *Theory of Robotics*, pp.143-147. Edited by D. Kopacek, I. Troch and K. Desoyer. IFAC Proceedings Series, No.3, Oxford, 1988.

[8] E. Schmitz. "Modeling and Control of a Planar Manipulator with an Elastic Forearm". *Proceedings 1989 IEEE International Conference on Robotics and Automation*, 2 (1989): 894-899.

[9] A. Yigit, R. A. Scott and A. G. Ulsoy. "Flexural motion of a Radially Rotating Beam Attached to a Rigid Body". *Journal of Sound and Vibration*, 121(2), (1988): 201-210.

[10] S. K. Biswas and R. D. Klafter. "Dynamic Modeling and Optimal Control of Flexible Robotic Manipulator". *Proceedings 1988 IEEE International Conference on Robotics and Automation*, 1 (1988): 15-20.

[11] P. J. Nathan and S. N. Singh. "Variable Structure Control of a Robotic Arm with Flexible Links". *Proceedings 1989 IEEE International Conference on Robotics and Automation*, 2 (1989): 882-887.

[12] E. Schmitz. "Dynamics and Control of a Planar Manipulator with Elastic Links". *Proceedings of 25th Conference on Decision and Control*, (December 1986): 1135-1139.

[13] A. G. Chassiakos and G. A. Bekey. "Pointwise Control of a Flexible Manipulator Arm". In *Robot Control (SYROCO '85)*, pp.181-185. Edited by L. Basañez, G. Ferraté and G. Saridis. IFAC Proceedings Series, No.9, Oxford, 1986.

[14] G. Yang and M. Donath. "Dynamic Model of a One-Link Robot Manipulator with Both Structural and Joint Flexibility". *Proceedings 1988 IEEE International Conference on Robotics and Automation*, 1 (1988): 476-481.

[15] W. J. Book. "Recursive Lagrangian Dynamics of Flexible Manipulator Arms". *The International Journal of Robotics Research*, 3, No. 3 (Fall 1984): 87-101.

[16] S. Djerassi and T. R. Kane. "Equations of Motion Governing the Deployment of a Flexible Linkage from a Spacecraft". *The Journal of the Astronautical Sciences*, 33, No. 4 (1985): 417-428.

[17] T. R. Kane, R. R. Ryan and A. K. Banerjee. "Dynamics of a Cantilever Beam Attached to a Moving Base". *Journal of Guidance, Control, and Dynamics*, 10, No. 2 (1987): 139-151.

[18] P. B. Usoro, R. Nadira and S. S. Mahil. "A Finite Element/Lagrange Approach to Modeling Lightweight Flexible Manipulators". *Journal of Dynamic Systems, Measurement, and Control*, 198 (September 1986): 198-205.

[19] W. H. Sunada and S. Dubowsky. "On the Dynamic Analysis and Behavior of Industrial Robotic Manipulators with Elastic Members". *Journal of Mechanisms, Transmissions, and Automation in Design*, 105 (March 1983): 42-51.

[20] D. A. Levinson and T. R. Kane. "Simulation of Large Motions of Nonuniform Beams in Orbit : Part I - The Cantilever Beam". *The Journal of the Astronautical Sciences*, 29, No. 3 (1981): 213-244.

[21] P. Chedmail and J. C. Bardiaux. "Experimental Validation of a Plane Flexible Robot Modeling". In *Theory of Robotics*, pp.137-142. Edited by D. Kopacek, I. Troch and K. Desoyer. IFAC Proceedings Series, No.3, Oxford, 1988.

[22] E. Van Den Bossche, L. Dugard and I. D. Landau. "Modeling and Identification of a Flexible Arm". *Proceedings of the American Control Conference*, 3 (1986): 1611-1616.

[23] C. Menq and J. Chen. "Dynamic Modeling and Payload-Adaptive Control of A Flexible Manipulator". *Proceedings 1988 IEEE International Conference on Robotics and Automation*, 1 (1988): 488-493.

[24] E. Bayo and M. Moulin. "An Efficient Computation of the Inverse Dynamics of Flexible Manipulators in the Time Domain". *Proceedings 1989 IEEE International Conference on Robotics and Automation*, 2 (1989): 710-715.

[25] E. Bayo. "Computed Torque for the Position Control of Open-Chain Flexible Robots". *Proceedings 1988 IEEE International Conference on Robotics and Automation*, 1 (1988): 316-321.

[26] G. Naganathan and A. H. Soni. "Non-Linear Flexibility Studies for Spatial Manipulators". *Proceedings 1986 IEEE International Conference on Robotics & Automation*, 1 (1986): 373-378.

[27] E. R. Christensen and S. W. Lee. "Nonlinear Finite Element Modeling of the Dynamics of Unrestrained Flexible Structures". *Computers & Structures*, 23, No. 6 (1986): 819-829.

[28] S. Cetinkunt and W. J. Book. "Symbolic Modeling of Flexible Manipulators". *Proceedings 1987 IEEE International Conference on Robotics & Automation*, 3 (1987): 2074-2080.

[29] P. Lucibello, F. Nicolò and R. Pimpinelli. "Automatic Symbolic Modelling of Robots with a Deformable Link". In *Theory of Robotics*, pp.131-135. Edited by D. Kopacek, I. Troch and K. Desoyer. IFAC Proceedings Series, No.3, Oxford, 1988.

[30] S. Nicosia, P. Tomei and A. Tornambe. "Dynamic Modeling of Flexible Robot Manipulators". *Proceedings 1986 IEEE International Conference on Robotics & Automation*, 1 (1986): 365-372.

[31] A. P. Tzes, S. Yurkovich and F. D. Langer. "A Symbolic Manipulation Package for Modeling of Rigid of Flexible Manipulators". *Proceedings 1988 IEEE International Conference on Robotics and Automation*, 3 (1988): 1526-1531.

[32] A. De Luca, P. Lucibello and F. Nicolò. "Automatic Symbolic Modelling and Nonlinear Control of Robots with Flexible Links". In *Robot Control Theory and Applications*, pp.62-70. Edited by K. Warwick and A. Pugh, London, 1988.

[33] Y. Sakawa, F. Matsuno and S. Fukushima. "Modeling and Feedback Control of a Flexible Arm". *Journal of Robotic Systems*, 2(4) (1985): 453-472.

[34] T. E. Alberts, S. L. Dickerson and W. J. Book. "Modeling and Control of Flexible Manipulators". *Society of Manufacturing Engineers(Technical Paper): MS85-524*, (1985): 1446-1459.

[35] J. Carusone, K. S. Buchan and G. M. T. D'Eleuterio. "End-Effector Tracking Control for Structurally Flexible Manipulators". *Proceedings of the American Control Conference*, (1989): 1389-1396.

[36] V. Feliu, K. S. Ratten and H. B. Brown, Jr. "Adaptive Control of a Single-Link Flexible Manipulator in the Presence of Joint Friction and Load Changes". *Proceedings 1988 IEEE International Conference on Robotics and Automation*, 3 (1988): 1036-1041.

[37] D. M. Rovner and R. H. Cannon, Jr. "Experiments Toward On-Line Identification and Control of a Very Flexible One-Link Manipulator". *The International Journal of Robotics Research*, 6, No.4 (1987): 3-19.

[38] W. J. Book and S. H. Lee. "Vibration Control of a Large Flexible Manipulator by a Small Robotic Arm". *Proceedings of the American Control Conference*, 2 (1989): 1377-1380.

[39] B. Siciliano and W. J. Book. "A Singular Perturbation Approach to Control of Lightweight Flexible Manipulators". *The International Journal of Robotics Research*, 7, No.4 (1988): 79-90.

[40] N. C. Singer and W. P. Seering. "Design and Comparison of Command Shaping Methods for Controlling Residual Vibration". *Proceedings 1989 IEEE International Conference on Robotics and Automation*, 2 (1989): 888-893.

[41] Integrated Systems Inc.. "MATRIXx 7.0 Release Notes". Santa Clara, October 1988.

[42] B. D. O. Anderson and J. B. Moore. "Linear System Optimisation with Prescribed Degree of Stability". *Proc. IEE*, 116, No. 12, (Dec. 1969):2083-2087.

[43] A. E. Bryson, Jr. and Y. Ho. "Applied Optimal Control". *Hemisphere Publishing Corporation*, New York, 1975.

[44] S. Timoshenko, D. H. Young and W. Weaver, Jr. "Vibration Problems in Engineering". *John Wiley & Sons*, New York, 1974.

11. APPENDIX A. UPPER TRIANGULAR ELEMENTS OF THE MATRIX AND THE RIGHT HAND SIDE VECTOR IN EQUATION 3.86

This appendix gives upper triangular elements of the matrix and the right hand side vector in Equation 3.86. Upper triangular elements of the matrix in Equation 3.86 are given as

$$
\begin{aligned}
P_{11} \;=\; & J_1 + \frac{1}{3}(\rho A)_1 \ell_1^3 + \left(m_a + m_b\right)\ell_1^2 + \left(J_a + J_b\right) \\
& + (\rho A)_2 \left(\ell_1^2 \ell_2 + \frac{1}{3}\ell_2^3 + \ell_1 \ell_2^2 cos\theta_2\right) \\
& + m_p \left(\ell_1^2 + \ell_2^2 + 2\ell_1 \ell_2 cos\theta_2\right) + J_p \\
& + \int_0^{\ell_1} (\rho A)_1 \left(\mathbf{a}^T \phi \phi^T \mathbf{a}\right) dr_1 + \left(m_a + m_b\right)\left(\mathbf{a}^T \phi_{\ell_1} \phi_{\ell_1}^T \mathbf{a}\right) \\
& + \int_0^{\ell_2} (\rho A)_2 \left[\left(\mathbf{a}^T \phi_{\ell_1} \phi_{\ell_1}^T \mathbf{a}\right) + \left(\mathbf{c}^T \psi \psi^T \mathbf{c}\right) - 2\ell_1 \left(\psi^T \mathbf{c}\right) sin\theta_2 \right. \\
& \qquad \left. + 2\left(\phi_{\ell_1}^T \mathbf{a}\right)\left\{r_2 sin\theta_2 + \left(\psi^T \mathbf{c}\right) cos\theta_2\right\}\right] dr_2 \\
& + m_p \left[\left(\mathbf{a}^T \phi_{\ell_1} \phi_{\ell_1}^T \mathbf{a}\right) + \left(\mathbf{c}^T \psi_{\ell_2} \psi_{\ell_2}^T \mathbf{c}\right) - 2\ell_1 \left(\psi_{\ell_2}^T \mathbf{c}\right) sin\theta_2 \right. \\
& \qquad \left. + 2\left(\phi_{\ell_1}^T \mathbf{a}\right)\left(\ell_2 sin\theta_2 + \left(\psi_{\ell_2}^T \mathbf{c}\right) cos\theta_2\right)\right]
\end{aligned}
\tag{11.1}
$$

$$
\begin{aligned}
\mathbf{P}_{12} \;=\; & \int_0^{\ell_1} (\rho A)_1 \left(r_1 \phi^T\right) dr_1 + \left(m_a + m_b\right)\ell_1 \phi_{\ell_1}^T + J_a \phi_{\ell_1}'^T \\
& + \int_0^{\ell_2} (\rho A)_2 \left(\ell_1 \phi_{\ell_1}^T + r_2 \phi_{\ell_1}^T cos\theta_2\right) dr_2 \\
& + m_p \left(\ell_1 \phi_{\ell_1}^T + \ell_2 \phi_{\ell_1}^T cos\theta_2\right)
\end{aligned}
\tag{11.2}
$$

$$
\begin{aligned}
&+\int_0^{\ell_2}(\rho A)_2\left[-\phi_{\ell_1}^T\left(\psi^T\mathbf{c}\right)sin\theta_2\right]dr_2\\
&+m_p\left[-\phi_{\ell_1}^T\left(\psi_{\ell_2}^T\mathbf{c}\right)sin\theta_2\right]\\
P_{13} \;=\; & J_b+\int_0^{\ell_2}(\rho A)_2\left(r_2^2+\ell_1 r_2 cos\theta_2\right)dr_2 \qquad (11.3)\\
&+m_p\left(\ell_2^2+\ell_1\ell_2 cos\theta_2\right)+J_p\\
&+\int_0^{\ell_2}(\rho A)_2\left[\left(\mathbf{c}^T\psi\psi^T\mathbf{c}\right)-\ell_1\left(\psi^T\mathbf{c}\right)sin\theta_2\right.\\
&\qquad\left.+\left(\phi_{\ell_1}^T\mathbf{a}\right)\left(r_2 sin\theta_2+\left(\psi^T\mathbf{c}\right)cos\theta_2\right)\right]dr_2\\
&+m_p\left[\left(\mathbf{c}^T\psi_{\ell_2}\psi_{\ell_2}^T\mathbf{c}\right)-\ell_1\left(\psi_{\ell_2}^T\mathbf{c}\right)sin\theta_2\right.\\
&\qquad\left.+\left(\phi_{\ell_1}^T\mathbf{a}\right)\left(\ell_2 sin\theta_2+\left(\psi_{\ell_2}^T\mathbf{c}\right)cos\theta_2\right)\right]\\
\mathbf{P}_{14} \;=\; & \int_0^{\ell_2}(\rho A)_2\left(\ell_1\psi^T cos\theta_2+r_2\psi^T\right)dr_2 \qquad (11.4)\\
&+m_p\left(\ell_1\psi_{\ell_2}^T cos\theta_2+\ell_2\psi_{\ell_2}^T\right)+J_p\psi_{\ell_2}^{\prime T}\\
&+\int_0^{\ell_2}(\rho A)_2\left[\left(\phi_{\ell_1}^T\mathbf{a}\right)\left(\psi^T\right)sin\theta_2\right]dr_2\\
&+m_p\left[\left(\phi_{\ell_1}^T\mathbf{a}\right)\left(\psi_{\ell_2}^T\right)sin\theta_2\right]\\
\mathbf{P}_{22} \;=\; & \int_0^{\ell_1}(\rho A)_1\left(\phi\phi^T\right)dr_1 \qquad (11.5)\\
&+\int_0^{\ell_2}(\rho A)_2\left(\phi_{\ell_1}\phi_{\ell_1}^T\right)dr_2\\
&+\left(m_a+m_b\right)\left(\phi_{\ell_1}\phi_{\ell_1}^T\right)+J_a\left(\phi_{\ell_1}^{\prime}\phi_{\ell_1}^{\prime T}\right)+m_p\left(\phi_{\ell_1}\phi_{\ell_1}^T\right)\\
\mathbf{P}_{23} \;=\; & \int_0^{\ell_2}(\rho A)_2\left(r_2\phi_{\ell_1}cos\theta_2\right)dr_2 \qquad (11.6)\\
&-\int_0^{\ell_2}(\rho A)_2\left[\left(\phi_{\ell_1}\right)\left(\psi^T\mathbf{c}\right)sin\theta_2\right]dr_2\\
&+m_p\left(\ell_2\phi_{\ell_1}cos\theta_2\right)-m_p\left(\phi_{\ell_1}\right)\left(\psi_{\ell_2}^T\mathbf{c}\right)sin\theta_2\\
\mathbf{P}_{24} \;=\; & \int_0^{\ell_2}(\rho A)_2\left(\phi_{\ell_1}\psi^T cos\theta_2\right)dr_2+m_p\left(\phi_{\ell_1}\psi_{\ell_2}^T cos\theta_2\right) \qquad (11.7)
\end{aligned}
$$

$$P_{33} = J_b + m_p\left(\ell_2^2\right) + J_p + m_p\left(\mathbf{c}^T\psi_{\ell_2}\psi_{\ell_2}^T\mathbf{c}\right) + \int_0^{\ell_2}(\rho A)_2\left(\mathbf{c}^T\psi\psi^T\mathbf{c}\right)dr_2 + \int_0^{\ell_2}(\rho A)_2\left(r_2^2\right)dr_2 \tag{11.8}$$

$$\mathbf{P}_{34} = \int_0^{\ell_2}(\rho A)_2\left(r_2\psi^T\right)dr_2 + m_p\left(\ell_2\psi_{\ell_2}^T\right) + J_p\left(\psi_{\ell_2}'^T\right) \tag{11.9}$$

$$\mathbf{P}_{44} = \int_0^{\ell_2}(\rho A)_2\left(\psi\psi^T\right)dr_2 + m_p\left(\psi_{\ell_2}\psi_{\ell_2}^T\right) + J_p\left(\psi_{\ell_2}'\psi_{\ell_2}'^T\right) \tag{11.10}$$

The right hand side vector in Equation 3.86 is given by

$$\begin{aligned} f_1(\mathbf{q},\dot{\mathbf{q}}) = & -2\int_0^{\ell_1}(\rho A)_1\left(\dot{\mathbf{a}}^T\phi\phi^T\mathbf{a}\right)\dot{\theta}_1 dr_1 \\ & -2\left(m_a+m_b\right)\left(\dot{\mathbf{a}}^T\phi_{\ell_1}\phi_{\ell_1}^T\mathbf{a}\right)\dot{\theta}_1 \\ & -\int_0^{\ell_2}(\rho A)_2\Big[2\left(\dot{\mathbf{a}}^T\phi_{\ell_1}\phi_{\ell_1}^T\mathbf{a}\right)\dot{\theta}_1 - \ell_1\left(\psi^T\dot{\mathbf{c}}\right)\dot{\theta}_2 sin\theta_2 \\ & \quad + \left(\phi_{\ell_1}^T\dot{\mathbf{a}}\right)\left(\psi^T\dot{\mathbf{c}}\right)sin\theta_2 + \left(\phi_{\ell_1}^T\mathbf{a}\right)\left(\psi^T\dot{\mathbf{c}}\right)\dot{\theta}_2 cos\theta_2 \\ & \quad +2\left(\dot{\theta}_1+\dot{\theta}_2\right)\left(\dot{\mathbf{c}}^T\psi\psi^T\mathbf{c}\right) \\ & \quad + \left(\ell_1\dot{\theta}_1 + \phi_{\ell_1}^T\dot{\mathbf{a}}\right)\Big\{-\left(\psi^T\dot{\mathbf{c}}\right)sin\theta_2 \\ & \qquad -r_2\dot{\theta}_2 sin\theta_2 - \left(\psi^T\mathbf{c}\right)\dot{\theta}_2 cos\theta_2\Big\} \\ & \quad +\dot{\theta}_1\left(\phi_{\ell_1}^T\dot{\mathbf{a}}\right)\Big\{r_2 sin\theta_2 + \left(\psi^T\mathbf{c}\right)cos\theta_2\Big\} \\ & \quad +\dot{\theta}_1\left(\phi_{\ell_1}^T\mathbf{a}\right)\Big\{r_2\dot{\theta}_2 cos\theta_2 + \left(\psi^T\dot{\mathbf{c}}\right)cos\theta_2 - \left(\psi^T\mathbf{c}\right)\dot{\theta}_2 sin\theta_2\Big\} \\ & \quad + \left(\dot{\theta}_1+\dot{\theta}_2\right)\Big\{-\ell_1\Big(\left(\psi^T\dot{\mathbf{c}}\right)sin\theta_2 + \left(\psi^T\mathbf{c}\right)\dot{\theta}_2 cos\theta_2\Big) \\ & \qquad -\ell_1 r_2\dot{\theta}_2 sin\theta_2 + \left(\phi_{\ell_1}^T\dot{\mathbf{a}}\right)\left(r_2 sin\theta_2 + \left(\psi^T\mathbf{c}\right)cos\theta_2\right) \\ & \qquad + \left(\phi_{\ell_1}^T\mathbf{a}\right)\left(r_2\dot{\theta}_2 cos\theta_2\right) \\ & \qquad + \left(\phi_{\ell_1}^T\mathbf{a}\right)\Big(\left(\psi^T\dot{\mathbf{c}}\right)cos\theta_2 - \left(\psi^T\mathbf{c}\right)\dot{\theta}_2 sin\theta_2\Big)\Big\}\Big]dr_2 \\ & -m_p\Big[2\left(\dot{\mathbf{a}}^T\phi_{\ell_1}\phi_{\ell_1}^T\mathbf{a}\right)\dot{\theta}_1 + \left(\psi_{\ell_2}^T\dot{\mathbf{c}}\right)\Big(\left(\phi_{\ell_1}^T\dot{\mathbf{a}}\right)sin\theta_2 - \ell_1\dot{\theta}_2 sin\theta_2\Big) \end{aligned} \tag{11.11}$$

$$
\begin{aligned}
&+\left(\phi_{\ell_1}^T \mathbf{a}\right)\left(\psi_{\ell_2}^T \dot{\mathbf{c}}\right)\dot{\theta}_2 cos\theta_2 + 2\left(\dot{\theta}_1+\dot{\theta}_2\right)\left(\dot{\mathbf{c}}^T \psi_{\ell_2}\psi_{\ell_2}^T \mathbf{c}\right)\\
&+\left(\ell_1\dot{\theta}_1+\phi_{\ell_1}^T\dot{\mathbf{a}}\right)\left\{-\left(\psi_{\ell_2}^T\dot{\mathbf{c}}\right)sin\theta_2\right.\\
&\quad\left.-\ell_2\dot{\theta}_2 sin\theta_2-\left(\psi_{\ell_2}^T\mathbf{c}\right)\dot{\theta}_2 cos\theta_2\right\}\\
&+\dot{\theta}_1\left(\phi_{\ell_1}^T\dot{\mathbf{a}}\right)\left\{\ell_2 sin\theta_2+\left(\psi_{\ell_2}^T\mathbf{c}\right)cos\theta_2\right\}\\
&+\dot{\theta}_1\left(\phi_{\ell_1}^T\mathbf{a}\right)\left\{\ell_2\dot{\theta}_2 cos\theta_2+\left(\psi_{\ell_2}^T\dot{\mathbf{c}}\right)cos\theta_2-\left(\psi_{\ell_2}^T\mathbf{c}\right)\dot{\theta}_2 sin\theta_2\right\}\\
&+\left(\dot{\theta}_1+\dot{\theta}_2\right)\left\{-\ell_1\left(\left(\psi_{\ell_2}^T\dot{\mathbf{c}}\right)sin\theta_2+\left(\psi_{\ell_2}^T\mathbf{c}\right)\dot{\theta}_2 cos\theta_2\right)\right.\\
&\quad-\ell_1\ell_2\dot{\theta}_2 sin\theta_2+\left(\phi_{\ell_1}^T\dot{\mathbf{a}}\right)\left(\ell_2 sin\theta_2+\left(\psi_{\ell_2}^T\mathbf{c}\right)cos\theta_2\right)\\
&\quad+\left(\phi_{\ell_1}^T\mathbf{a}\right)\left(\ell_2\dot{\theta}_2 cos\theta_2\right)\\
&\quad\left.+\left(\phi_{\ell_1}^T\mathbf{a}\right)\left(\left(\psi_{\ell_2}^T\dot{\mathbf{c}}\right)cos\theta_2-\left(\psi_{\ell_2}^T\mathbf{c}\right)\dot{\theta}_2 sin\theta_2\right)\right\}\Big]\\
&-K_{t_1}\dot{\theta}_1\\
&-\int_0^{\ell_1}(\rho A)_1 g\left[\left(\phi^T\mathbf{a}\right)cos\theta_1+r_1 sin\theta_1\right]dr_1\\
&-\left(m_a+m_b\right)g\left[\left(\phi_{\ell_1}^T\mathbf{a}\right)cos\theta_1+\ell_1 sin\theta_1\right]\\
&-\int_0^{\ell_2}(\rho A)_2 g\left[\left(\phi_{\ell_1}^T\mathbf{a}\right)cos\theta_1+\ell_1 sin\theta_1\right.\\
&\qquad+\left\{\left(\psi^T\mathbf{c}\right)cos\theta_2+r_2 sin\theta_2\right\}cos\theta_1\\
&\qquad\left.-\left\{\left(\psi^T\mathbf{c}\right)sin\theta_2-r_2 cos\theta_2\right\}sin\theta_1\right]dr_2\\
&-m_p g\left[\left(\phi_{\ell_1}^T\mathbf{a}\right)cos\theta_1+\ell_1 sin\theta_1\right.\\
&\quad+\left\{\left(\psi_{\ell_2}^T\mathbf{c}\right)cos\theta_2+\ell_2 sin\theta_2\right\}cos\theta_1\\
&\quad\left.-\left\{\left(\psi_{\ell_2}^T\mathbf{c}\right)sin\theta_2-\ell_2 cos\theta_2\right\}sin\theta_1\right]\\
&+\frac{1}{2}\int_0^{\ell_1}(\rho A)_1 g\left[sin\theta_1\int_0^{r_1}\left(\mathbf{a}^T\phi'\phi'^T\mathbf{a}\right)d\xi_1\right]dr_1\\
&+\frac{1}{2}\int_0^{\ell_1}\left(m_a+m_b+m_p\right)g sin\theta_1\left(\mathbf{a}^T\phi'\phi'^T\mathbf{a}\right)dr_1
\end{aligned}
$$

$$
\begin{aligned}
&+\frac{1}{2}\int_0^{\ell_2}(\rho A)_2 g\left[sin\theta_1\int_0^{\ell_1}\left(\mathbf{a}^T\phi'\phi'^T\mathbf{a}\right)dr_1\right]dr_2\\
&+\frac{1}{2}\int_0^{\ell_2}(\rho A)_2 g\left(sin\theta_2 cos\theta_1+cos\theta_2 sin\theta_1\right)\\
&\qquad\qquad\left[\int_0^{r_2}\left(\mathbf{c}^T\psi'\psi'^T\mathbf{c}\right)d\xi_2\right]dr_2\\
&+\frac{1}{2}m_p g\left(sin\theta_2 cos\theta_1+cos\theta_2 sin\theta_1\right)\int_0^{\ell_2}\left(\mathbf{c}^T\psi'\psi'^T\mathbf{c}\right)dr_2
\end{aligned}
$$

$$
\begin{aligned}
\mathbf{f}_2(\mathbf{q},\dot{\mathbf{q}}) \;=\; &\int_0^{\ell_2}(\rho A)_2\left[\phi_{\ell_1}\left(\psi^T\dot{\mathbf{c}}\right)\dot{\theta}_2 sin\theta_2\right.\\
&\quad+\left(\dot{\theta}_1+\dot{\theta}_2\right)\left(\phi_{\ell_1}\right)\left\{r_2\dot{\theta}_2 sin\theta_2\right.\\
&\qquad\left.\left.+\left(\psi^T\dot{\mathbf{c}}\right)sin\theta_2+\left(\psi^T\mathbf{c}\right)\dot{\theta}_2 cos\theta_2\right\}\right]dr_2\\
&+m_p\left[\phi_{\ell_1}\left(\psi_{\ell_2}^T\dot{\mathbf{c}}\right)\dot{\theta}_2 sin\theta_2\right.\\
&\quad+\left(\dot{\theta}_1+\dot{\theta}_2\right)\left(\phi_{\ell_1}\right)\left\{\ell_2\dot{\theta}_2 sin\theta_2\right.\\
&\qquad\left.\left.+\left(\psi_{\ell_2}^T\dot{\mathbf{c}}\right)sin\theta_2+\left(\psi_{\ell_2}^T\mathbf{c}\right)\dot{\theta}_2 cos\theta_2\right\}\right]\\
&+\int_0^{\ell_1}(\rho A)_1\left[\left(\phi\phi^T\mathbf{a}\right)\dot{\theta}_1^2\right]dr_1\\
&+m_a\left[\left(\phi_{\ell_1}\phi_{\ell_1}^T\mathbf{a}\right)\dot{\theta}_1^2\right]+m_b\left[\left(\phi_{\ell_1}\phi_{\ell_1}^T\mathbf{a}\right)\dot{\theta}_1^2\right]\\
&+\int_0^{\ell_2}(\rho A)_2\left[\left(\phi_{\ell_1}\phi_{\ell_1}^T\mathbf{a}\right)\dot{\theta}_1^2+\dot{\theta}_1\left(\phi_{\ell_1}\right)\left(\psi^T\dot{\mathbf{c}}\right)sin\theta_2\right.\\
&\quad\left.+\left(\dot{\theta}_1+\dot{\theta}_2\right)\dot{\theta}_1\left(\phi_{\ell_1}\right)\left\{r_2 sin\theta_2+\left(\psi^T\mathbf{c}\right)cos\theta_2\right\}\right]dr_2\\
&+m_p\left[\left(\phi_{\ell_1}\phi_{\ell_1}^T\mathbf{a}\right)\dot{\theta}_1^2+\dot{\theta}_1\left(\phi_{\ell_1}\right)\left(\psi_{\ell_2}^T\dot{\mathbf{c}}\right)sin\theta_2\right.\\
&\quad\left.+\left(\dot{\theta}_1+\dot{\theta}_2\right)\dot{\theta}_1\left(\phi_{\ell_1}\right)\left\{\ell_2 sin\theta_2+\left(\psi_{\ell_2}^T\mathbf{c}\right)cos\theta_2\right\}\right]\\
&-\int_0^{\ell_1}(EI)_1\left(\phi''\phi''^T\mathbf{a}\right)dr_1\\
&-K_{t_2}\left(\phi'_{\ell_1}\phi'^T_{\ell_1}\mathbf{a}-\theta_2\phi'_{\ell_1}\right)\\
&-\int_0^{\ell_1}(\rho A)_1\left[g\left(\phi\right)sin\theta_1\right]dr_1-\left(m_a+m_b\right)g\left(\phi_{\ell_1}\right)sin\theta_1
\end{aligned}
\qquad (11.12)
$$

$$
\begin{aligned}
& -\int_0^{\ell_2}(\rho A)_2\left[g\left(\phi_{\ell_1}\right)sin\theta_1\right]dr_2 - m_p g\left(\phi_{\ell_1}\right)sin\theta_1 \\
& -\int_0^{\ell_1}(\rho A)_1 g\left[cos\theta_1\int_0^{r_1}\left(\phi'\phi'^T\mathbf{a}\right)d\xi_1\right]dr_1 \\
& -\int_0^{\ell_1}\left(m_a+m_b+m_p\right)gcos\theta_1\left(\phi'\phi'^T\mathbf{a}\right)dr_1 \\
& -\int_0^{\ell_2}(\rho A)_2 g\left[cos\theta_1\int_0^{\ell_1}\left(\phi'\phi'^T\mathbf{a}\right)dr_1\right]dr_2 \\
f_3(\mathbf{q},\dot{\mathbf{q}}) \;=\; & -\int_0^{\ell_2}(\rho A)_2\Big[2\left(\dot\theta_1+\dot\theta_2\right)\left(\dot{\mathbf{c}}^T\psi\psi^T\mathbf{c}\right) \\
& \quad +\dot\theta_1\left(\phi_{\ell_1}^T\dot{\mathbf{a}}\right)\left\{r_2 sin\theta_2+\left(\psi^T\mathbf{c}\right)cos\theta_2\right\} \\
& \quad +\left(\ell_1\dot\theta_1+\phi_{\ell_1}^T\dot{\mathbf{a}}\right)\left\{-\left(\psi^T\dot{\mathbf{c}}\right)sin\theta_2\right. \\
& \qquad \left.-r_2\dot\theta_2 sin\theta_2-\left(\psi^T\mathbf{c}\right)\dot\theta_2 cos\theta_2\right\} \\
& \quad +\dot\theta_1\left(\phi_{\ell_1}^T\mathbf{a}\right)\left\{\left(\psi^T\dot{\mathbf{c}}\right)cos\theta_2\right. \\
& \qquad \left.+r_2\dot\theta_2 cos\theta_2-\left(\psi^T\mathbf{c}\right)\dot\theta_2 sin\theta_2\right\}\Big]dr_2 \\
& -m_p\Big[2\left(\dot\theta_1+\dot\theta_2\right)\left(\dot{\mathbf{c}}^T\psi_{\ell_2}\psi_{\ell_2}^T\mathbf{c}\right) \\
& \quad +\dot\theta_1\left(\phi_{\ell_1}^T\dot{\mathbf{a}}\right)\left\{\ell_2 sin\theta_2+\left(\psi_{\ell_2}^T\mathbf{c}\right)cos\theta_2\right\} \\
& \quad +\left(\ell_1\dot\theta_1+\phi_{\ell_1}^T\dot{\mathbf{a}}\right)\left\{-\left(\psi_{\ell_2}^T\dot{\mathbf{c}}\right)sin\theta_2\right. \\
& \qquad \left.-\ell_2\dot\theta_2 sin\theta_2-\left(\psi_{\ell_2}^T\mathbf{c}\right)\dot\theta_2 cos\theta_2\right\} \\
& \quad +\dot\theta_1\left(\phi_{\ell_1}^T\mathbf{a}\right)\left(\ell_2\dot\theta_2 cos\theta_2\right) \\
& \quad +\dot\theta_1\left(\phi_{\ell_1}^T\mathbf{a}\right)\left\{\left(\psi_{\ell_2}^T\dot{\mathbf{c}}\right)cos\theta_2-\left(\psi_{\ell_2}^T\mathbf{c}\right)\dot\theta_2 sin\theta_2\right\}\Big] \\
& +\int_0^{\ell_2}(\rho A)_2\Big[-\left(\phi_{\ell_1}^T\dot{\mathbf{a}}\right)\left(\psi^T\dot{\mathbf{c}}\right)sin\theta_2 \\
& \quad -\ell_1\dot\theta_1\left(\psi^T\dot{\mathbf{c}}\right)sin\theta_2+\dot\theta_1\left(\phi_{\ell_1}^T\mathbf{a}\right)\left(\psi^T\dot{\mathbf{c}}\right)cos\theta_2 \\
& \quad +\left(\dot\theta_1+\dot\theta_2\right)\left\{\left(\ell_1\dot\theta_1+\phi_{\ell_1}^T\dot{\mathbf{a}}\right)\left(-r_2 sin\theta_2-\left(\psi^T\mathbf{c}\right)cos\theta_2\right)\right.
\end{aligned}
\tag{11.13}
$$

$$
\begin{aligned}
&\quad +\dot{\theta}_1\left(\phi_{\ell_1}^T\mathbf{a}\right)\left(r_2cos\theta_2-\left(\psi^T\mathbf{c}\right)sin\theta_2\right)\Big\}\Big]\,dr_2\\
&+m_p\Big[-\left(\phi_{\ell_1}^T\dot{\mathbf{a}}\right)\left(\psi_{\ell_2}^T\dot{\mathbf{c}}\right)sin\theta_2\\
&\quad -\ell_1\dot{\theta}_1\left(\psi_{\ell_2}^T\dot{\mathbf{c}}\right)sin\theta_2+\dot{\theta}_1\left(\phi_{\ell_1}^T\mathbf{a}\right)\left(\psi_{\ell_2}^T\dot{\mathbf{c}}\right)cos\theta_2\\
&\quad +\left(\dot{\theta}_1+\dot{\theta}_2\right)\Big\{\left(\ell_1\dot{\theta}_1+\phi_{\ell_1}^T\dot{\mathbf{a}}\right)\left(-\ell_2sin\theta_2-\left(\psi_{\ell_2}^T\mathbf{c}\right)cos\theta_2\right)\\
&\quad +\dot{\theta}_1\left(\phi_{\ell_1}^T\mathbf{a}\right)\left(\ell_2cos\theta_2-\left(\psi_{\ell_2}^T\mathbf{c}\right)sin\theta_2\right)\Big\}\Big]\\
&+K_{t_2}\left(\phi_{\ell_1}^{\prime T}\mathbf{a}-\theta_2\right)\\
&-\int_0^{\ell_2}(\rho A)_2g\Big[\Big\{-\left(\psi^T\mathbf{c}\right)sin\theta_2+r_2cos\theta_2\Big\}sin\theta_1\\
&\quad +\Big\{\left(\psi^T\mathbf{c}\right)cos\theta_2+r_2sin\theta_2\Big\}cos\theta_1\Big]\,dr_2\\
&-m_pg\Big[\Big\{-\left(\psi_{\ell_2}^T\mathbf{c}\right)sin\theta_2+\ell_2cos\theta_2\Big\}sin\theta_1\\
&\quad +\Big\{\left(\psi_{\ell_2}^T\mathbf{c}\right)cos\theta_2+\ell_2sin\theta_2\Big\}cos\theta_1\Big]\\
&+\frac{1}{2}\int_0^{\ell_2}(\rho A)_2g\big(cos\theta_2sin\theta_1+sin\theta_2cos\theta_1\big)\\
&\qquad\qquad\Big[\int_0^{r_2}\left(\mathbf{c}^T\psi'\psi'^T\mathbf{c}\right)d\xi_2\Big]\,dr_2\\
&+\frac{1}{2}m_pg\big(cos\theta_2sin\theta_1+sin\theta_2cos\theta_1\big)\int_0^{\ell_2}\left(\mathbf{c}^T\psi'\psi'^T\mathbf{c}\right)dr_2
\end{aligned}
$$

$$
\begin{aligned}
\mathbf{f}_4(\mathbf{q},\dot{\mathbf{q}}) \;=\; &-\int_0^{\ell_2}(\rho A)_2\Big[-\left(\phi_{\ell_1}^T\dot{\mathbf{a}}\right)\left(\psi\right)\dot{\theta}_2sin\theta_2-\ell_1\dot{\theta}_1\dot{\theta}_2\left(\psi\right)sin\theta_2\\
&\quad +\dot{\theta}_1\left(\phi_{\ell_1}^T\dot{\mathbf{a}}\right)\left(\psi\right)sin\theta_2+\dot{\theta}_1\dot{\theta}_2\left(\phi_{\ell_1}^T\mathbf{a}\right)\left(\psi\right)cos\theta_2\Big]\,dr_2\\
&-m_p\Big[-\left(\phi_{\ell_1}^T\dot{\mathbf{a}}\right)\left(\psi_{\ell_2}\right)\dot{\theta}_2sin\theta_2-\ell_1\dot{\theta}_1\dot{\theta}_2\left(\psi_{\ell_2}\right)sin\theta_2\\
&\quad +\dot{\theta}_1\left(\phi_{\ell_1}^T\dot{\mathbf{a}}\right)\left(\psi_{\ell_2}\right)sin\theta_2+\dot{\theta}_1\dot{\theta}_2\left(\phi_{\ell_1}^T\mathbf{a}\right)\left(\psi_{\ell_2}\right)cos\theta_2\Big]\\
&+\int_0^{\ell_2}(\rho A)_2\Big[\left(\dot{\theta}_1+\dot{\theta}_2\right)^2\left(\psi\psi^T\mathbf{c}\right)\\
&\quad -\left(\dot{\theta}_1+\dot{\theta}_2\right)\left(\ell_1\dot{\theta}_1+\phi_{\ell_1}^T\dot{\mathbf{a}}\right)\left(\psi\right)sin\theta_2
\end{aligned}
\qquad (11.14)
$$

$$
\begin{aligned}
&+\left(\dot{\theta}_1+\dot{\theta}_2\right)\dot{\theta}_1\left(\phi_{\ell_1}^T\mathbf{a}\right)\left(\psi\right)cos\theta_2\Big]\,dr_2\\
&+m_p\Big[\left(\dot{\theta}_1+\dot{\theta}_2\right)^2\left(\psi_{\ell_2}\psi_{\ell_2}^T\mathbf{c}\right)\\
&\quad-\left(\dot{\theta}_1+\dot{\theta}_2\right)\left(\ell_1\dot{\theta}_1+\phi_{\ell_1}^T\dot{\mathbf{a}}\right)\left(\psi_{\ell_2}\right)sin\theta_2\\
&\quad+\left(\dot{\theta}_1+\dot{\theta}_2\right)\dot{\theta}_1\left(\phi_{\ell_1}^T\mathbf{a}\right)\left(\psi_{\ell_2}\right)cos\theta_2\Big]\\
&-\int_0^{\ell_2}(EI)_2\left(\psi''\psi''^T\mathbf{c}\right)dr_2\\
&-\int_0^{\ell_2}(\rho A)_2 g\Big[(\psi)\,cos\theta_2 sin\theta_1+(\psi)\,sin\theta_2 cos\theta_1\Big]dr_2\\
&-m_p g\Big[\left(\psi_{\ell_2}\right)cos\theta_2 sin\theta_1+\left(\psi_{\ell_2}\right)sin\theta_2 cos\theta_1\Big]\\
&-\int_0^{\ell_2}(\rho A)_2 g\left(-sin\theta_2 sin\theta_1+cos\theta_2 cos\theta_1\right)\\
&\qquad\qquad\Big[\int_0^{r_2}\left(\psi'\psi'^T\mathbf{c}\right)d\xi_2\Big]\,dr_2\\
&-m_p g\left(-sin\theta_2 sin\theta_1+cos\theta_2 cos\theta_1\right)\int_0^{\ell_2}\left(\mathbf{c}^T\psi'\psi'^T\mathbf{c}\right)dr_2
\end{aligned}
$$

12. APPENDIX B. NONZERO ELEMENTS OF THE MATRIX IN EQUATION 4.31

This appendix gives nonzero elements of the matrix in Equation 4.31.

$$
\begin{aligned}
S_{11} &= \frac{g}{\omega^2} \\
S_{23} &= \alpha \\
S_{25} &= \alpha \\
S_{32} &= -cosh(\alpha l_1) \\
S_{33} &= -sinh(\alpha l_1) \\
S_{34} &= -cos(\alpha l_1) \\
S_{35} &= -sin(\alpha l_1) \\
S_{36} &= \frac{g}{\omega^2} \\
S_{48} &= \beta \\
S_{410} &= \beta \\
S_{52} &= \omega^2(m_a + m_b)cosh(\alpha l_1) + (EI)_1\alpha^3 sinh(\alpha l_1) \\
S_{53} &= \omega^2(m_a + m_b)sinh(\alpha l_1) + (EI)_1\alpha^3 cosh(\alpha l_1) \\
S_{54} &= \omega^2(m_a + m_b)cos(\alpha l_1) + (EI)_1\alpha^3 sin(\alpha l_1) \\
S_{55} &= \omega^2(m_a + m_b)sin(\alpha l_1) - (EI)_1\alpha^3 cos(\alpha l_1)
\end{aligned}
$$

$$
\begin{aligned}
S_{56} &= m_p g + (\rho A)_2 \ell_2 g \\
S_{57} &= \omega^2 m_p \cosh(\beta\ell_2) + \frac{1}{\beta}\omega^2(\rho A)_2 \sinh(\beta\ell_2) \\
S_{58} &= \omega^2 m_p \sinh(\beta\ell_2) + \frac{1}{\beta}\omega^2(\rho A)_2 \big(\cosh(\beta\ell_2) - 1\big) \\
S_{59} &= \omega^2 m_p \cos(\beta\ell_2) + \frac{1}{\beta}\omega^2(\rho A)_2 \sin(\beta\ell_2) \\
S_{510} &= \omega^2 m_p \sin(\beta\ell_2) + \frac{1}{\beta}\omega^2(\rho A)_2 \big(-\cos(\beta\ell_2) + 1\big) \\
S_{61} &= K_{t_2} \\
S_{62} &= -(EI)_1\alpha^2 \cosh(\alpha\ell_1) + \omega^2 J_a \alpha \sinh(\alpha\ell_1) - K_{t_2}\alpha \sinh(\alpha\ell_1) \\
S_{63} &= -(EI)_1\alpha^2 \sinh(\alpha\ell_1) + \omega^2 J_a \alpha \cosh(\alpha\ell_1) - K_{t_2}\alpha \cosh(\alpha\ell_1) \\
S_{64} &= (EI)_1\alpha^2 \cos(\alpha\ell_1) - \omega^2 J_a \alpha \sin(\alpha\ell_1) + K_{t_2}\alpha \sin(\alpha\ell_1) \\
S_{65} &= (EI)_1\alpha^2 \sin(\alpha\ell_1) + \omega^2 J_a \alpha \cos(\alpha\ell_1) - K_{t_2}\alpha \cos(\alpha\ell_1) \\
S_{66} &= K_{t_2} \\
S_{77} &= m_p\omega^2 \cosh(\beta\ell_2) + (EI)_2\beta^3 \sinh(\beta\ell_2) \\
S_{78} &= m_p\omega^2 \sinh(\beta\ell_2) + (EI)_2\beta^3 \cosh(\beta\ell_2) \\
S_{79} &= m_p\omega^2 \cos(\beta\ell_2) + (EI)_2\beta^3 \sin(\beta\ell_2) \\
S_{710} &= m_p\omega^2 \sin(\beta\ell_2) - (EI)_2\beta^3 \cos(\beta\ell_2) \\
S_{87} &= -(EI)_2\beta^2 \cosh(\beta\ell_2) + J_p\omega^2\beta \sinh(\beta\ell_2) \\
S_{88} &= -(EI)_2\beta^2 \sinh(\beta\ell_2) + J_p\omega^2\beta \cosh(\beta\ell_2) \\
S_{89} &= (EI)_2\beta^2 \cos(\beta\ell_2) - J_p\omega^2\beta \sin(\beta\ell_2) \\
S_{810} &= (EI)_2\beta^2 \sin(\beta\ell_2) + J_p\omega^2\beta \cos(\beta\ell_2) \\
S_{91} &= -(m_a + m_b + m_p)\frac{g^2}{\omega^2} - K_{t_1} + \omega^2(J_1 + J_b) \\
&\quad + g\left\{(m_a + m_b)\ell_1 + m_p(\ell_1 + \ell_2)\right\} - (\rho A)_1\frac{g^2}{\omega^2}\ell_1
\end{aligned}
$$

$$+\frac{1}{2}(\rho A)_1 g\ell_1^2 - (\rho A)_2\frac{g^2}{\omega^2}\ell_2 + (\rho A)_2 g\ell_1\ell_2 + \frac{1}{2}(\rho A)_2 g\ell_2^2$$

$$\begin{aligned}
S_{92} &= -(m_a+m_b)g\cosh(\alpha\ell_1) + \omega^2(m_a+m_b)\ell_1\cosh(\alpha\ell_1) \\
&\quad + J_a\omega^2\alpha\sinh(\alpha\ell_1) - (\rho A)_1\frac{g}{\alpha}\sinh(\alpha\ell_1) \\
&\quad + (\rho A)_1\frac{\omega^2}{\alpha^2}\Big((\alpha\ell_1)\sinh(\alpha\ell_1) - \cosh(\alpha\ell_1) + 1\Big) \\
S_{93} &= -(m_a+m_b)g\sinh(\alpha\ell_1) + \omega^2(m_a+m_b)\ell_1\sinh(\alpha\ell_1) \\
&\quad + J_a\omega^2\alpha\cosh(\alpha\ell_1) - (\rho A)_1\frac{g}{\alpha}\Big(\cosh(\alpha\ell_1) - 1\Big) \\
&\quad + (\rho A)_1\frac{\omega^2}{\alpha^2}\Big((\alpha\ell_1)\cosh(\alpha\ell_1) - \sinh(\alpha\ell_1)\Big) \\
S_{94} &= -(m_a+m_b)g\cos(\alpha\ell_1) + \omega^2(m_a+m_b)\ell_1\cos(\alpha\ell_1) \\
&\quad - J_a\omega^2\alpha\sin(\alpha\ell_1) - (\rho A)_1\frac{g}{\alpha}\sin(\alpha\ell_1) \\
&\quad + (\rho A)_1\frac{\omega^2}{\alpha^2}\Big(\cos(\alpha\ell_1) + (\alpha\ell_1)\sin(\alpha\ell_1) - 1\Big) \\
S_{95} &= -(m_a+m_b)g\sin(\alpha\ell_1) + \omega^2(m_a+m_b)\ell_1\sin(\alpha\ell_1) \\
&\quad + J_a\omega^2\alpha\cos(\alpha\ell_1) + (\rho A)_1\frac{g}{\alpha}\Big(\cos(\alpha\ell_1) - 1\Big) \\
&\quad + (\rho A)_1\frac{\omega^2}{\alpha^2}\Big(\sin(\alpha\ell_1) - (\alpha\ell_1)\cos(\alpha\ell_1)\Big) \\
S_{96} &= -m_p\frac{g^2}{\omega^2} + \omega^2 J_b + m_p g(\ell_1+\ell_2) \\
&\quad + (\rho A)_2\left(-\frac{g^2}{\omega^2}\ell_2 + g\ell_1\ell_2 + \frac{1}{2}g\ell_2^2\right) \\
S_{97} &= -m_p g\cosh(\beta\ell_2) + m_p(\ell_1+\ell_2)\omega^2\cosh(\beta\ell_2) + J_p\omega^2\beta\sinh(\beta\ell_2) \\
&\quad + (\rho A)_2(-g+\omega^2\ell_1)\frac{1}{\beta}\sinh(\beta\ell_2) \\
&\quad + (\rho A)_2\frac{\omega^2}{\beta^2}\Big((\beta\ell_2)\sinh(\beta\ell_2) - \cosh(\beta\ell_2) + 1\Big) \\
S_{98} &= -m_p g\sinh(\beta\ell_2) + m_p(\ell_1+\ell_2)\omega^2\sinh(\beta\ell_2) + J_p\omega^2\beta\cosh(\beta\ell_2)
\end{aligned}$$

$$+(\rho A)_2(-g+\omega^2\ell_1)\frac{1}{\beta}\Big(cosh\,(\beta\ell_2)-1\Big)$$

$$+(\rho A)_2\frac{\omega^2}{\beta^2}\Big((\beta\ell_2)\,cosh\,(\beta\ell_2)-sinh\,(\beta\ell_2)\Big)$$

$$S_{99} = -m_p g cos\,(\beta\ell_2)+m_p(\ell_1+\ell_2)\omega^2 cos\,(\beta\ell_2)-J_p\omega^2\beta sin\,(\beta\ell_2)$$

$$+(\rho A)_2(-g+\omega^2\ell_1)\frac{1}{\beta}sin\,(\beta\ell_2)$$

$$+(\rho A)_2\frac{\omega^2}{\beta^2}\Big(cos\,(\beta\ell_2)+(\beta\ell_2)\,sin\,(\beta\ell_2)-1\Big)$$

$$S_{910} = -m_p g sin\,(\beta\ell_2)+m_p(\ell_1+\ell_2)\omega^2 sin\,(\beta\ell_2)+J_p\omega^2\beta cos\,(\beta\ell_2)$$

$$+(\rho A)_2(-g+\omega^2\ell_1)\frac{1}{\beta}\Big(-cos\,(\beta\ell_2)+1\Big)$$

$$+(\rho A)_2\frac{\omega^2}{\beta^2}\Big(sin\,(\beta\ell_2)-(\beta\ell_2)\,cos\,(\beta\ell_2)\Big)$$

$$S_{101} = -K_{t_2}+\omega^2 J_b+m_p g\ell_2+\frac{1}{2}g(\rho A)_2\ell_2^2$$

$$S_{102} = K_{t_2}\alpha sinh\,(\alpha\ell_1)+m_p g cosh\,(\alpha\ell_1)+(\rho A)_2 g\ell_2 cosh\,(\alpha\ell_1)$$

$$S_{103} = K_{t_2}\alpha cosh\,(\alpha\ell_1)+m_p g sinh\,(\alpha\ell_1)+(\rho A)_2 g\ell_2 sinh\,(\alpha\ell_1)$$

$$S_{104} = -K_{t_2}\alpha sin\,(\alpha\ell_1)+m_p g cos\,(\alpha\ell_1)+(\rho A)_2 g\ell_2 cos\,(\alpha\ell_1)$$

$$S_{105} = K_{t_2}\alpha cos\,(\alpha\ell_1)+m_p g sin\,(\alpha\ell_1)+(\rho A)_2 g\ell_2 sin\,(\alpha\ell_1)$$

$$S_{106} = -K_{t_2}-m_p\frac{g^2}{\omega^2}+\omega^2 J_b+m_p g\ell_2+(\rho A)_2\left(-\frac{g^2}{\omega^2}\ell_2+\frac{1}{2}g\ell_2^2\right)$$

$$S_{107} = -m_p g cosh\,(\beta\ell_2)+\omega^2 m_p\ell_2 cosh\,(\beta\ell_2)+\omega^2 J_p\beta sinh\,(\beta\ell_2)$$

$$-(\rho A)_2\frac{g}{\beta}sinh\,(\beta\ell_2)+(\rho A)_2\frac{\omega^2}{\beta^2}\Big((\beta\ell_2)\,sinh\,(\beta\ell_2)-cosh\,(\beta\ell_2)+1\Big)$$

$$S_{108} = -m_p g sinh\,(\beta\ell_2)+\omega^2 m_p\ell_2 sinh\,(\beta\ell_2)+\omega^2 J_p\beta cosh\,(\beta\ell_2)$$

$$-(\rho A)_2\frac{g}{\beta}\Big(cosh\,(\beta\ell_2)-1\Big)+(\rho A)_2\frac{\omega^2}{\beta^2}\Big((\beta\ell_2)\,cosh\,(\beta\ell_2)-sinh\,(\beta\ell_2)\Big)$$

$$S_{109} = -m_p g cos\,(\beta\ell_2)+\omega^2 m_p\ell_2 cos\,(\beta\ell_2)-\omega^2 J_p\beta sin\,(\beta\ell_2)$$

$$
\begin{aligned}
& -(\rho A)_2 \frac{g}{\beta} sin\,(\beta \ell_2) + (\rho A)_2 \frac{\omega^2}{\beta^2} \Big(cos\,(\beta \ell_2) + (\beta \ell_2)\, sin\,(\beta \ell_2) - 1 \Big) \\
S_{1010} \;=\; & -m_p g sin\,(\beta \ell_2) + \omega^2 m_p \ell_2 sin\,(\beta \ell_2) + \omega^2 J_p \beta cos\,(\beta \ell_2) \\
& +(\rho A)_2 \frac{g}{\beta} \Big(cos\,(\beta \ell_2) - 1 \Big) + (\rho A)_2 \frac{\omega^2}{\beta^2} \Big(sin\,(\beta \ell_2) - (\beta \ell_2)\, cos\,(\beta \ell_2) \Big)
\end{aligned}
$$

13. APPENDIX C. EIGENVECTOR FOR EXACT SOLUTION

This appendix presents two methods for finding the eigenvectors of exact solution. The eigenvectors can be analytically found by substituting the eigenvalues into the characteristic matrix, and then analytically solving the homogeneous linear system for a set of (Θ_1, b_1, b_2, b_3, b_4,Θ_2, d_1, d_2, d_3, d_4). The analytical procedure to find eigenvectors is illustrated as follows.

First, manipulating terms of the first, second, and fourth equations of the homogeneous linear system (Equation 4.31) yields the following three equations.

$$b_1 = -b_3 - S_{11}\Theta_1 \tag{13.1}$$

$$b_2 = -\frac{S_{25}}{S_{23}}b_4 + \frac{\Theta_1}{S_{23}} \tag{13.2}$$

$$\Theta_2 = -\Theta_1 + S_{48}d_2 + S_{410}d_4 \tag{13.3}$$

Substituting Equations 13.1, 13.2 and 13.3 into the sixth equation of the homogeneous linear system (Equation 4.31) yields the expression for b_3.

$$b_3 = R_{31}\Theta_1 + R_{34}b_4 + R_{38}d_2 + R_{310}d_4 \tag{13.4}$$

where the coefficients, R_{31},R_{34}, R_{38} and R_{310} are represented by

$$R_{31} = \frac{-\left(S_{61} - S_{62}S_{11} + \frac{S_{63}}{S_{23}} - S_{66}\right)}{-S_{62} + S_{64}}$$

$$R_{34} = \frac{-\left(\frac{-S_{63}S_{25}}{S_{23}} + S_{65}\right)}{-S_{62} + S_{64}}$$

$$R_{38} = \frac{-S_{66}S_{48}}{-S_{62} + S_{64}}$$

$$R_{310} = \frac{-S_{66}S_{410}}{-S_{62} + S_{64}}$$

Substituting Equations 13.1 – 13.4 into the third equation of the homogeneous system (Equation 4.31) yields the expression for b_4.

$$b_4 = R_{41}\Theta_1 + R_{47}d_1 + R_{48}d_2 + R_{49}d_3 + R_{410}d_4 \tag{13.5}$$

The coefficients R_{41}, R_{47}, R_{48}, R_{49} and R_{410} are defined by

$$R_{41} = \frac{\left[-(-S_{32} + S_{34})R_{31} + S_{32}S_{11} - \frac{S_{33}}{S_{23}} + S_{36}\right]}{[R4d]}$$

$$R_{47} = -\frac{1}{[R4d]}$$

$$R_{48} = \frac{\left[-(-S_{32} + S_{34})R_{38} - S_{36}S_{48}\right]}{[R4d]}$$

$$R_{49} = -\frac{1}{[R4d]}$$

$$R_{410} = \frac{\left[-(-S_{32} + S_{34})R_{310} - S_{36}S_{410}\right]}{[R4d]}$$

where the common denominator $R4d$ is given by

$$R4d = (-S_{32} + S_{24})R_{34} - \frac{S_{33}S_{25}}{S_{23}} + S_{35}$$

Substituting the Equations 13.1 – 13.5 into the fifth equation of the homogeneous system (Equation 4.31) yields the expression for d_1.

$$d_1 = R_{71}\Theta_1 + R_{78}d_2 + R_{79}d_3 + R_{710}d_4 \tag{13.6}$$

In the Equation 13.6, the coefficients are given by

$$\begin{aligned}
R_{71} &= -\Big[S_{51} - S_{52}S_{11} + \frac{S_{53}}{S_{23}} + (-S_{52} + S_{54})R_{31} + S_{55}R_{41} \\
&\quad -S_{56} + \Big\{(-S_{52} + S_{54})R_{34} - \frac{S_{53}S_{25}}{S_{23}}\Big\}R_{41}\Big] \;/\; [R7d] \\
R_{78} &= -\Big[S_{55}R_{48} + S_{56}S_{48} + S_{58} + (-S_{52} + S_{54})R_{38} \\
&\quad + \Big\{(-S_{52} + S_{54})R_{34} - \frac{S_{53}S_{25}}{S_{23}}\Big\}R_{48}\Big] \;/\; [R7d] \\
R_{79} &= -\frac{\Big[S_{55}R_{49} + S_{59} + \Big\{(-S_{52} + S_{54})R_{34} - \frac{S_{53}S_{25}}{S_{23}}\Big\}R_{49}\Big]}{[R7d]} \\
R_{710} &= -\Big[S_{55}R_{410} + S_{56}S_{410} + S_{510} + (-S_{52} + S_{54})R_{310} \\
&\quad + \Big\{(-S_{52} + S_{54})R_{34} - \frac{S_{53}S_{25}}{S_{23}}\Big\}R_{410}\Big] \;/\; [R7d]
\end{aligned}$$

where the common denominator $R7d$ is given by

$$R7d = S_{55}R_{47} + S_{57} + \Big\{(-S_{52} + S_{54})R_{34} - \frac{S_{53}S_{25}}{S_{23}}\Big\}R_{47}$$

When the Equations 13.1 – 13.6 are substituted into the ninth equation of the homogeneous system (Equation 4.31), the expression for d_2 is given by

$$d_2 = R_{81}\Theta_1 + R_{89}d_3 + R_{810}d_4 \tag{13.7}$$

In the Equation 13.7, the coefficients are given by

$$R_{81} = -\Big[S_{91} - S_{92}S_{11} + \frac{S_{93}}{S_{23}} - S_{96} + S_{97}R_{71} + (-S_{92} + S_{94})R_{31}$$

$$+\left\{(-S_{92}+S_{94})R_{34}-\frac{S_{93}S_{25}}{S_{23}}+S_{95}\right\}(R_{41}+R_{47}R_{71})\Big]$$
$$/\ [R8d]$$

$$R_{89} = -\Big[S_{97}R_{79}+S_{99}$$
$$+\left\{(-S_{92}+S_{94})R_{34}-\frac{S_{93}S_{25}}{S_{23}}+S_{95}\right\}(R_{47}R_{79}+R_{49})\Big]$$
$$/\ [R8d]$$

$$R_{810} = -\Big[(-S_{92}+S_{94})R_{310}+S_{96}S_{410}+S_{97}R_{710}+S_{910}$$
$$+\left\{(-S_{92}+S_{94})R_{34}-\frac{S_{93}S_{25}}{S_{23}}+S_{95}\right\}(R_{47}R_{710}+R_{410})\Big]$$
$$/\ [R8d]$$

where the common denominator $R8d$ is given by

$$R8d = (-S_{92}+S_{94})R_{38}+S_{96}S_{48}+S_{97}R_{78}+S_{98}$$
$$+\left\{(-S_{92}+S_{94})R_{34}-\frac{S_{93}S_{25}}{S_{23}}+S_{95}\right\}(R_{47}R_{78}+R_{48})$$

Substituting Equations 13.6 and 13.7 the the seventh equation of the homogeneous system (Equation 4.31) yields the expression for d_3.

$$d_3 = R_{91}\Theta_1 + R_{910}d_4 \tag{13.8}$$

Where the coefficients are given by

$$R_{91} = -\frac{\left[S_{77}R_{71}+(S_{77}R_{78}+S_{78})R_{81}\right]}{[R9d]}$$

$$R_{910} = -\frac{\left[(S_{77}R_{78}+S_{78})R_{810}+S_{77}R_{710}+S_{710}\right]}{[R9d]}$$

where the common denominator $R9d$ is given by

$$R9d = (S_{77}R_{78} + S_{78})R_{89} + S_{77}R_{79} + S_{79}$$

Finally, substituting Equations 13.6 - 13.8 into the eighth equation of the homogeneous system (Equation 4.31), the following relationship is found between d_4 and Θ_1.

$$d_4 = R_{101}\Theta_1 \tag{13.9}$$

Where the coefficient is given by

$$\begin{aligned} R_{101} \;=\; & -\Big[S_{87}R_{71} + (S_{87}R_{78} + S_{88})R_{81} \\ & + (S_{87}R_{78} + S_{88})R_{89}R_{91} + S_{87}R_{79}R_{91} + S_{89}R_{91}\Big] \;/ \\ & \Big[(S_{87}R_{78} + S_{88})R_{89}R_{910} + S_{87}R_{79}R_{910} + S_{89}R_{910} \\ & + (S_{87}R_{78} + S_{88})R_{810} + S_{87}R_{710} + S_{810}\Big] \end{aligned}$$

To find an eigenvector, the value of each element of the characteristic matrix is evaluated by substituting an eigenvalue into the matrix. Θ_1 is arbitrarily set because an eigenvector can be scaled arbitrary. Then, d_4 is calculated from the Equation 13.9. Θ_1 and d_4 are substituted into Equation 13.8 and then d_3 is computed. With the same procedure, an eigenvector can be found by sequentially substituting previously computed elements of the eigenvector to the calculation of the next element in the inverse order.

Another simpler way to find eigenvectors [44] is from direct comparison between the given homogeneous system (Equation 4.31) and the formal definition for the inverse of a characteristic matrix. Even though there does not exist the inverse matrix of the system characteristic matrix because the determinant of the matrix is

zero, the formal definition of the inverse of the characteristic matrix is defined by

$$\left[S_{ij}\right]^{-1} = \frac{\left[S_{ij}\right]^{a}}{det\left[S_{ij}\right]} \tag{13.10}$$

where $\left[S_{ij}\right]^{a}$ denotes the adjoint matrix of $\left[S_{ij}\right]$. By a speculation, the following relationship may be established

$$\left[S_{ij}\right]\left[S_{ij}\right]^{a} = \left[S_{ij}\right]\left[S_{ij}\right]^{-1} det\left[S_{ij}\right] = 0 \tag{13.11}$$

since $det\left[S_{ij}\right]$ is equal to zero. Thus, it yields the following equation.

$$\left[S_{ij}\right]\left[S_{ij}\right]^{a} = 0 \tag{13.12}$$

When the Equation 13.12 is compared with the homogeneous system (Equation 4.31), it is apparent that an eigenvector is proportion to any nonzero column of the adjoint characteristic matrix $\left[S_{ij}\right]^{a}$. If it is required, each column of the adjoint matrix can be scaled arbitrary.

14. APPENDIX D. UPPER TRIANGULAR ELEMENTS OF THE MATRICES IN EQUATION 7.1

This appendix gives upper triangular elements of the matrices in Equation 6.1.

$$
\begin{aligned}
M_{11} &= J_1 + \frac{1}{3}(\rho A)_1 \ell_1^3 + \left(m_a + m_b\right) \ell_1^2 + \left(J_a + J_b\right) \\
&\quad + (\rho A)_2 \left(\ell_1^2 \ell_2 + \frac{1}{3}\ell_2^3 + \ell_1 \ell_2^2\right) \\
&\quad + m_p \left(\ell_1^2 + \ell_2^2 + 2\ell_1 \ell_2\right) + J_p
\end{aligned} \tag{14.1}
$$

$$
\begin{aligned}
\mathrm{M}_{12} &= \int_0^{\ell_1} (\rho A)_1 \left(r_1 \phi^T\right) dr_1 + \left(m_a + m_b\right) \ell_1 \phi_{\ell_1}^T + J_a \phi_{\ell_1}'^T \\
&\quad + (\rho A)_2 \left(\ell_1 \ell_2 + \frac{1}{2}\ell_2^2\right) \phi_{\ell_1}^T + m_p \left(\ell_1 + \ell_2\right) \phi_{\ell_1}^T
\end{aligned} \tag{14.2}
$$

$$
\begin{aligned}
M_{13} &= J_b + (\rho A)_2 \left(\frac{1}{3}\ell_2^3 + \frac{1}{2}\ell_1 \ell_2^2\right) \\
&\quad + m_p \left(\ell_2^2 + \ell_1 \ell_2\right) + J_p
\end{aligned} \tag{14.3}
$$

$$
\begin{aligned}
\mathrm{M}_{14} &= \int_0^{\ell_2} (\rho A)_2 \left(\ell_1 \psi^T + r_2 \psi^T\right) dr_2 \\
&\quad + m_p \left(\ell_1 \psi_{\ell_2}^T + \ell_2 \psi_{\ell_2}^T\right) + J_p \psi_{\ell_2}'^T
\end{aligned} \tag{14.4}
$$

$$
\begin{aligned}
\mathrm{M}_{22} &= \int_0^{\ell_1} (\rho A)_1 \left(\phi \phi^T\right) dr_1 + (\rho A)_2 \ell_2 \left(\phi_{\ell_1} \phi_{\ell_1}^T\right) \\
&\quad + \left(m_a + m_b + m_p\right) \left(\phi_{\ell_1} \phi_{\ell_1}^T\right) + J_a \left(\phi_{\ell_1}' \phi_{\ell_1}'^T\right)
\end{aligned} \tag{14.5}
$$

$$
\mathrm{M}_{23} = \frac{1}{2}(\rho A)_2 \ell_2^2 \left(\phi_{\ell_1}\right) + m_p \left(\ell_2 \phi_{\ell_1}\right) \tag{14.6}
$$

$$
\mathrm{M}_{24} = \int_0^{\ell_2} (\rho A)_2 \left(\phi_{\ell_1} \psi^T\right) dr_2 + m_p \left(\phi_{\ell_1} \psi_{\ell_2}^T\right) \tag{14.7}
$$

$$M_{33} = J_b + m_p\left(\ell_2^2\right) + J_p + \frac{1}{3}(\rho A)_2 \ell_2^3 \tag{14.8}$$

$$\mathbf{M}_{34} = \int_0^{\ell_2} (\rho A)_2 \left(r_2 \psi^T\right) dr_2 + m_p\left(\ell_2 \psi_{\ell_2}^T\right) + J_p\left(\psi_{\ell_2}'^T\right) \tag{14.9}$$

$$\mathbf{M}_{44} = \int_0^{\ell_2} (\rho A)_2 \left(\psi \psi^T\right) dr_2 + m_p\left(\psi_{\ell_2} \psi_{\ell_2}^T\right) + J_p\left(\psi_{\ell_2}' \psi_{\ell_2}'^T\right) \tag{14.10}$$

$$K_{11} = K_{t_1} + \left(m_a + m_b\right) g \ell_1 + m_p g\left(\ell_1 + \ell_2\right) + \frac{1}{2}(\rho A)_1 g \ell_1^2 + (\rho A)_2 g\left(\ell_1 \ell_2 + \frac{1}{2}\ell_2^2\right) \tag{14.11}$$

$$\mathbf{K}_{12} = \left(m_a + m_b + m_p\right) g \phi_{\ell_1}^T + \int_0^{\ell_1} (\rho A)_1 g\left(\phi^T\right) dr_1 + (\rho A)_2 g \ell_2 \left(\phi_{\ell_1}^T\right) \tag{14.12}$$

$$K_{13} = m_p g \ell_2 + \frac{1}{2}(\rho A)_2 g \ell_2^2 \tag{14.13}$$

$$\mathbf{K}_{14} = m_p g\left(\psi_{\ell_2}^T\right) + \int_0^{\ell_2} (\rho A)_2 g\left(\psi^T\right) dr_2 \tag{14.14}$$

$$\mathbf{K}_{22} = \int_0^{\ell_1} (EI)_1 \left(\phi'' \phi''^T\right) dr_1 + K_{t_2}\left(\phi_{\ell_1}' \phi_{\ell_1}'^T\right) + \left(m_a + m_b + m_p\right) g \int_0^{\ell_1} \left(\phi' \phi'^T\right) dr_1 + \int_0^{\ell_1} (\rho A)_1 g \left[\int_0^{r_1} \left(\phi' \phi'^T\right) d\xi_1\right] dr_1 + (\rho A)_2 g \ell_2 \int_0^{\ell_2} \left(\phi' \phi'^T\right) dr_1 \tag{14.15}$$

$$\mathbf{K}_{23} = -K_{t_2} \phi_{\ell_1}' \tag{14.16}$$

$$\mathbf{K}_{24} = \mathbf{0} \tag{14.17}$$

$$K_{33} = K_{t_2} + m_p g \ell_2 + \frac{1}{2}(\rho A)_2 g \ell_2^2 \tag{14.18}$$

$$\mathbf{K}_{34} = m_p g\left(\psi_{\ell_2}^T\right) + \int_0^{\ell_2} (\rho A)_2 g\left(\psi^T\right) dr_2 \tag{14.19}$$

$$\mathbf{K}_{44} = \int_0^{\ell_2} (EI)_2 \left(\psi'' \psi''^T\right) dr_2 + m_p g \int_0^{\ell_2} \left(\psi' \psi'^T\right) dr_2 + \int_0^{\ell_2} (\rho A)_2 g \left[\int_0^{r_2} \left(\psi' \psi'^T\right) d\xi_2\right] dr_2 \tag{14.20}$$

15. APPENDIX E. EXPERIMENTAL PROCEDURES

15.1 Torsional Spring Constants Measurement

Torsional spring constants for upper and lower joints are measured by applying a weight to an extended arm and measuring the displacement at the end of the arm. Figure 15.1 shows the schematic diagram for measuring torsional spring constants.

Moment balance about a point O is given as

$$-K_t\theta + \big(WC\big)cos\theta + \frac{mg\,d}{2}cos\theta = 0 \tag{15.1}$$

where mg is a weight of the extended arm for measuring the displacement and W is a supplied weight to give a static displacement to the arm. If the angle θ is small, the following two terms are approximated as

$$\begin{aligned} cos\theta &\approx 1 \\ \theta &\approx \frac{h}{d} \end{aligned}$$

Then, Equation 15.1 becomes

$$-K_t\frac{h}{d} + WC + \frac{mg\,d}{2} = 0 \tag{15.2}$$

LVDT(Linear-Variable Differential Transformer) is used to measure the static

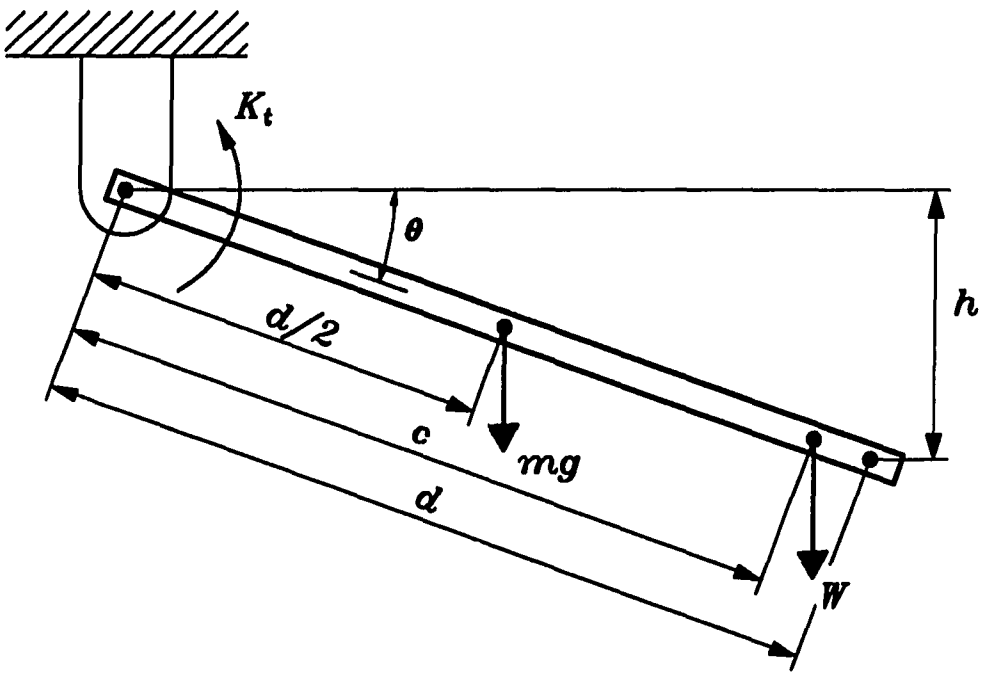

Figure 15.1: A schematic diagram for measuring torsional spring constants

displacement of the arm. The displacement h is given as

$$h = S_d\left(V - V_0\right) \tag{15.3}$$

where S_d is LVDT sensitivity, V_0 is the initial voltage and V is the voltage when a weight is applied.

Substituting Equation 15.3 into Equation 15.2 and rearranging the equation to give an expression for a weight W yields

$$W = \left(\frac{K_t\, S_d}{C\, d}\right) V - \left(\frac{K_t\, S_d\, V_0}{C\, d} + \frac{mg\, d}{2C}\right) \tag{15.4}$$

A set of data is made for a spring by applying several different weights and measuring their voltages. This data set is fit to a straight line by least squares approximation. Figure 15.2 shows a plot for least squares straight line approximation to the set of measured data points.

Equation 15.4 has slope

$$S_l = \frac{K_t\, S_d}{C\, d} \tag{15.5}$$

and is calculated from the least squares fit. Therefore, the torsional spring constant is given as

$$K_t = \frac{S_l\, C\, d}{S_d} \tag{15.6}$$

15.2 Mass Moment of Inertia J_1 Measurement

It is difficult to analytically estimate the mass moment of inertia J_1 because several components are involved in the rotational behavior such as the shaft, bearing, a mounting block, hooks to hold tension springs, the tension springs, an extended arm to hold a LVDT core and a LVDT core.

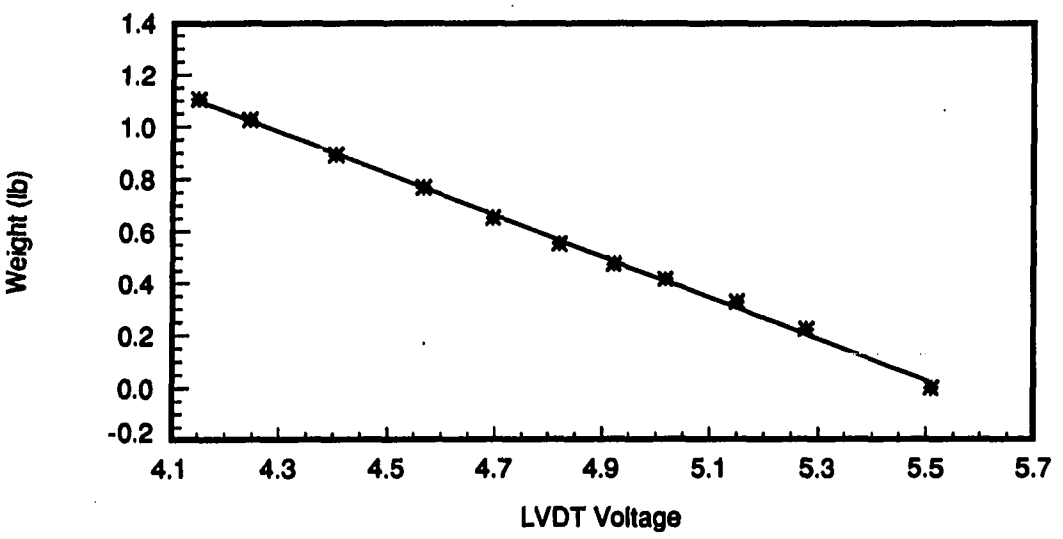

Figure 15.2: A least squares straight line approximation to a data set

If it is assumed that all inertia is concentrated in the upper linker's shaft, the differential equation of motion without including elastic arms is given as

$$J_1\ddot{\theta} + K_{t_1}\theta = 0 \tag{15.7}$$

where K_{t_1} is a measured torsional spring constant and J_1 is mass moment of inertia to be measured.

The eigenvalue of the system is given as

$$\omega^2 = \frac{K_{t_1}}{J_1} \tag{15.8}$$

The torsional spring constant K_{t_1} is a measured value. When the natural frequency is measured, mass moment of inertia J_1 is estimated as

$$J_1 = \frac{K_{t_1}}{\omega^2} = \frac{K_{t_1}}{(2\pi f)^2} \tag{15.9}$$

Table 15.1: Measurement equipments

EQUIPMENT	MODEL or TYPE	COMPANY
Dual Channel Signal Analyzer	Type 2032	Brüel & Kjaer
LVDT	7DCDT - 1000	Hewlett Packard
Voltmeter		United Systems Corporation
Charge Amplifier	Model 504	Kistler
Charge Amplifier	Model 504D	Kistler
Accelerometer	Model 2222B DV51	Endevco
Accelerometer	Model 2222B HS/2	Endevco

15.3 Measurement of Natural Frequencies

This section describes the experimental procedures for measuring natural frequencies. Measurement equipment used for the experimental is shown in Table 15.1. One LVDT transducer and two accelerometers are used to measure the motion of elastic two arms system. A dual channel signal analyzer is used to analyze the signals. One channel is used for the LVDT transducer or the accelerometer attached on the upper arm, and the other channel is used for a signal from an accelerometer attached on the lower arm.

The LVDT is connected to a direct input channel of the dual channel signal analyzer through a voltmeter, and either accelerometer is connected to direct input channel of the signal analyzer through a charge amplifier which converts charge signals to voltage signals.

Storage time constant 200 seconds in the charge amplifiers which establishes the output signal decay rate when a step input is applied to the amplifier is used to pick

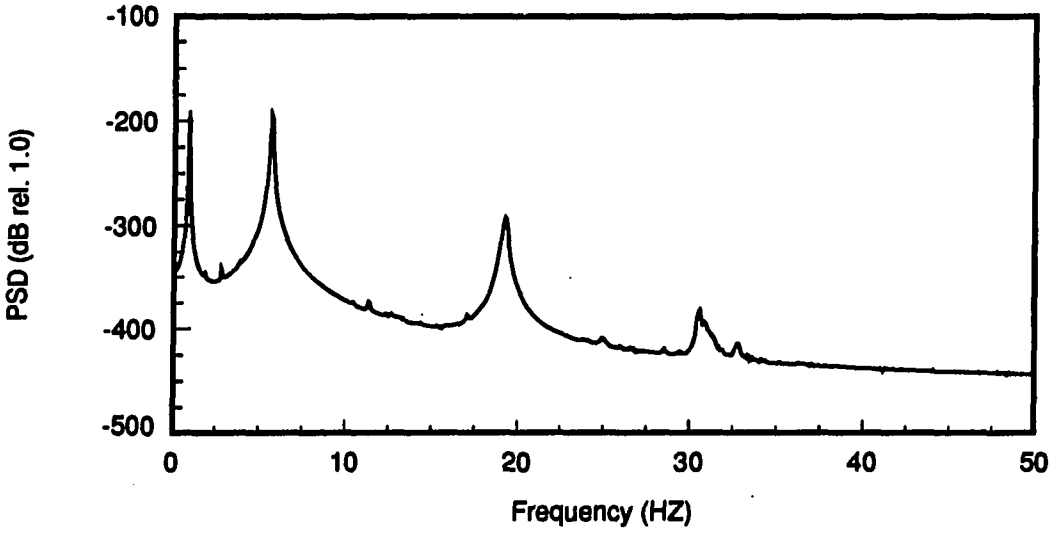

Figure 15.3: A frequency response of the flexible system

up frequencies of the flexible system.

For the measurement set up of the dual channel signal analyzer, the dual spectrum averaging mode is used. The frequency span is adjusted dependent on the frequencies to be measured. The frequency span 6.25 or 12.5 Hz is used for the first two frequencies, and a frequency span of 50 Hz is used for the first four frequencies. Baseband operation is used with a rectangular window weighting.

The flexible system is excited by applying a soft impact force on the system. Figure 15.3 shows a frequency response of the flexible system. The first four frequencies 0.9375 Hz, 5.6875 Hz, 19.250 Hz and 30.625 Hz are shown in the figure.

16. APPENDIX F. LINEARIZED EQUATIONS OF MOTION WITH RESPECT TO AN ARBITRARY EQUILIBRIUM POINT

This appendix gives equations of motion linearized with respect to an arbitrary equilibrium point. The equations of motion include the shortening effect.

$$
\begin{aligned}
&\Big[J_1+\tfrac{1}{3}(\rho A)_1\ell_1^3+(m_a+m_b)\ell_1^2+(J_a+J_b+J_p) \qquad (16.1)\\
&+(\rho A)_2\left(\ell_1^2\ell_2+\tfrac{1}{3}\ell_2^3+\ell_1\ell_2^2 cos\theta_{20}\right)+m_p\left(\ell_1^2+\ell_2^2+2\ell_1\ell_2 cos\theta_{20}\right)\\
&+\int_0^{\ell_1}(\rho A)_1\left(\mathbf{a}_0^T\phi\phi^T\mathbf{a}_0^T\right)dr_1+(m_a+m_b)\left(\mathbf{a}_0^T\phi_{\ell_1}\phi_{\ell_1}^T\mathbf{a}_0\right)\\
&+\int_0^{\ell_2}(\rho A)_2\Big\{\left(\mathbf{a}_0^T\phi_{\ell_1}\phi_{\ell_1}^T\mathbf{a}_0\right)+\left(\mathbf{c}_0^T\psi\psi^T\mathbf{c}_0\right)\\
&-2\ell_1\left(\psi^T\mathbf{c}_0\right)sin\theta_{20}+2\left(\phi_{\ell_1}^T\mathbf{a}_0\right)\left(r_2 sin\theta_{20}+\psi^T\mathbf{c}_0 cos\theta_{20}\right)\Big\}dr_2\\
&+m_p\Big\{\left(\mathbf{a}_0^T\phi_{\ell_1}\phi_{\ell_1}^T\mathbf{a}_0\right)+\left(\mathbf{c}_0^T\psi_{\ell_2}\psi_{\ell_2}^T\mathbf{c}_0\right)\\
&-2\ell_1\left(\psi_{\ell_2}^T\mathbf{c}_0\right)sin\theta_{20}+2\left(\phi_{\ell_1}^T\mathbf{a}_0\right)\left(\ell_2 sin\theta_{20}+\psi_{\ell_2}^T\mathbf{c}_0 cos\theta_{20}\right)\Big\}\Big]\ddot{\theta}_1\\
&+\Big[\int_0^{\ell_1}(\rho A)_1\left(r_1\phi^T\right)dr_1+(m_a+m_b)\ell_1\phi_{\ell_1}^T+J_a\phi_{\ell_1}'^T\\
&+\int_0^{\ell_2}(\rho A)_2\left\{\ell_1\phi_{\ell_1}^T+r_2\phi_{\ell_1}^T cos\theta_{20}-\phi_{\ell_1}^T\left(\psi^T\mathbf{c}_0\right)sin\theta_{20}\right\}dr_2\\
&+m_p\left\{\ell_1\phi_{\ell_1}^T+\ell_2\phi_{\ell_1}^T cos\theta_{20}-\phi_{\ell_1}^T\left(\psi_{\ell_2}^T\mathbf{c}_0\right)sin\theta_{20}\right\}\Big]\ddot{\mathbf{a}}\\
&+\Big[J_b+\int_0^{\ell_2}(\rho A)_2\left(r_2^2+\ell_1 r_2 cos\theta_{20}\right)dr_2\\
&+m_p\left(\ell_2^2+\ell_1\ell_2 cos\theta_{20}\right)+J_p
\end{aligned}
$$

$$+\int_0^{\ell_2}(\rho A)_2\left\{\left(\mathbf{c}_0^T\psi\psi^T\mathbf{c}_0\right)-\ell_1\left(\psi^T\mathbf{c}_0\right)sin\theta_{20}\right.$$
$$\left.+\left(\phi_{\ell_1}^T\mathbf{a}_0\right)\left(r_2 sin\theta_{20}+\psi^T\mathbf{c}_0 cos\theta_{20}\right)\right\}dr_2$$
$$+m_p\left\{\left(\mathbf{c}_0^T\psi_{\ell_2}\psi_{\ell_2}^T\mathbf{c}_0\right)-\ell_1\left(\psi_{\ell_2}^T\mathbf{c}_0\right)sin\theta_{20}\right.$$
$$\left.+\left(\phi_{\ell_1}^T\mathbf{a}_0\right)\left(\ell_2 sin\theta_{20}+\psi_{\ell_2}^T\mathbf{c}_0 cos\theta_{20}\right)\right\}\Big]\ddot{\theta}_2$$
$$+\Big[\int_0^{\ell_2}(\rho A)_2\left\{\ell_1\psi^T cos\theta_{20}+r_2\psi^T+\left(\phi_{\ell_1}^T\mathbf{a}_0\right)\psi^T sin\theta_{20}\right\}dr_2$$
$$+m_p\left\{\ell_1\psi_{\ell_2}^T cos\theta_{20}+\ell_2\psi_{\ell_2}^T+\left(\phi_{\ell_1}^T\mathbf{a}_0\right)\psi_{\ell_2}^T sin\theta_{20}\right\}\Big]\ddot{\mathbf{c}}$$
$$+\Big[\int_0^{\ell_1}(\rho A)_1 g\left(-\phi^T\mathbf{a}_0 sin\theta_{10}+r_1 cos\theta_{10}\right)dr_1$$
$$+(m_a+m_b)g\left(-\phi_{\ell_1}^T\mathbf{a}_0 sin\theta_{10}+\ell_1 cos\theta_{10}\right)$$
$$+\int_0^{\ell_2}(\rho A)_2 g\left\{-\left(\phi_{\ell_1}^T\mathbf{a}_0 sin\theta_{10}\right)+\left(\ell_1 cos\theta_{10}\right)\right.$$
$$-\left(\psi^T\mathbf{c}_0\right)\left(cos\theta_{20}sin\theta_{10}+sin\theta_{20}cos\theta_{10}\right)$$
$$\left.-(r_2)\left(sin\theta_{20}sin\theta_{10}-cos\theta_{20}cos\theta_{10}\right)\right\}dr_2$$
$$+m_p g\left\{-\left(\phi_{\ell_1}^T\mathbf{a}_0 sin\theta_{10}\right)+\left(\ell_1 cos\theta_{10}\right)\right.$$
$$-\left(\psi_{\ell_2}^T\mathbf{c}_0\right)\left(cos\theta_{20}sin\theta_{10}+sin\theta_{20}cos\theta_{10}\right)$$
$$\left.-(\ell_2)\left(sin\theta_{20}sin\theta_{10}-cos\theta_{20}cos\theta_{10}\right)\right\}$$
$$-\frac{1}{2}\int_0^{\ell_1}(\rho A)_1 g(cos\theta_{10})\left\{\int_0^{r_1}\left(\mathbf{a}_0^T\phi'\phi'^T\mathbf{a}_0\right)d\xi_1\right\}dr_1$$
$$-\frac{1}{2}\int_0^{\ell_1}(m_a+m_b)g(cos\theta_{10})\left(\mathbf{a}_0^T\phi'\phi'^T\mathbf{a}_0\right)dr_1$$
$$-\frac{1}{2}\int_0^{\ell_2}(\rho A)_2 g(cos\theta_{10})\left\{\int_0^{\ell_1}\left(\mathbf{a}_0^T\phi'\phi'^T\mathbf{a}_0\right)dr_1\right\}dr_2$$
$$+\frac{1}{2}\int_0^{\ell_2}(\rho A)_2 g\left(sin\theta_{20}sin\theta_{10}-cos\theta_{20}cos\theta_{10}\right)\int_0^{r_2}\left(\mathbf{c}_0^T\psi'\psi'^T\mathbf{c}_0\right)d\xi_2 dr_2$$
$$-\frac{1}{2}m_p g(cos\theta_{10})\int_0^{\ell_1}\left(\mathbf{a}_0^T\phi'\phi'^T\mathbf{a}_0\right)dr_1$$

$$+\frac{1}{2}m_p g\left(sin\theta_{20}sin\theta_{10} - cos\theta_{20}cos\theta_{10}\right)\int_0^{\ell_2}\left(\mathbf{c}_0^T\psi'\psi'^T\mathbf{c}_0\right)dr_2\Big]\tilde{\theta}_1$$

$$+\Big[\int_0^{\ell_1}(\rho A)_1\, g\left(\phi^T cos\theta_{10}\right)dr_1 + \int_0^{\ell_2}(\rho A)_2\, g\left(\phi_{\ell_1}^T cos\theta_{10}\right)dr_2$$

$$+\left(m_a + m_b + m_p\right)g\left(\phi_{\ell_1}^T cos\theta_{10}\right)$$

$$-\int_0^{\ell_1}(\rho A)_1\, g\left(sin\theta_{10}\right)\Big\{\int_0^{r_1}\left(\mathbf{a}_0^T\phi'\phi'^T\right)d\xi_1\Big\}dr_1$$

$$-\int_0^{\ell_1}\left(m_a + m_b + m_p\right)g\left(sin\theta_{10}\right)\left(\mathbf{a}_0^T\phi'\phi'^T\right)dr_1$$

$$-\int_0^{\ell_2}(\rho A)_2\, g\left(sin\theta_{10}\right)\Big\{\int_0^{\ell_1}\left(\mathbf{a}_0^T\phi'\phi'^T\right)dr_1\Big\}dr_2\Big]\tilde{\mathbf{a}}$$

$$+\Big[\int_0^{\ell_2}(\rho A)_2\, g\Big\{-\left(\psi^T\mathbf{c}_0\right)\left(sin\theta_{20}cos\theta_{10} + cos\theta_{20}sin\theta_{10}\right)$$

$$+\left(r_2\right)\left(cos\theta_{20}cos\theta_{10} - sin\theta_{20}sin\theta_{10}\right)\Big\}\,dr_2$$

$$+m_p g\Big\{-\left(\psi_{\ell_2}^T\mathbf{c}_0\right)\left(sin\theta_{20}cos\theta_{10} + cos\theta_{20}sin\theta_{10}\right)$$

$$+\left(\ell_2\right)\left(cos\theta_{20}cos\theta_{10} - sin\theta_{20}sin\theta_{10}\right)\Big\}$$

$$-\frac{1}{2}\int_0^{\ell_2}(\rho A)_2\, g\left(cos\theta_{20}cos\theta_{10} - sin\theta_{20}sin\theta_{10}\right)\int_0^{r_2}\left(\mathbf{c}_0^T\psi'\psi'^T\mathbf{c}_0\right)d\xi_2 dr_2$$

$$+\frac{1}{2}m_p g\left(-cos\theta_{20}cos\theta_{10} + sin\theta_{20}sin\theta_{10}\right)\int_0^{\ell_2}\left(\mathbf{c}_0^T\psi'\psi'^T\mathbf{c}_0\right)dr_2\Big]\tilde{\theta}_2$$

$$+\Big[\int_0^{\ell_2}(\rho A)_2\, g\left(\psi^T\right)\left(cos\theta_{20}cos\theta_{10} - sin\theta_{20}sin\theta_{10}\right)dr_2$$

$$+m_p g\left(\psi_{\ell_2}^T\right)\left(cos\theta_{20}cos\theta_{10} - sin\theta_{20}sin\theta_{10}\right)$$

$$-\int_0^{\ell_2}(\rho A)_2\, g\left(sin\theta_{20}cos\theta_{10} + cos\theta_{20}sin\theta_{10}\right)\int_0^{r_2}\left(\mathbf{c}_0^T\psi'\psi'^T\right)d\xi_2 dr_2$$

$$-m_p g\left(sin\theta_{20}cos\theta_{10} + cos\theta_{20}sin\theta_{10}\right)\int_0^{\ell_2}\left(\mathbf{c}_0^T\psi'\psi'^T\right)dr_2\Big]\tilde{\mathbf{c}}$$

$$= u_1$$

$$\Big[\int_0^{\ell_1}(\rho A)_1\left(r_1\phi\right)dr_1 + \left(m_a + m_b\right)\left(\ell_1\phi_{\ell_1}\right) + J_a\phi'_{\ell_1} \quad (16.2)$$

$$+\int_0^{\ell_2}(\rho A)_2\left\{\ell_1\phi_{\ell_1}+r_2\phi_{\ell_1}cos\theta_{20}-\phi_{\ell_1}\left(\psi^T c_0\right)sin\theta_{20}\right\}dr_2$$
$$+m_p\left\{\ell_1\phi_{\ell_1}+\ell_2\phi_{\ell_1}cos\theta_{20}-\phi_{\ell_1}\left(\psi_{\ell_2}^T c_0\right)sin\theta_{20}\right\}\Big]\ddot{\tilde{\theta}}_1$$
$$+\Big[\int_0^{\ell_1}(\rho A)_1\left(\phi\phi^T\right)dr_1+\left(m_a+m_b\right)\left(\phi_{\ell_1}\phi_{\ell_1}^T\right)+J_a\left(\phi'_{\ell_1}\phi'^T_{\ell_1}\right)$$
$$+\int_0^{\ell_2}(\rho A)_2\left(\phi_{\ell_1}\phi_{\ell_1}^T\right)dr_2+m_p\left(\phi_{\ell_1}\phi_{\ell_1}^T\right)\Big]\ddot{\tilde{a}}$$
$$+\Big[\int_0^{\ell_2}(\rho A)_2\left\{r_2\phi_{\ell_1}cos\theta_{20}-\phi_{\ell_1}\left(\psi^T c_0\right)sin\theta_{20}\right\}dr_2$$
$$+m_p\left\{\ell_2\phi_{\ell_1}cos\theta_{20}-\phi_{\ell_1}\left(\psi_{\ell_2}^T c_0\right)sin\theta_{20}\right\}\Big]\ddot{\tilde{\theta}}_2$$
$$+\Big[\int_0^{\ell_2}(\rho A)_2\left(\phi_{\ell_1}\psi^T cos\theta_{20}\right)dr_2+m_p\left(\phi_{\ell_1}\psi_{\ell_2}^T cos\theta_{20}\right)\Big]\ddot{\tilde{c}}$$
$$+\Big[\int_0^{\ell_1}(\rho A)_1 g\left(\phi cos\theta_{10}\right)dr_1+\int_0^{\ell_2}(\rho A)_2 g\left(\phi_{\ell_1}cos\theta_{10}\right)dr_2$$
$$+\left(m_a+m_b+m_p\right)g\left(\phi_{\ell_1}cos\theta_{10}\right)$$
$$-\int_0^{\ell_1}(\rho A)_1 g\left(sin\theta_{10}\right)\left\{\int_0^{r_1}\left(\phi'\phi'^T a_0\right)d\xi_1\right\}dr_1$$
$$-\int_0^{\ell_1}\left(m_a+m_b+m_p\right)gsin\theta_{10}\left(\phi'\phi'^T a_0\right)dr_1$$
$$-\int_0^{\ell_2}(\rho A)_2 g\left(sin\theta_{10}\right)\left\{\int_0^{\ell_1}\left(\phi'\phi'^T a_0\right)dr_1\right\}dr_2\Big]\tilde{\theta}_1$$
$$+\Big[\int_0^{\ell_1}(EI)_1\left(\phi''\phi''^T\right)dr_1$$
$$+\int_0^{\ell_1}(\rho A)_1 g\left(cos\theta_{10}\right)\left\{\int_0^{r_1}\left(\phi'\phi'^T\right)d\xi_1\right\}dr_1$$
$$+\int_0^{\ell_1}\left(m_a+m_b+m_p\right)g\left(cos\theta_{10}\right)\left(\phi'\phi'^T\right)dr_1$$
$$+\int_0^{\ell_2}(\rho A)_2 gcos\theta_{10}\left\{\int_0^{\ell_1}\left(\phi'\phi'^T\right)dr_1\right\}dr_2\Big]\tilde{a}$$
$$=-u_2\left(\phi'\right)$$
$$\Big[\int_0^{\ell_2}(\rho A)_2\left\{\left(\ell_1 r_2 cos\theta_{20}+r_2^2\right)+\left(c_0^T\psi\psi^T c_0\right)\right. \qquad (16.3)$$

$$
\begin{aligned}
&-\ell_1\left(\psi^T \mathbf{c}_0\right) sin\theta_{20} + \left(\phi_{\ell_1}^T \mathbf{a}_0\right)\left(r_2 sin\theta_{20} + \psi^T \mathbf{c}_0 cos\theta_{20}\right)\Big\}\, dr_2 \\
&\qquad + m_p\Big\{\left(\ell_1 \ell_2 cos\theta_{20} + \ell_2^2\right) + \left(\mathbf{c}_0^T \psi_{\ell_2} \psi_{\ell_2}^T \mathbf{c}_0\right) \\
&-\ell_1\left(\psi_{\ell_2}^T \mathbf{c}_0\right) sin\theta_{20} + \left(\phi_{\ell_1}^T \mathbf{a}_0\right)\left(\ell_2 sin\theta_{20} + \psi_{\ell_2}^T \mathbf{c}_0 cos\theta_{20}\right)\Big\} \\
&\qquad + J_b + J_p\Big]\ddot{\tilde{\theta}}_1 \\
&\quad + \Big[\int_0^{\ell_2} (\rho A)_2 \Big\{\left(r_2 cos\theta_{20} - \psi^T \mathbf{c}_0 sin\theta_{20}\right)\left(\phi_{\ell_1}^T\right)\Big\}\, dr_2 \\
&\qquad + m_p\Big\{\left(\ell_2 cos\theta_{20} - \psi_{\ell_2}^T \mathbf{c}_0 sin\theta_{20}\right)\left(\phi_{\ell_1}^T\right)\Big\}\Big]\ddot{\tilde{\mathbf{a}}} \\
&\qquad + \Big[\int_0^{\ell_2} (\rho A)_2 \left(r_2^2 + \mathbf{c}_0^T \psi \psi^T \mathbf{c}_0\right)\, dr_2 \\
&\qquad + J_b + J_p + m_p\left(\ell_2^2 + \mathbf{c}_0^T \psi_{\ell_2} \psi_{\ell_2}^T \mathbf{c}_0\right)\Big]\ddot{\tilde{\theta}}_2 \\
&\quad + \Big[\int_0^{\ell_2} (\rho A)_2 \left(r_2 \psi^T\right) dr_2 + m_p\left(\ell_2 \psi_{\ell_2}^T\right) + J_P \psi_{\ell_2}'^T\Big]\ddot{\tilde{\mathbf{c}}} \\
&\quad + \Big[\int_0^{\ell_2} (\rho A)_2\, g\Big\{-\left(\psi^T \mathbf{c}_0\right)\left(sin\theta_{20} cos\theta_{10} + cos\theta_{20} sin\theta_{10}\right) \\
&\qquad + \left(r_2\right)\left(cos\theta_{20} cos\theta_{10} - sin\theta_{20} sin\theta_{10}\right)\Big\}\, dr_2 \\
&\qquad + m_p g\Big\{-\left(\psi_{\ell_2}^T \mathbf{c}_0\right)\left(sin\theta_{20} cos\theta_{10} + cos\theta_{20} sin\theta_{10}\right) \\
&\qquad + \left(\ell_2\right)\left(cos\theta_{20} cos\theta_{10} - sin\theta_{20} sin\theta_{10}\right)\Big\} \\
&-\frac{1}{2}\int_0^{\ell_2} (\rho A)_2\, g\left(cos\theta_{20} cos\theta_{10} - sin\theta_{20} sin\theta_{10}\right)\int_0^{r_2}\left(\mathbf{c}_0^T \psi' \psi'^T \mathbf{c}_0\right) d\xi_2 dr_2 \\
&\qquad + \frac{1}{2} m_p g\left(-cos\theta_{20} cos\theta_{10} + sin\theta_{20} sin\theta_{10}\right)\int_0^{\ell_2}\left(\mathbf{c}_0^T \psi' \psi'^T \mathbf{c}_0\right) dr_2\Big]\tilde{\theta}_1 \\
&\quad + \Big[\int_0^{\ell_2} (\rho A)_2\, g\Big\{-\left(\psi^T \mathbf{c}_0\right)\left(cos\theta_{20} sin\theta_{10} + sin\theta_{20} cos\theta_{10}\right) \\
&\qquad + \left(r_2\right)\left(cos\theta_{20} cos\theta_{10} - sin\theta_{20} sin\theta_{10}\right)\Big\}\, dr_2 \\
&\qquad + m_p g\Big\{-\left(\psi_{\ell_2}^T \mathbf{c}_0\right)\left(cos\theta_{20} sin\theta_{10} + sin\theta_{20} cos\theta_{10}\right) \\
&\qquad + \left(\ell_2\right)\left(cos\theta_{20} cos\theta_{10} - sin\theta_{20} sin\theta_{10}\right)\Big\}
\end{aligned}
$$

$$
\begin{aligned}
&+\frac{1}{2}\int_0^{\ell_2}(\rho A)_2\, g\big(sin\theta_{20}sin\theta_{10}-cos\theta_{20}cos\theta_{10}\big)\int_0^{r_2}\left(\mathbf{c}_0^T\psi'\psi'^T\mathbf{c}_0\right)d\xi_2 dr_2\\
&\quad+\frac{1}{2}m_p g\big(sin\theta_{20}sin\theta_{10}-cos\theta_{20}cos\theta_{10}\big)\int_0^{\ell_2}\left(\mathbf{c}_0^T\psi'\psi'^T\mathbf{c}_0\right)dr_2\Big]\tilde{\theta}_2\\
&\quad+\Big[\int_0^{\ell_2}(\rho A)_2\, g\Big\{-\left(\psi^T\right)\big(sin\theta_{20}sin\theta_{10}-cos\theta_{20}cos\theta_{10}\big)\Big\}dr_2\\
&\qquad+m_p g\Big\{-\left(\psi_{\ell_2}^T\right)\big(sin\theta_{20}sin\theta_{10}-cos\theta_{20}cos\theta_{10}\big)\Big\}\\
&-\int_0^{\ell_2}(\rho A)_2\, g\big(cos\theta_{20}sin\theta_{10}+sin\theta_{20}cos\theta_{10}\big)\int_0^{r_2}\left(\mathbf{c}_0^T\psi'\psi'^T\right)d\xi_2 dr_2\\
&\quad-m_p g\big(cos\theta_{20}sin\theta_{10}+sin\theta_{20}cos\theta_{10}\big)\int_0^{\ell_2}\left(\mathbf{c}_0^T\psi'\psi'^T\right)dr_2\Big]\tilde{\mathbf{c}}\\
&\qquad\qquad=u_2\\
&\quad\Big[\int_0^{\ell_2}(\rho A)_2\left\{\ell_1\psi cos\theta_{20}+r_2\psi+\left(\phi_{\ell_1}^T\mathbf{a}_0\right)\psi sin\theta_{20}\right\}dr_2\\
&+m_p\left\{\ell_1\psi_{\ell_2}cos\theta_{20}+\ell_2\psi_{\ell_2}+\left(\phi_{\ell_1}^T\mathbf{a}_0\right)\psi_{\ell_2}sin\theta_{20}\right\}+J_p\psi'_{\ell_2}\Big]\ddot{\tilde{\theta}}_1\\
&\quad+\Big[\int_0^{\ell_2}(\rho A)_2\left(\psi\phi_{\ell_1}^T cos\theta_{20}\right)dr_2+\left(\psi_{\ell_2}\phi_{\ell_1}^T cos\theta_{20}\right)\Big]\ddot{\tilde{\mathbf{a}}}\\
&\quad+\Big[\int_0^{\ell_2}(\rho A)_2\left(r_2\psi\right)dr_2+m_p\left(\ell_2\psi_{\ell_2}\right)+J_p\left(\psi'_{\ell_2}\right)\Big]\ddot{\tilde{\theta}}_2\\
&+\Big[\int_0^{\ell_2}(\rho A)_2\left(\psi\psi^T\right)dr_2+m_p\left(\psi_{\ell_2}\psi{\ell_2}^T\right)+J_p\left(\psi'_{\ell_2}\psi'^T_{\ell_2}\right)\Big]\ddot{\tilde{\mathbf{c}}}\\
&\quad+\Big[\int_0^{\ell_2}(\rho A)_2\, g\Big\{(\psi)\big(cos\theta_{20}cos\theta_{10}-sin\theta_{20}sin\theta_{10}\big)\Big\}dr_2\\
&\qquad+m_p g\Big\{\left(\psi_{\ell_2}\right)\big(cos\theta_{20}cos\theta_{10}-sin\theta_{20}sin\theta_{10}\big)\Big\}\\
&-\int_0^{\ell_2}(\rho A)_2\, g\big(sin\theta_{20}cos\theta_{10}+cos\theta_{20}sin\theta_{10}\big)\int_0^{r_2}\left(\psi'\psi'^T\mathbf{c}_0\right)d\xi_2 dr_2\\
&\quad-m_p g\big(sin\theta_{20}cos\theta_{10}+cos\theta_{20}sin\theta_{10}\big)\int_0^{\ell_2}\left(\psi'\psi'^T\mathbf{c}_0\right)dr_2\Big]\tilde{\theta}_1\\
&\quad+\Big[\int_0^{\ell_2}(\rho A)_2\, g\Big\{-(\psi)\big(sin\theta_{20}sin\theta_{10}-cos\theta_{20}cos\theta_{10}\big)\Big\}dr_2\\
&\qquad+m_p g\Big\{-\left(\psi_{\ell_2}\right)\big(sin\theta_{20}sin\theta_{10}-cos\theta_{20}cos\theta_{10}\big)\Big\}
\end{aligned}
\tag{16.4}
$$

$$
\begin{aligned}
&- \int_0^{\ell_2} (\rho A)_2 \, g\left(cos\theta_{20} sin\theta_{10} + sin\theta_{20} cos\theta_{10}\right) \int_0^{r_2} \left(\psi' \psi'^T \mathbf{c}_0\right) d\xi_2 dr_2 \\
&\qquad - m_p g\left(cos\theta_{20} sin\theta_{10} + sin\theta_{20} cos\theta_{10}\right) \int_0^{\ell_2} \left(\psi' \psi'^T \mathbf{c}_0\right) dr_2 \Big] \tilde{\theta}_2 \\
&\qquad + \Big[\int_0^{\ell_2} (EI)_2 \left(\psi'' \psi''^T\right) \, dr_2 \\
&+ \int_0^{\ell_2} (\rho A)_2 \, g\left(-sin\theta_{20} sin\theta_{10} + cos\theta_{20} cos\theta_{10}\right) \int_0^{r_2} \left(\psi' \psi'^T\right) d\xi_2 dr_2 \\
&\qquad + m_p g\left(-sin\theta_{20} sin\theta_{10} + cos\theta_{20} cos\theta_{10}\right) \int_0^{\ell_2} \left(\psi' \psi'^T\right) dr_2 \Big] \tilde{\mathbf{c}} \\
&\qquad = \mathbf{0}
\end{aligned}
$$